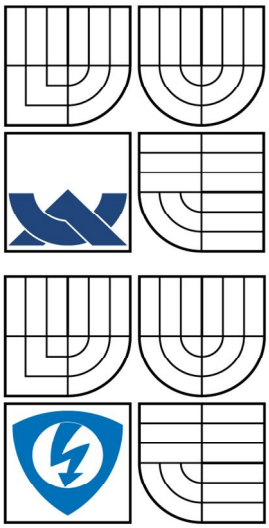

VYSOKÉ UČENÍ TECHNICKÉ V BRNĚ
BRNO UNIVERSITY OF TECHNOLOGY

FAKULTA ELEKTROTECHNIKY A KOMUNIKAČNÍCH TECHNOLOGIÍ
ÚSTAV FYZIKY

FACULTY OF ELECTRICAL ENGINEERING AND COMMUNICATION
DEPARTMENT OF PHYSICS

NELINEÁRNÍ ELEKTRO-ULTRAZVUKOVÁ SPEKTROSKOPIE REZISTORŮ

NON-LINEAR ELECTRO-ULTRASONIC SPECTROSCOPY OF RESISTIVE MATERIALS

DOKTORSKÁ PRÁCE
DOCTORAL THESIS

AUTOR PRÁCE — Ing. PAVEL TOFEL
AUTHOR

VEDOUCÍ PRÁCE — Prof. Ing. RNDr. JOSEF ŠIKULA, DrSc.
SUPERVISOR

BRNO 2011

Keywords:

Electric signal, Ultrasonic signal, electrical resistance modulation, ultrasonic wave, piezoresistive effect, crack, resonant frequency, damping, electro acoustic effect

Klíčová slova:

Elektrický signál, Ultrazvukový signál, modulace elektrického odporu, ultrazvuková vlna, piezoresistivní efekt, prasklina, rezonanční frekvence, tlumení, elektro akustický efekt

Abstract

All materials contain cracks and micro-cracks in structure. My aim is to detect these cracks. Electro-Ultrasonic spectroscopy is a non–destructive testing method which describes quality and reliability of a tested sample. Tested sample is excited by the harmonic electrical signal of frequency f_E and ultrasonic signal of frequency f_U. A new harmonic signal of the frequency f_i is created as a result of electrical resistance change due to the variation of the crack effective area by ultrasonic excitation. The intermodulation frequency f_i is given by the subtraction of excitation frequencies f_E and f_U. Amplitude of the intermodulation signal at frequency f_i is influenced by the electric current, which flows through the sample structure, and resistance change, which is ultrasonically induced due to the defects and unhomogeneities in a sample structure. High sensitivity of this method comes from the fact that the frequencies of exciting sources and measured signal are on different frequencies. The signal-to-noise ratio and high sensitivity for NDT analyses are based on the application of electrical filters for attenuation of exciting signals in signal preprocessing. Experimental verification of this method was performed on various samples such as magnesium alloy, aluminium and dural plates, both without and with cracks, varisotors, MOS FET transistor, rock samples, monocrystals Si and CdTe. This work presents a new non-destructive testing method of solids with metallic electrical conductivity, monocrystals, resistive materials and electronic devices.

Abstrakt

Elektro-ultrazvuková spektroskopie je založena na interakci dvou signálů, elektrického střídavého signálu s frekvencí f_E a ultrazvukového signálu s frekvencí f_U. Ultrazvukový signál mění vzdálenost mezi vodivými zrny ve vzorku a tím mění jeho celkový elektrický odpor R. Změna odporu ΔR je proměnná s frekvencí ultrazvukového signálu f_U. Vzorek, který obsahuje mnoho defektů ve své struktuře, vykazuje vysokou změnu odporu ΔR v porovnání se vzorkem bez defektů při stejné hodnotě ultrazvukového a elektrického signálu. V disertační práci je popsána elektro-ultrazvuková metoda na tlustovrstvých rezistorech, hořčíkových slitinách, monokrystalech Si a CdTe, varistorech a také jeden z prvních pokusů aplikace elektro-ultrazvukové spektroskopie na horninové vzorky a tak diagnostikovat jejich stav poškození. V našem případě byl proměřen vzorek žuly. Jelikož se jedná o nedestruktivní metodu testování, tak má tato metoda velmi perspektivní budoucnost. Tato metoda je citlivá na všechny defekty ve vzorku. Její výhodou je, že se měří velikost signálu ne frekvenci danou rozdílem nebo součtem budících frekvencí f_E a f_U a tím se dá dosáhnout vysoké citlivosti. V mém případě byl vždy měřen signál na rozdílové frekvenci $f_i = f_E - f_U$.

Prohlašuji, že jsem disertační práci v celém rozsahu vypracoval samostatně pod odborným vedením svého školitele Prof. Ing. RNDr. Josefa Šikuly, DrSc., s použitím odborné literatury, kterou jsem všechnu citoval v seznamu literatury.

Jako autor uvedené práce dále prohlašuji, že v souvislosti s touto prací jsem neporušil autorská práva třetích osob a jsem si plně vědom následků porušení ustanovení § 11 a autorského zákona č. 121/2000 Sb., včetně možných trestněprávních důsledků vyplývajících z ustanovení § 152 trestního zákona č. 140/1961 Sb.

V Brně dne 26.10.2011 ……

Pavel Tofel

Děkuji tímto za cenné rady a připomínky svému školiteli Prof. RNDr. Ing. Josefu Šikulovi, DrSc. a kolegům, kteří mi vyšli vstříc praktickými radami a připomínkami.

TOFEL, P. *Nelineární elektro-ultrazvuková spektroskopie rezistorů.* Brno: Vysoké učení technické v Brně, Fakulta elektrotechniky a komunikačních technologií, 2012. 85 s. Vedoucí disertační práce prof. Ing. RNDr. Josef Šikula, DrSc..

Table of Contents

List of Figures

1. Introduction

The non-destructive testing (NDT) has become important discipline. The main advantage of NDT is detection of the defects and cracks in the tested material without damage the sample. This way I can chose the samples which have not meet the standards. If a sample contains some defects, the next step is to localize the crack and define its properties (the crack length, crack width, whether the crack will change its geometry in the future, etc.). The effort is to establish the lifetime of sample or product, and separate the samples with short lifetimes. In this manner, I eliminate the fatal damage if the product fails. The non- destructive methods are very interesting because the sample or product is tested without the changes of its properties.

A lot of non-destructive testing methods are based on the ultrasonic (ultrasound) signal. These methods analyze reflection, absorption and interference of the mechanical wave. These methods have some limitations. The tested sample must have a simple shape and made from a homogeneous material. Reflection of the ultrasonic wave from the edge of tested sample is parasitic signal which can be evaluated as defect or crack in the sample. The testing of the samples of small shape which are comparable with the ultrasonically induced mechanical wave length is very difficult. In this case ultrasonic signal with frequency over 10 MHz is used. But ultrasonic signal with higher frequency has higher absorption coefficient also. Therefore testing is performed on thin layers where the tested sample is situated in the liquid medium. The testing of samples with un-homogeneities structure and of difficult shape is impossible due to many parasitic signals.

There is wide spectrum of non-destructive methods. One of the new perspective methods is non-linear ultrasonic spectroscopy, which is useful for testing materials of complicated shapes, composite materials including connection feud and testing materials on the micro-structural level.

Non-linear ultrasonic spectroscopy is based on the non-linear interaction of mechanical wave with atoms of solid body in the sample. Cracks and defects are the sources of un-harmonic oscillations of atoms in the material structure and crystal lattice due to nonlinear effects. That is why higher harmonics signals appear in the measured spectrum. Non-linear ultrasonic spectroscopy is a very important non-destructive method for testing solid material because it's independent on the shape.

Electro-ultrasonic spectroscopy is based on interaction of ultrasonic signal and electric signal in conductive materials. Ultrasonic signal changes the contact area between conducting grains in the sample, thus resistance of the sample is modulated by frequency of ultrasonic excitation. Defects and cracks in the sample structure are the sources of new intermodulation signal. The frequency of new intermodulation signal is given by the superposition or subtraction of exciting frequencies. This method is very sensitive because is evaluating intermodulation signal on the frequency different than exciting frequencies electrical and ultrasonic signal.

Electromagnetic and acoustic emission can localize the new rising cracks or defects. Non-linear ultrasonic spectroscopy and electro-ultrasonic spectroscopy are sensitive on all cracks or defects in the sample structure, thus the quality and reliability of materials can be described. It is possible to estimate the lifetime of products by different size and structure.

1.1. State of art

The basic principles of selected methods for non-destructive testing:

SIMONRUS and SIMONRAS belong to group of new NDT techniques. These methods evaluate non-linear effects in dependence on a shift of resonant frequency. SIMONRUS (Single Mode Nonlinear Resonance Ultrasound Spectroscopy) is used for higher ultrasonic frequency and SIMONRAS (Single Mode Nonlinear Resonance Acoustic Spectroscopy) is used for lower acoustic frequency [1].

The pulse echo method (PE) evaluates the proportion of echo by the boundary-line and back reflection. One sensor is used as ultrasonic transmitter and receiver. Defects in the material cause a decrease in the reflection amplitude. Method is limited by the minimal thickness of measured sample, where the measured echoes are possible to distinguish. Basic types of ultrasonic testing is illustrate in Fig. 1.1.

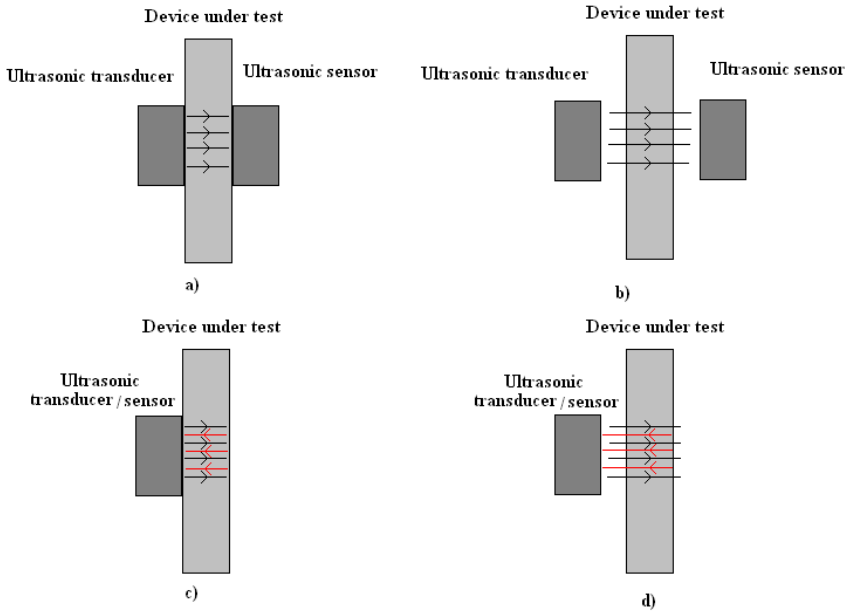

Fig. 1.1: Basic types of ultrasonic testing

Through-transmission ultrasonic methods (TTU) consist of two sensors where the first sensor is used as generator and second one is used as receiver. The amplitude of measured ultrasonic signal is evaluated in the TTU method. The measured sample is situated between ultrasonic transmitter and ultrasonic receiver. The sensitivity of TTU methods is influenced by the position of ultrasonic transmitter and receiver. The higher sensitivity is ensured by the ultrasonic receiver situated strictly against ultrasonic transmitter. Cracks and defects in the material cause a decrease in measured amplitude of ultrasonic signal [2].

The measuring velocity of propagation longitudinal waves and damping is provided by vertically situated ultrasonic sensor to the direction of fibers in the sample matrix. The thickness of the sample must be defined. The velocity of propagation of longitudinal waves is a function of proportion the sample matrix. Damping depends on the delamination, microstructure defects, resin content and proportional capacity of fibers and resin.

Next method of ultrasonic testing is based on back-scattering of ultrasonic wave. Testing aparature rotates around a sample and signal of back-scattered wave is evaluated as a function of angular displacement. Sample with cracks has higher amplitude of the scattered wave then the sample without cracks.

High frequency bond tester (HFBT) is based on special narrow-band transducers which generate continuum ultrasonic field in a specimen. The frequency depends on thickness and type of measured material and it is within the range of 25 to 500 kHz. If the thickness of the sample is changed, the load of the transmitter will be changed, and resonant frequency of the transmitter will be shifted. The level of amplitude describes the size of crack and phase describes the thickness of a tested material.

Pitch-catch is method that uses two search units. The first search unit is used as transmitter for generation of ultrasonic signal and second used as a receiver. The pitch-catch method involves a set-up in which transmitter and receiver are located at the same side of tested object. The velocity lag of ultrasonic wave depends on defects and un-homogeneities in the sample. The amplitude of the measured signal describes delamination because energy is disappearing for the high quality connection point in the material. Phase describes the stiffness in the area of non-connecting for measured material. Ultrasonic waves, which are reflected once or multiple times from the back-wall of the object or refracted by a discontinuity, are recorded and analyzed for visualization.

The Mechanical Impedance Analysis (MIA) is another of the methods of NDT. MIA was developed to investigate bonded structures and composite materials and to discover damages that cause a stiffness diminished of the surface, especially in the aerospace field. This method detects, locates and evaluates defects, such as voids, delaminations, inclusions and other similar defects found in materials. MIA is a low frequency non-resonant method that employs a continuous wave. The probe contains two piezo-electric crystals. The excitation of the crystal transforms electrical signal into vibrations and, by the reverse procedure, the modified vibrations on the receiving crystal are converted back into electrical signals. When the probe is in free air, there is no net strain of the receiving crystal. When the probe tip is placed on the material under test, the receiving crystal is restricted, creating a strain and thus an output is produced. The degree of restriction is conditioned by the local stiffness and mass of material in the structure below the probe. The method has a number of advantages over other bond testing equipment. It is independent of the material type, it does not require couplant, one single transducer is used for all the applications. MIA is known also as „Bond-tester“.

Simple NDT method is based on sample excitation by hammer. Sample with cracks has different frequency spectrum then sample without cracks and then spectral analysis or also hearing is able to distinguish between sample with cracks and without one.

Electromagnetic (EME) and acoustic emission (AE) signals may be observed when solid materials are mechanically stressed. These signals may be used for indication of micro-crack formations in stressed materials. The cracks generation in the solids is accompanied by the redistribution of the electric charge. The crack walls are electrically charged and their vibrations produce time variable dipole moments. Hence the individual cracks become electromagnetic field sources, which can be measured by appropriate sensors, it is known as EME. The signal of acoustic emission (AE) is generated simultaneously with the EME signal. The time delay between both signals is caused by different propagation velocities of the acoustic

and electromagnetic signals in the sample under examination. The AE signal time latency to the EME signal arrival provides information about the distance of the crack from the AE sensor. In case of the AE signal multi-channel measurement, one can get the useful information about the crack position in the stressed material, when three sensors are used at least. AE and EME are belongs to passive NDT methods. Example of AE signal is shown in Fig. 1.2.

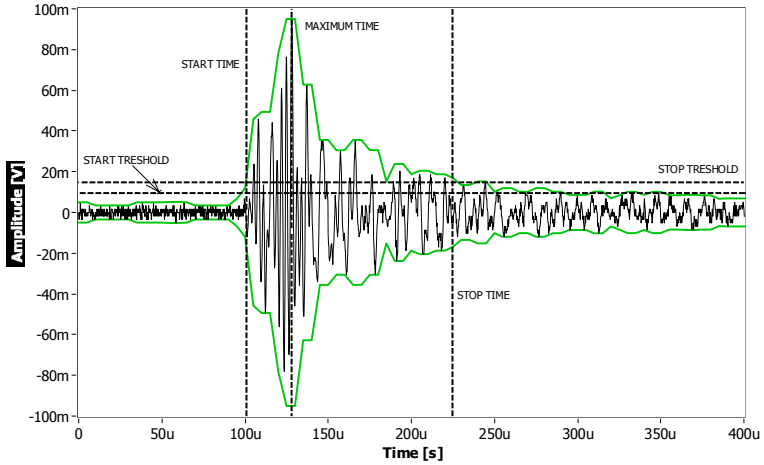

Fig. 1.2: A real-time processing of AE signal (Trcka. T.)

Non-linear ultrasonic spectroscopy is based on the non-linear effects, which are generated near the defects in the sample structure and crystal lattice. The oscillations of atoms are unharmonic in the vicinity of defects because potential energy is not a quadratic function of atom location. It is reason for generation of unharmonics oscillations of atoms and generate on of the second, third and higher harmonic signals in the signal spectra also. Non-linear ultrasonic spectroscopy belongs to perspective NDT methods for solids testing. This method was detailed describe in [3]. Measurement by this method is described in many papers for example [4, 5, 6 and 7].

All NDT methods from the field of ultrasonic spectroscopy are based on the reflection of mechanical waves, absorption and interference. The examination of defects and cracks or other inhomogeneities in the sample structure is difficult when the defects are unevenly situated inside the sample structure. If the size of the examined sample is too small with correspondence to wave length of mechanical oscillations and sample has a complicated shape, it is also difficult to examine by the ultrasonic spectroscopy.

1.2. Electro-ultrasonic background

Phenomenon of the electro-ultrasonic spectroscopy is closely related to electro-acoustic effects. These effects are result of a coupling between acoustic and electric fields. Mostly, this phenomenon occurs when ultrasound actuates on the fluid which contains ions which have an electric charge. Ultrasonic signal moves with ions and then this motion generates the AC electric signal.

Electro-acoustic effect was firstly observed by Debye in 1933 [8]. Electric signal is generated when the acoustic wave passes through the homogeneous fluid. He used sound with

longitudinal wave on the fluid and he discovered the difference in the effective mass or friction coefficient between anion and cation. This difference generates AC electric potential between various points in a sound wave.

Streaming Vibration current was demonstrated in 1948 by Williams [9]. Electric AC signal is generated when acoustic wave pass through a porous body in which the pores are filled with fluid.

Double layer compression is a structure that appears on a surface of object that is placed into a liquid and acoustic signal is actuating on the fluid [10]. The sound waves generate local pressure change, thus the length of double layer is changing (see Fig. 1.3).

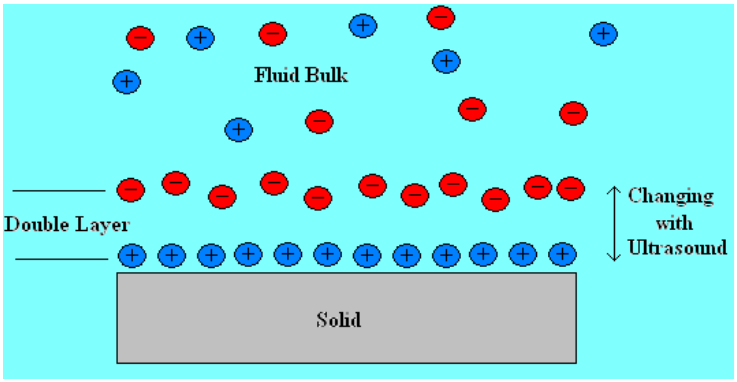

Fig. 1.3: Positively charged solid on the fluid

Colloid Vibration Potential (CVI) was described in 1938 by Hermans and Rutgers. It is used for characterizing the ζ – potential of dispersions and emulsions. Theory was written by O´Brian [11], where is CVI described by dynamic electrophoretic mobility μ_d:

$$\mathrm{CVI} = A\Phi\mu_d \frac{n_p - n_m}{n_m} \tag{1.1}$$

Where: A – calibration constant which is dependent on the frequency and independent on the shape of particles, Φ – volume fraction of dispersed phase, n_p – density of particles, n_m – density of the fluid.

More information about electrophoretic mobility which is similar to electrophoretic mobility in electro-phoresis theory is described in [12].

Acousto-electric effect occurs by the transfer of momentum from the ultrasonic wave to the electrons. It is due to bunching of electrons in the potential minima of the periodic electric field created and accompanying the sound wave. The electrons create an acousto-electric current by following the wave motion. An acousto electric field E_{ae} is measured, and is related to the attenuation α_{sw} of the sound wave:

$$\alpha_{sw} = (eNv_s/2I_{aw})E_{ae} \tag{1.2}$$

with v_s the sound velocity and I_{aw} the intensity of the acoustic wave. Here, the doping level is smaller than in relaxation case.

If one applies a DC electric field E_{dc} parallel to the sound wave direction, the electrons gain a drift velocity:

$$v_d = \mu E_{dc} \tag{1.3}$$

with μ the mobility. If the drift velocity exceeds the sound velocity v_s, the electrons move ahead of the sound wave and will be further accelerated and de-accelerated depending on the sign of the sound wave field. This leads on average to amplification [13].

A new principle of non-destructive testing is presented. Proposed method is based on the effect of ultrasonic vibrations on electron transport in samples with scattered centers and the defects as cracks affecting electrical conductivity. The effect of the mechanical wave motion on electrons in conducting solids, so called acoustoelectric effect, has been analyzed in many papers (see e.g. Akshiser [14], Parmenter [15], Inreich [16]). The principal of acoustoelectric effect consists in the generation of DC electric voltage on the measured sample as a result of single traveling longitudinal acoustic wave moving along a long uniform rod of material.

2. Aims of the dissertation

The principal aim of this dissertation is to study a new non-destructive method to test resistors. This method is based on the interaction between the ultrasonic wave and the AC electric current. Ultrasonic phonons have an influence on transfer electrons located near defects. The aim is to find out the experimental information about the influence of ultrasonic phonons on the mobility of electrons. Due to different physical origins of ultrasonic and electric signals the electro-ultrasonic spectroscopy is supposed to provide higher resolution sensitivity for measured samples. The project is based on works of grants such as Non-linear ultrasonic spectroscopy in solids and Increasing the dynamic range of the analog signal pre-treatment (Nelineární ultrazvuková spektroskopie v pevných látkách and Zvyšování dynamického rozsahu systému s analogovým předzpracováním signálu).

2.1. Reason for electro-ultrasonic spectroscopy

Nowadays special attention is given to non-destructive methods of quality testing and the reliability of electronic devices. These methods keep the original parameters of the sample under the test. The electro-ultrasonic spectroscopy is a new method based on the interaction of two signals, the ultrasonic signal and the AC electrical signal. The high resolution of the electro-ultrasonic method is expected due to the fact that the measured signal is on the intermodulation frequency which differs from exciting frequencies.

Principal aims are:

- Experimental study of the dependence of amplitude spectral density on the intermodulation frequency vs. amplitude of electrical AC voltage for constant ultrasonic excitation
- Experimental study of the dependence of the amplitude spectral density on the intermodulation frequency vs. the amplitude of the ultrasonic excitation for the constant electrical AC voltage
- Study the influence of the ultrasonic signal on both the sample structure and the resistance change which is induced by the ultrasonic signal
- Establish the influence of ultrasonic phonons on the mobility of electrons
- Measure many samples by means of electro-ultrasonic spectroscopy

3. Theory of electro-ultrasonic spectroscopy

It is very useful to use two exciting signals with different frequencies. The measured signal has the frequency which is given by the subtraction or superposition of exciting frequencies. In this way I get high sensitivity of evaluating by this method. Is it possible used two ultrasonic actuators which are generating ultrasonic signal on the two different frequencies (important for non-conducting samples), or one ultrasonic actuator and electric AC or DC signal. If is apply one ultrasonic actuator and electric DC so the measuring signal is on the frequency given by the ultrasonic actuator. I measured by this method the samples of polymer based thick film layers resistors. If is apply one ultrasonic actuator on the frequency f_U and electric AC signal on the frequency f_E, I get new intermodulation signal on the frequency $f_i = f_E - f_U$ or $f_I = f_E + f_U$. My doctoral work is aimed on the electro-ultrasonic spectroscopy. I have measured many different samples by this method and results and discussions are shown on this work.

The electro-ultrasonic spectroscopy was used as a non-destructive testing method for conductive samples. This method can be used as a diagnostic tool for the quality and reliability assessment. The sample resistance is influenced by the ultrasonic signal. The ultrasonic signal changes the contact area between the conducting grains in the sample structure and then resistance is modulated by the frequency of ultrasonic excitation. The electrical charge and also the electrical current flowing through the sample structure are conserved. In case the contact area between the conducting grains is changing then the current density is changed. This leads to the resistivity change of measured structure. It is suppose that for the sample with more defects in the structure the influence of the ultrasonic signal is more pronounced and the resistance change is higher.

3.1. The frequency spectrum of electro-ultrasonic spectroscopy

Electro-ultrasonic spectroscopy is based on the two signals, how is illustrated in Fig. 3.1. Electric AC signal variable with frequency f_E and ultrasonic signal, which is generated by the ultrasonic actuator, variable with frequency f_U.

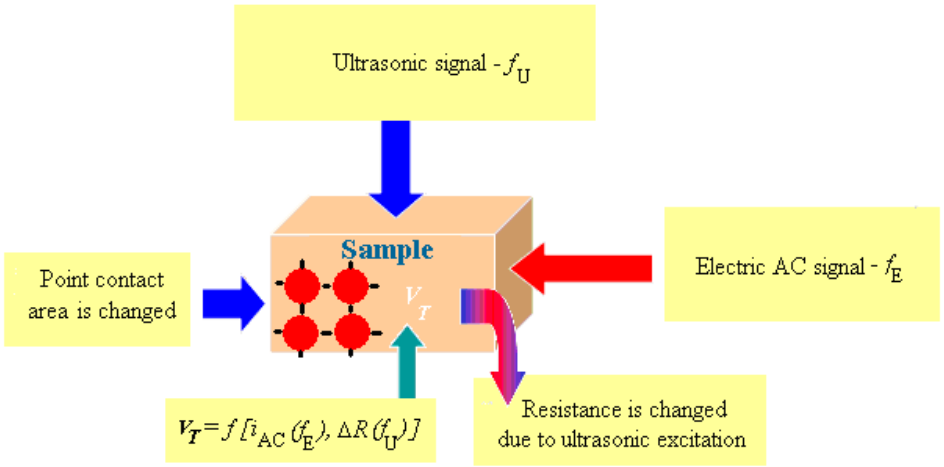

Fig. 3.1: Electro-ultrasonic spectroscopy

The total voltage V_T can is given by electric current flowing through the sample and ultrasonic excited resistance change:

$$V_T = f\left[i_{AC}(f_E), \Delta R(f_U)\right] \tag{3.1}$$

Where: i_{AC} – electric AC current amplitude, f_E, f_U - frequency of electric and ultrasonic excitation respectively, ΔR_M - amplitude of the resistance change due to the ultrasonic excitation

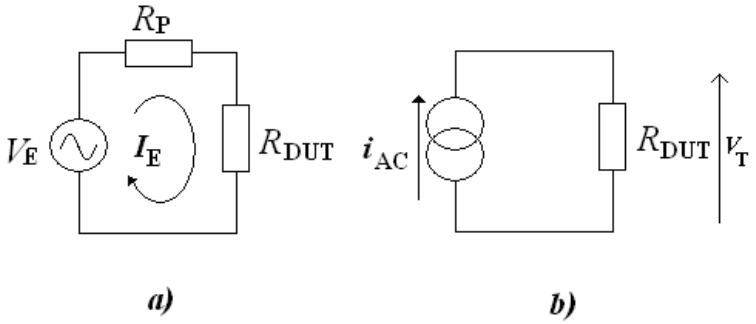

Fig. 3.2: Electric circuit with resistance of the sample R_{DUT}

The measured sample with resistance R_{DUT} and protective resistor R_P were connected to the electric generator, as it is shown in Fig. 3.2 *a*). Protective resistor R_P and generator are generating electric AC current i_{AC}, (Fig. 3.2 *b*). The voltage V_T measured on the sample is:

$$V_T = R_{DUT} \cdot i_{AC} \cos(\omega_E t) \tag{3.2}$$

When the sample is fixed on the ultrasonic actuator which is generating ultrasonic signal with frequency f_U, then the resistance of the sample is changing with the amplitude ΔR. Resistance change is varying with frequency f_U also, (Fig. 3.3). The voltage V_T measured on the sample is given by:

$$V_T = \left(R_{DUT} + \Delta R\right) \cdot i_{AC} \cos\left(\omega_E t\right) \tag{3.3}$$

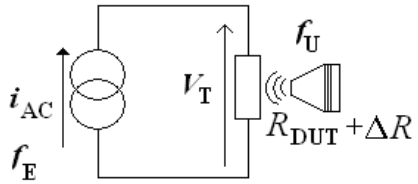

Fig. 3.3: Electric circuit and ultrasonic transducer which influence the sample resistance

The resistance change ΔR is dependents on the amplitude of the mechanical vibration x_t:

$$x_t = M \cdot V_U \cdot \cos\left(\omega_U t\right) \tag{3.4}$$

where V_U is voltage connected to the ultrasonic actuator and M is ultrasonic constant which is different for each frequency f_U. Then the resistance ΔR is given by:

$$\Delta R = k_U \cdot x_t \tag{3.5}$$

where k_U is ultrasonic transfer constant and it is different for each material of the sample. Voltage V_T is:

$$V_T = (R_{DUT} + \Delta R) \cdot I_{AC} \cos(\omega_E t) = [R_{DUT} + k_U \cdot M \cdot V_U \cos(\omega_U t)] \cdot I_{AC} \cos(\omega_E t) = \quad (3.6)$$

$$R_{DUT} \cdot I_{AC} \cos(\omega_E t) + \frac{1}{2} k_u \cdot M \cdot V_U \cdot I_{AC} [\cos(\omega_E t - \omega_U t) + \cos(\omega_E t + \omega_U t)]$$

The resultant voltage spectrum is given by voltage at frequency f_E which consists of resistance of the sample R_{DUT} and AC current flowing through the sample. Sideband voltages are created by resistance change ΔR and AC current flowing through the sample structure also. The result spectrum is shown in Fig. 3.4.

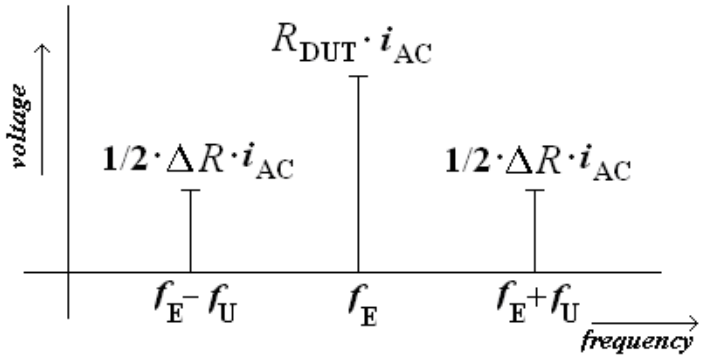

Fig. 3.4: The theoretic result spectrum of the electro-ultrasonic spectroscopy

I am able to study the influence of the ultrasonic signal on the resistor structure. If the sample is connected to the DC voltage or shorted, and fixed on the ultrasonic actuator this is generating the ultrasonic signal of frequency f_U. I have measured the spectral density of voltage V_s created on the studied sample.

$$V_s = I_{DC} \cdot \Delta R_M \sin \omega_U t \quad (3.7)$$

where: I_{DC} – DC electric current flowing through the structure

This voltage is proportional to the ultrasonic excited resistance change ΔR and it is value depends on the sample structure. I can observe the piezoelectric effect on my samples – the voltage of frequency f_U is measured on the samples even when the sample is shorted.

3.2. Model of electro-ultrasonic spectroscopy

Ultrasonic signal evokes the resistance change in the sample due to geometry change. The resistance change can be given by:

- Changes the geometry of the sample
- Changes the area of cracks in the sample structure
- Has influence on the charge carrier mobility

The intermodulation voltage is depends on:

- Tenzometric effect

- Deformation of cracks due to ultrasonic vibration
- Interaction between carrier of electric charge and structural defects-mobility

3.2.1. Piezoresistive effect

This situation is comparable with piezoresistive effect when the conductivity of the sample is changing due to deformation of geometry sample.
Electric resistance of material which has length L and cross-section area A is given by:

$$R = \rho \cdot \frac{L}{A} \tag{3.8}$$

where ρ is electrical resistivity and it is given for each material.

For a bar is a resistance:

$$R = \rho \cdot \frac{L}{D^2} \tag{3.9}$$

where D is thickness and width of the material

If the natural logarithm is applied, then:

$$\ln(R) = \ln(\rho) + \ln(L) - 2\ln(D) \tag{3.10}$$

When it suppose that:

$$\ln(x) = \int_1^x \frac{\mathrm{d}x'}{x'} \text{ or } \mathrm{d}\ln(x) = \frac{\mathrm{d}x}{x} \tag{3.11}$$

It can be obtain the equation for a resistance change:

$$\frac{\mathrm{d}R}{R} = \frac{\mathrm{d}\rho}{\rho} + \frac{\mathrm{d}L}{L} - 2\frac{\mathrm{d}D}{D} \tag{3.12}$$

If the sample is deformed in the longitudinal directions, it can be written for small deformations:

$$\varepsilon = \frac{\Delta L}{L} \tag{3.13}$$

Hover, the cross-section area is also changed due to the Poisson's ratio υ.

$$\varepsilon_T = -\upsilon \cdot \varepsilon = \frac{\mathrm{d}D}{D} = -\upsilon \frac{\mathrm{d}L}{L} \Rightarrow -2\frac{\mathrm{d}D}{D} = 2 \cdot \upsilon \cdot \varepsilon \tag{3.14}$$

Then the resistance change is given:

$$\frac{\mathrm{d}R}{R} = \frac{\mathrm{d}\rho}{\rho} + \varepsilon + 2 \cdot \upsilon \cdot \varepsilon = \varepsilon(1 + 2\upsilon) + \frac{\mathrm{d}\rho}{\rho} \tag{3.15}$$

The resistance change is measured when the material is deformed by stress. It is much known as piezoresistive effect. When a bar is strained with a uniaxial force, as in Fig 3.5, a phenomenon known as Poisson Strain causes the girth of the bar, D, to contract in the transverse, or

perpendicular, direction. The magnitude of this transverse contraction is a material property indicated by its Poisson's Ratio.

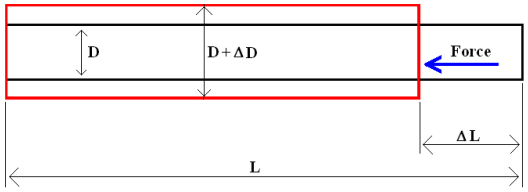

Fig. 3.5: Definition of Strain, piezoresistive effect

The resistance change for tenzometers is given by:

$$\frac{\Delta R}{R} = \mathrm{GF} \cdot \varepsilon \tag{3.16}$$

where: ΔR is resistance change, R is electrical resistance, GF is gauge factor and ε is strain .

Gauge factor is constant for small deformations and it is characteristic for each material. It was found that a material with inhomogeneities has higher number of gauge factor then homogeneous material [17]. It is obvious that Gauge factor is dependent on the electrical resistivity and Poisson's Ratio.

$$\mathrm{GF} = \frac{\frac{\Delta R}{R}}{\varepsilon} = 1 + 2\upsilon + \frac{\frac{\Delta \rho}{\rho}}{\varepsilon} \tag{3.18}$$

Hover, the resistance change is dependent on the temperature also:

$$\frac{\Delta R}{R} = \mathrm{GF} \cdot \varepsilon + \alpha_{\mathrm{T}} \Delta\theta \tag{3.19}$$

where α_{T} is temperature coefficient and $\Delta\theta$ is temperature change

Electrical resistance is defined as

$$\rho = \frac{1}{\sigma} \tag{3.20}$$

where the σ is electrical conductivity of material
Electrical conductivity of homogenous, isotropic solid material is defined follows

$$\sigma = n_{\mathrm{e}} |e| \mu_{\mathrm{e}} + n_{\mathrm{h}} |e| \mu_{\mathrm{h}} \tag{3.21}$$

Where n_{e} / n_{h} are electrons / holes density, $|e|$ is absolute value of the charge on an electron (hole), μ_{e} / μ_{h} are electron and hole mobility. It supposes that the conductivity of the material is changed due to deformations.

3.2.2. Ultrasonic signal

Ultrasonic signal, which is applied on the sample, has frequency range 15 kHz to 150 kHz. The wavelength of the ultrasonic signal is smaller then mean free path of carriers, so the ultrasonic signal has not influence on the carriers directly. Ultrasonic signal changes the geometry of the sample only, on the range of elastic deformations (it is non-destructive

geometry change). Then the standing waves are excited on the sample and resistance of the sample is changing similarly to piezoresistive effect. Amplitude of the standing wave is defined:

$$y = 2y_0 \cos(\omega t) \sin(kx) \tag{3.22}$$

when y_0 is the amplitude of the wave, ω is angular frequency, k is wave number, x and t is variables for longitudinal position and time respectively.
At locations $x = 0, \lambda/2, \lambda, 3\lambda/2\ldots$called the nodes, amplitude is always zero whereas at locations $x = \lambda/4, 3\lambda/4, 5\lambda/4\ldots$called the anti-nodes, amplitude is maximum.

Objects which are deformed by the force F in the range of elastic deformations can be described by Hooke's law. Region of elastic deformations is shown in Fig. 3.6.

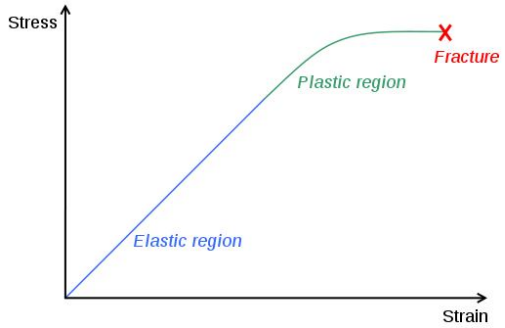

Fig. 3.6: Definition of Strain and Stress

For example a rod of any elastic material can by represented as a linear spring. The rod has length L and cross-sectional area A. Its extension (strain) ε is linearly proportional to its tensile stress σ, by a constant factor:

$$\sigma = E\varepsilon \tag{3.23}$$

or

$$\Delta L = \frac{F}{EA} L = \frac{\sigma}{E} L \tag{3.24}$$

where the E is a Young's modulus
In the case of three-dimensional stress state, the generalized form of Hooke's law is written as:

$$\sigma_{ij} = c_{ijkl}\varepsilon_{kl} \tag{3.25}$$

where the c is called the stiffness tensor or the elastic tensor
In matrix form, Hooke's law for isotropic material can be written as

$$\begin{bmatrix} \varepsilon_{11} \\ \varepsilon_{22} \\ \varepsilon_{33} \\ 2\varepsilon_{23} \\ 2\varepsilon_{31} \\ 2\varepsilon_{12} \end{bmatrix} = \begin{bmatrix} \varepsilon_{11} \\ \varepsilon_{22} \\ \varepsilon_{33} \\ \gamma_{23} \\ \gamma_{31} \\ \gamma_{12} \end{bmatrix} = \frac{1}{E} \begin{bmatrix} 1 & -\nu & -\nu & 0 & 0 & 0 \\ -\nu & 1 & -\nu & 0 & 0 & 0 \\ -\nu & -\nu & 1 & 0 & 0 & 0 \\ 0 & 0 & 0 & 2(1+\nu) & 0 & 0 \\ 0 & 0 & 0 & 0 & 2(1+\nu) & 0 \\ 0 & 0 & 0 & 0 & 0 & 2(1+\nu) \end{bmatrix} \begin{bmatrix} \sigma_{11} \\ \sigma_{22} \\ \sigma_{33} \\ \sigma_{23} \\ \sigma_{31} \\ \sigma_{12} \end{bmatrix} \tag{3.26}$$

where $\gamma_{ij} = 2\varepsilon_{ij}$ is the engineering shear strain

The inverse relation may be written as

$$\begin{bmatrix}\sigma_{11}\\ \sigma_{22}\\ \sigma_{33}\\ \sigma_{23}\\ \sigma_{31}\\ \sigma_{12}\end{bmatrix} = \frac{E}{(1+\nu)(1-2\nu)}\begin{bmatrix}1-\nu & \nu & \nu & 0 & 0 & 0\\ \nu & 1-\nu & \nu & 0 & 0 & 0\\ \nu & \nu & 1-\nu & 0 & 0 & 0\\ 0 & 0 & 0 & (1-2\nu)/2 & 0 & 0\\ 0 & 0 & 0 & 0 & (1-2\nu)/2 & 0\\ 0 & 0 & 0 & 0 & 0 & (1-2\nu)/2\end{bmatrix}\begin{bmatrix}\varepsilon_{11}\\ \varepsilon_{22}\\ \varepsilon_{33}\\ 2\varepsilon_{23}\\ 2\varepsilon_{31}\\ 2\varepsilon_{12}\end{bmatrix} \tag{3.27}$$

For anisotropic material the Hooke's law in matrix notation is

$$[\sigma] = \begin{bmatrix}\sigma_{11}\\ \sigma_{22}\\ \sigma_{33}\\ \sigma_{23}\\ \sigma_{31}\\ \sigma_{12}\end{bmatrix} \equiv \begin{bmatrix}\sigma_1\\ \sigma_2\\ \sigma_3\\ \sigma_4\\ \sigma_5\\ \sigma_6\end{bmatrix} \tag{3.28}$$

The strain is defined as

$$[\varepsilon] = \begin{bmatrix}\varepsilon_{11}\\ \varepsilon_{22}\\ \varepsilon_{33}\\ 2\varepsilon_{23}\\ 2\varepsilon_{31}\\ 2\varepsilon_{12}\end{bmatrix} \equiv \begin{bmatrix}\varepsilon_1\\ \varepsilon_2\\ \varepsilon_3\\ \varepsilon_4\\ \varepsilon_5\\ \varepsilon_6\end{bmatrix} \tag{3.29}$$

Then the stiffness tensor c can be expressed as

$$[C] = \begin{bmatrix}c_{1111} & c_{1122} & c_{1133} & c_{1123} & c_{1131} & c_{1112}\\ c_{2211} & c_{2222} & c_{2233} & c_{2223} & c_{2231} & c_{2212}\\ c_{3311} & c_{3322} & c_{3333} & c_{3323} & c_{3331} & c_{3312}\\ c_{2311} & c_{2322} & c_{2333} & c_{2323} & c_{2331} & c_{2312}\\ c_{3111} & c_{3122} & c_{3133} & c_{3123} & c_{3131} & c_{3112}\\ c_{1211} & c_{1222} & c_{1233} & c_{1223} & c_{1231} & c_{1212}\end{bmatrix} \equiv \begin{bmatrix}C_{11} & C_{12} & C_{13} & C_{14} & C_{15} & C_{16}\\ C_{12} & C_{22} & C_{23} & C_{24} & C_{25} & C_{26}\\ C_{13} & C_{23} & C_{33} & C_{34} & C_{35} & C_{36}\\ C_{14} & C_{24} & C_{34} & C_{44} & C_{45} & C_{46}\\ C_{15} & C_{25} & C_{35} & C_{45} & C_{55} & C_{56}\\ C_{16} & C_{26} & C_{36} & C_{46} & C_{56} & C_{66}\end{bmatrix} \tag{3.30}$$

and Hooke's law is written as

$$[\sigma] = [C][\varepsilon] \text{ or } \sigma_i = C_{ij}\varepsilon_j \tag{3.31}$$

3.3. Model of the metallic sample

I modeled a sample of the aluminum (shape of prism length L = 0.1m, width W = 0.005m and thickness t = 0.002m) in program COMSOL. Inside the sample I created 9 bubbles, which have represents defects. Radius of the bubbles was changed from $r = 0.5\text{x}10^{-3}$m to $0.8\text{x}10^{-3}$m with step $0.1\text{x}10^{-3}$m. The model of the sample is shown in Fig. 3.7.

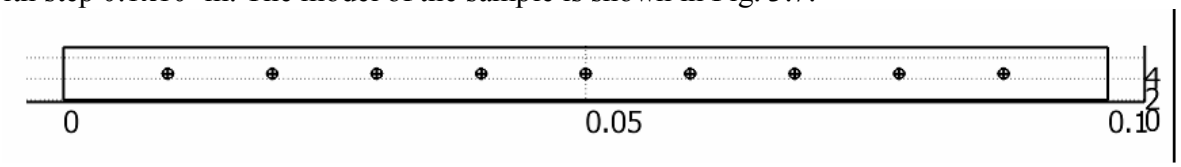

Fig. 3.7: Model of the aluminum sample in COMSOL

COMSOL founded the resonant frequencies of the sample in the range 20 kHz to 45 kHz. The material properties are defined in the stress-charge form, in which the user has to specify the elasticity matrix, the coupling matrix, the relative permittivity matrix, and the density. These matrices are defined as follow:

Elastic matrix [C_E]

$$C = \begin{bmatrix} 1.27e11 & 8.02e10 & 8.46e10 & 0 & 0 & 0 \\ 8.02e10 & 1.27e11 & 8.46e10 & 0 & 0 & 0 \\ 8.46e10 & 8.46e10 & 1.17e11 & 0 & 0 & 0 \\ 0 & 0 & 0 & 2.29e10 & 0 & 0 \\ 0 & 0 & 0 & 0 & 2.29e10 & 0 \\ 0 & 0 & 0 & 0 & 0 & 2.34e10 \end{bmatrix} \text{Pa} \tag{3.32}$$

Coupling matrix [e]:

$$e = \begin{bmatrix} 0 & 0 & 0 & 0 & 17.0345 & 0 \\ 0 & 0 & 0 & 17.0345 & 0 & 0 \\ -6.62281 & -6.62281 & 23.2403 & 0 & 0 & 0 \end{bmatrix} \text{C}/\text{m}^2 \tag{3.33}$$

Relative permittivity matrix [ε_{rS}]:

$$\varepsilon_{rS} = \begin{bmatrix} 1704.40 & 0 & 0 \\ 0 & 1704.40 & 0 \\ 0 & 0 & 1433.61 \end{bmatrix} \text{kg}/\text{m}^3 \tag{3.34}$$

Density:

$$\rho = 8040\,\text{kg}/\text{m}^3 \tag{3.35}$$

The resonant frequencies computed by COMSOL are shown in Tab. 1.

No.	Frequency (Hz)	Type of basic wave on the sample
1.	21396	transversal wave
2.	24525	torsion wave
3.	25984	transversal wave
4.	30814	transversal wave
5.	33251	transversal wave
6.	34488	torsion wave
7.	38559	longitudinal wave
8.	41293	transversal wave
9.	41371	transversal wave
10.	44530	torsion wave

Tab. 1: Resonant frequencies of the aluminum sample

The left side of the sample was fixed and second side of the sample was free. Total displacement on the sample for longitudinal wave is shown in Fig. 3.8. Blue color is signifying for minimal displacement, it is amplitude of oscillations is zero.

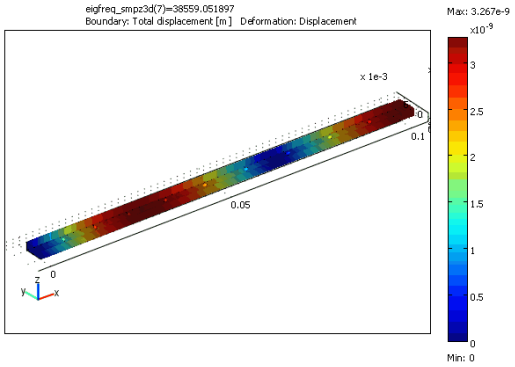

Fig. 3.8: Longitudinal waves, frequency $f = 38559$ Hz

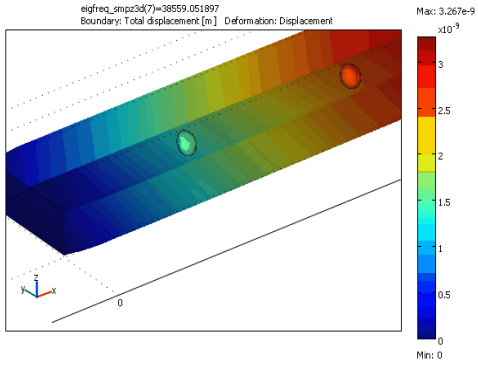

Fig. 3.9: Longitudinal waves – detail on the first and second bubbles

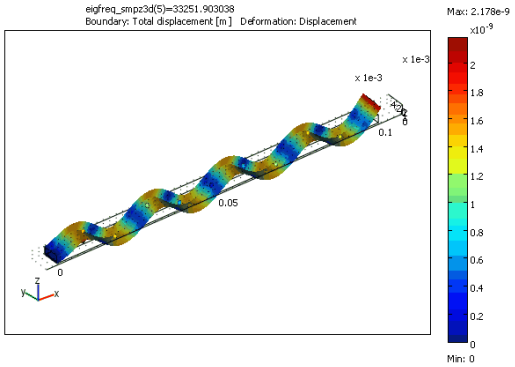

Fig. 3.10: Transversal waves, frequency $f = 33251$ Hz

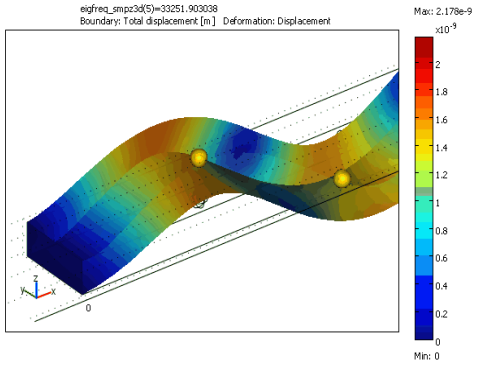

Fig. 3.11: Transversal waves – detail on the first and second bubbles

On the other hand the red color is signifying for maximal displacement and amplitude of oscillations on the sample is maximal. Detail of the geometry changes the first and second bubbles (defects) is shown in Fig. 3.9. Transversal wave on the sample has negligible influence on the geometry change of the bubbles inside the sample (Fig. 3.10 and Fig. 3.11 for detail view). The biggest influence on the bubbles geometry change was observed for torsion wave on the sample (see Fig. 3.12. and 3.13.)

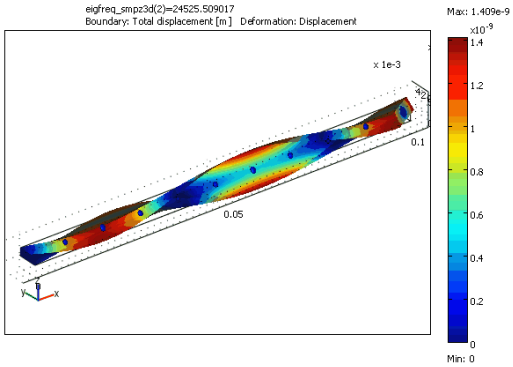

Fig. 3.12: Torsion waves, frequency $f = 24525$ Hz

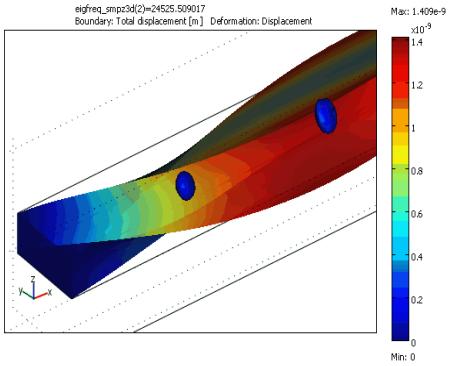

Fig. 3.13: Torsion waves – detail on the first and second bubbles

It is clear that geometry change inside the sample is dependent on the type of wave (longitudinal, transversal or torsion wave), frequency of oscillations and position where is defect situated inside the sample. Orientation of cracks considering to waving spreading is important also. I have evaluated the geometry change each bubble inside the sample for longitudinal wave, how is shown in Fig. 3.14.

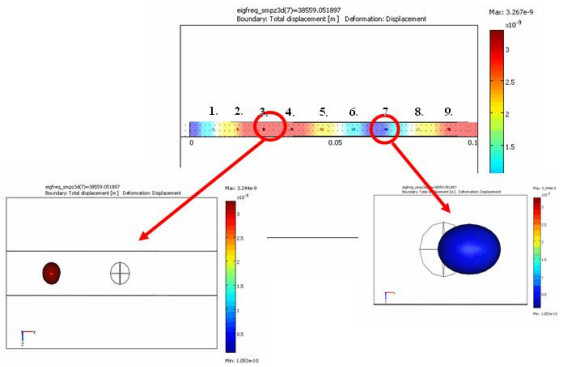

Fig. 3.14: Model of the aluminum sample in COMSOL with longitudinal oscillations

Geometry change of bubbles due to longitudinal oscillations on the sample dependent on the position and phase is shown in Fig. 3.15. - Fig.3.23. It is obviously that the biggest inside structure change is near the place of minimal displacement and minimal geometry change is observed for bubbles situated in the place maximal displacement.

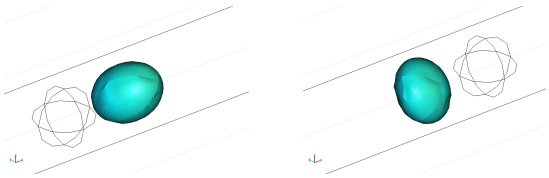

Fig. 3.15: Bubble on 1. position Phase 0° and 180°

Fig. 3.16: Bubble on 2. position Phase 0° and 180°

Fig. 3.17: Bubble on 3. position Phase 0° and 180°

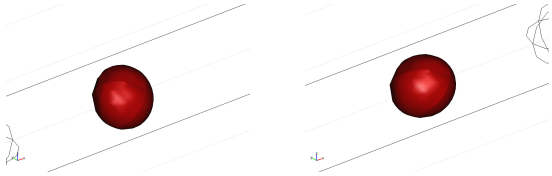

Fig. 3.18: Bubble on 4. position Phase 0° and 180°

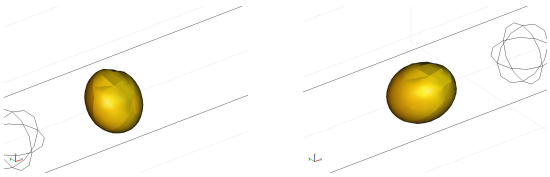

Fig. 3.19: Bubble on 5. position Phase 0° and 180°

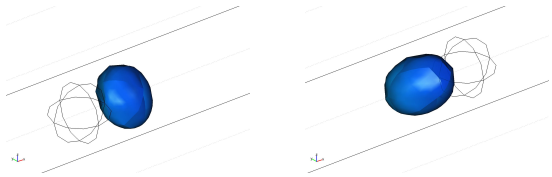

Fig. 3.20: Bubble on 6. position Phase 0° and 180°

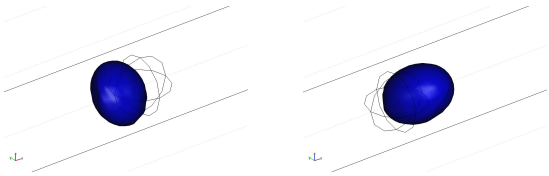

Fig. 3.21: Bubble on 7. position Phase 0° and 180°

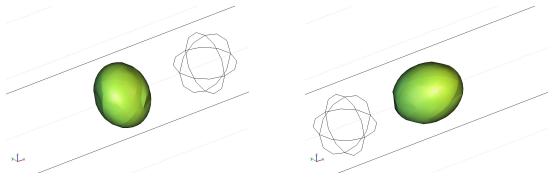

Fig. 3.22: Bubble on 8. position Phase 0° and 180°

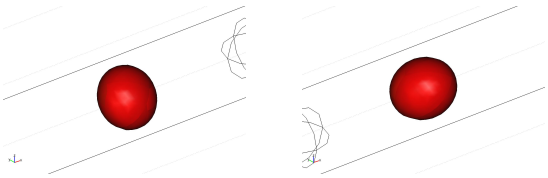

Fig. 3.23: Bubble on 9. position Phase 0° and 180°

The first and seventh bubbles are maximal deformed. These bubbles are situated in the place with minimal displacements. On the other hand the bubbles situated in place with maximal displacements there is minimal influence on the geometry change of the bubble.

Results from these figures can be the map of geometry change factor (in this case in x-direction), which is shown in Fig. 3.24. The map describes how much is changing internal structure in material for a given frequency of mechanical oscillations on the sample. In other words, how much will be the crack geometry changed inside the material and it is dependent on the position of crack in the sample. It is due to the standing waves excited on the sample.

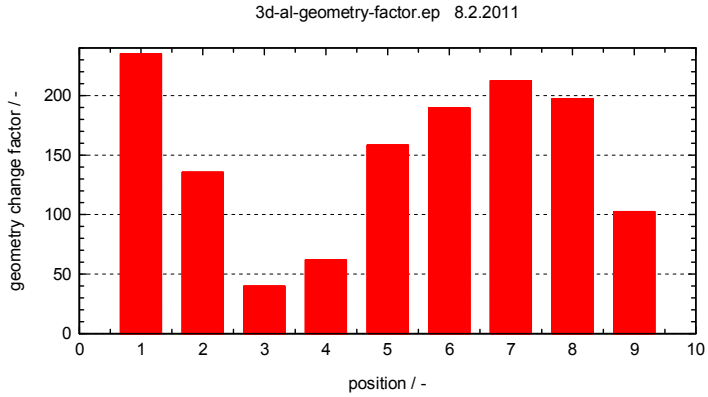

Fig. 3.24: The map of the geometry change factor x-direction

The ultrasonic signal changes the geometry the sample and cracks inside the sample structure, then must be changing the current density near the place of cracks and defects. The current density is constant for sample without cracks. If the sample contains some defects or cracks the current density is uneven distribution in area of cracks. The distribution of the current density on the alumina sample, which has a hole in the middle of the sample, is shown in Fig. 3.25. Electric current flowing throw the sample was $I = 1$A.

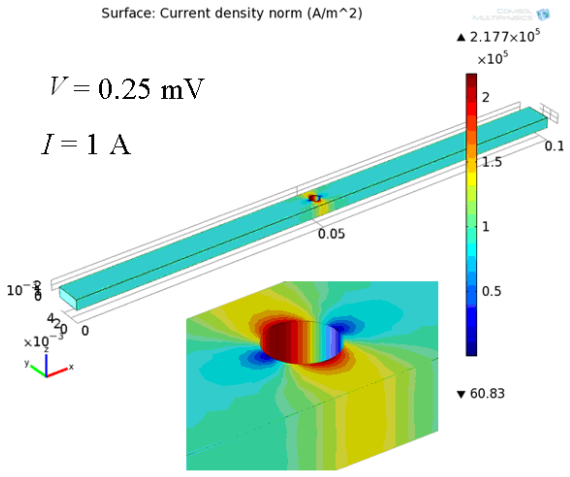

Fig. 3.25: Current density distribution on the Model of the aluminum sample in COMSOL

Electric current is defined follows

$$\vec{I} = \int_A \vec{J} \mathrm{d}\vec{A} \tag{3.36}$$

where $\vec{J}$ is the vector of current density and A is cross-section area
Ohm's law is defined in differential form follows

$$\vec{J} = \sigma \cdot \vec{E} \tag{3.37}$$

where σ is conductivity and $\vec{E}$ is vector of electric field

The resistance change due to deformation near the crack is possible replace by serial and parallel combination of resistors. For example aluminum sample with simple crack of prism shape, how is shown in Fig. 3.26. Crack is situated on center of the sample. The current density distribution has two levels approximately. Electric current flowing through the sample is $I = 1\text{A}$. Current density is about $J = 1.10^5$ A/m^2 for the parts except crack. For the area of crack is current density about $J = 1.5.10^5$ A/m^2 for each side. The value of resistor R_1 is given by the length and cross-section area of the sample between left side and crack. If the crack is situated on the center of the sample, so part behind the crack and right side is the same value R_1. Resistance R_2 is given by the geometry also and it is for each arm of the sample in area of crack. The total resistance of the sample will be given by serial combination of resistors R_1 and parallel combination of resistors R_2 (see Fig. 3.26).

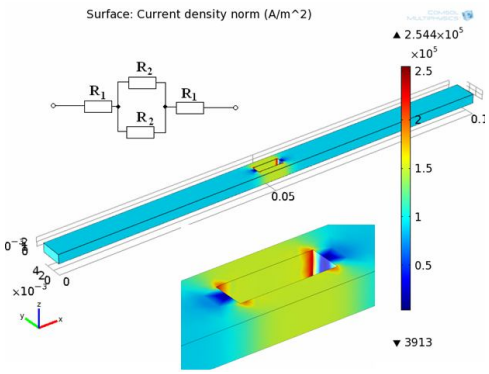

Fig. 3.26: Current density distribution on the Model of the aluminum sample with crack of prism shape in COMSOL

Then ultrasonic signal changes the geometry of the sample, changes the geometry of the cracks and then the resistance of the sample are changing also. Next question is about the tunnel effect and ballistic effect, near the area of crack. Ultrasonic signal, which is generated by the ultrasonic transmitter, changes the geometry of the cracks in the sample structure. This is illustrated in Fig. 3.27, where crack opens up and closes up during ultrasonic excitations. For assume that the hatched area represents a distance that electron can overcome by tunneling effect or ballistic effect. The geometry of the cracks is changing with frequency which corresponds with frequency of the ultrasonic excitation f_U. The resulting resistance change depends on the size of crack, shape of crack, number of cracks and orientation of cracks against direction of the ultrasonic wave.

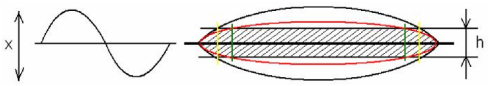

Fig. 3.27: Change of the cracks geometry due to ultrasonic excitation

3.4. Model of the thick film resistors

Thick film resistor is based on the substrate and thick film resistive past, how is shown in Fig. 3.28. In this case the gauge factor is dependent on the poisons ration of the substrate and poisons ratio of the thick film. The value of gauge factor is dependent on the direction of applied

strain. Gauge factor, when a strain ε is applied across the length of the resistor, parallel to the current flow, is given by:

$$GF_L = GF\left[1-\nu_S-\nu_F\left(\frac{1-\nu_S}{1-\nu_F}\right)\right]+1+\nu_S+\nu_F\left(\frac{1-\nu_S}{1-\nu_F}\right) \tag{3.38}$$

and

$$GF = \frac{GF_L - 1-\nu_S-\nu_F\left[(1-\nu_S)/(1-\nu_F)\right]}{1-\nu_S-\nu_F\left[(1-\nu_S)/(1-\nu_F)\right]} \tag{3.39}$$

where GF_L is the gauge factor quoted in papers and datasheets, ν_S is poison ration of the substrate and ν_F is poison ration of the film.

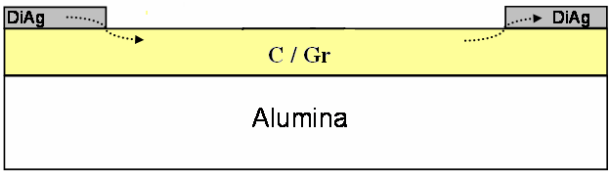

Fig. 3.28: Thick film resistor structure

For transverse gauge factor GF_T, when the strain is applied normal to the length of resistor, then:

$$GF_T = GF\left[1-\nu_S-\nu_F\left(\frac{1-\nu_S}{1-\nu_F}\right)\right]-\nu_S+\nu_F\left(\frac{1-\nu_S}{1-\nu_F}\right)-1 \tag{3.40}$$

or

$$GF_T = GF_L - 2(1+\nu_S) \tag{3.41}$$

Gauge factor for polymer thick film resistor is more described in [18]

3.5. Model of semiconductors

The piezoresistive effect in the semiconductors was discovered by Smith in 1954. The resistances of semiconductors, commonly silicon, are very sensitive to strain. The gauge factor of the silicon is between -50 ÷ 200 and it is dependent on the type (P-type or N-type) of silicon. The piezoresistive effect on semiconductors is described by equation 20. Semiconductors are very sensitive on the temperature change also. Piezoresistive effect on semiconductors is known as piezo-junction effect. If semiconductor is stressed, it is dimensional change, where is changed number of carriers and their average mobility. Unlike metals, when the resistivity change under stress dominates over the dimensional change [13]. The piezoresistive effect depends on the carrier concentration and crystallographic orientation with respect to the applied stress.

$$\frac{\Delta\rho}{\rho_0} = \pi_L\sigma \tag{3.42}$$

Where π_L is the longitudinal piezoresistive coefficient and ρ_0 is the resistivity for unstressed material. The resulting gauge factor is given by equation 3.19 [19, 20].

3.6. Other effects influence the deformations

If in the simple case the conductive grains are in form of the ball then the ultrasonic signal changes the geometry of these grains on the oblate spheroid, this is shown in Fig. 3.14 and Fig. 3.15.

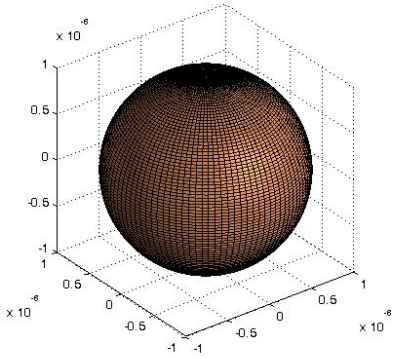

Fig. 3.29: The conductive grain of the ball shape without actuation of ultrasonic signal

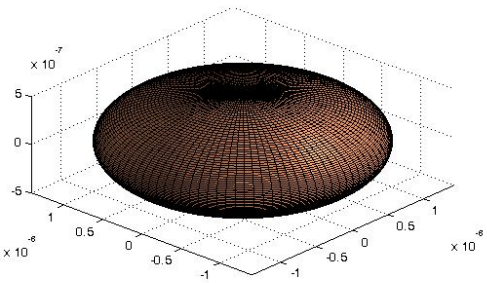

Fig. 3.30: The geometry change of the conductive grain into oblate spheroid by the ultrasonic signal

Electron can tunnel on the depth of 10^{-9} m from each conductive grain into the next one. If the size of the conductive grains is known, it is possible to found the effective area responsible for transport electrons. The effective area d is changing during the actuating of the ultrasonic signal on conductive grain, this is illustrated in Fig. 3.16 and Fig. 3.17.

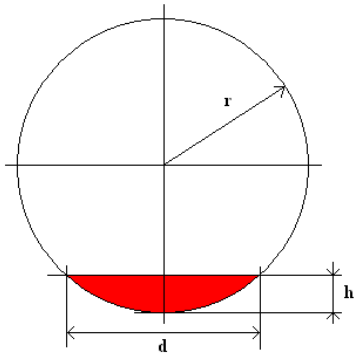

Fig. 3.31: Effective area responsible for transport electrons on the conductive grain without actuating of the ultrasonic signal

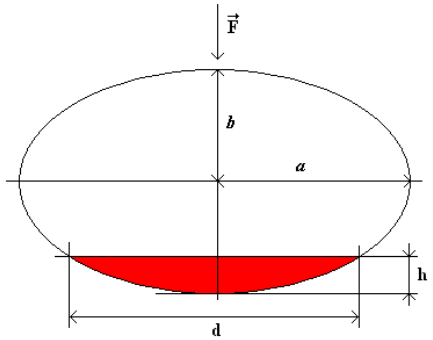

Fig. 3.32: Effective area responsible for transport electrons on the conductive grain with actuating of the ultrasonic signal

For example, if the diameter of the conductive grain is $r = 10^{-6}$m then the size of effective area d for the oblate spheroid is:

$$d = \pi \cdot \left(a^2 \cdot \left(1 - \left(\frac{b-h}{b} \right)^2 \right) \right) \tag{10}$$

where diameter b is given by:

$$b = r - \frac{h}{2} \tag{11}$$

and diameter a is given by:

$$a = \sqrt{\frac{r^3}{\left(r - \frac{h}{2}\right)}} \tag{12}$$

The dependence of the effective area d on the level of the ball compression is shown in Fig. 3.18. It is strongly non-linear dependence.

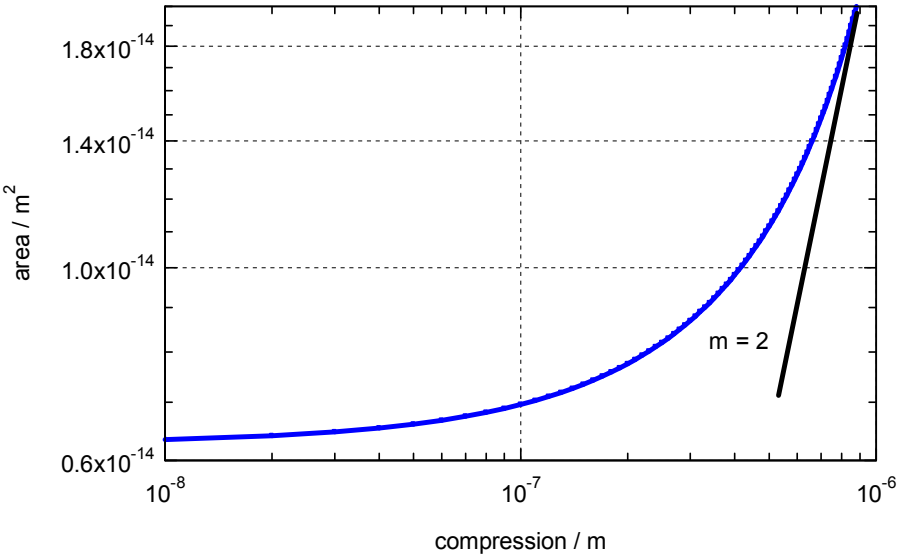

Fig. 3.33: Effective area of the conductive grain vs. compression

4. Measurement setup

The measurement of the small resistance change can be realized of several techniques. If the ultrasonic signal evokes very small geometry change then the resistance change will be slight also. The resistance change due to ultrasonic signal depends on many factors and it is order of 10^{-7} % of original resistance. Simple and common technique for measurement resistance is current injection shown in Fig. 4.1. It is measurement of resistance accurate to about 0.1% at best. The resulting voltage is given by the Ohm's Law. In this case is needed a source of constant current I_{AC}.

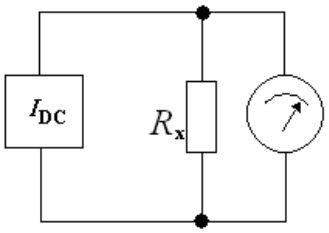

Fig. 4.1: Current injection circuit

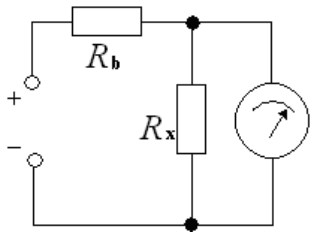

Fig. 4.2: Ballast circuit

Ballast circuit is similar to the current injection but avoids the need constant current source. The ballast resistor R_b which is connected in series with measured resistor R_x creates the constant current source. Maximal sensitivity occurs when resistor $R_b = R_x$. Circuit connected with ballast resistor R_b is shown in Fig. 4.2. Voltage measured on resistor R_x is given by:

$$V_x = \frac{R_x}{R_x + R_b} V_{IN}, \tag{4.1}$$

where V_{IN} is voltage connected to the circuit and V_x is measured voltage on the resistor R_x

Most sensitive method for measuring resistance, capacitance or inductance is connected to the Wheatstone bridge. The basic circuit of Wheatstone bridge is shown in Fig. 4.3. Voltage measured between two arms of Wheatstone bridge is given:

$$V_x = \left[\frac{R_d}{R_c + R_d} - \frac{R_b}{R_a + R_b} \right] V_{IN}, \tag{4.1}$$

The voltage V_x is zero, when the circuit is balanced and it is provided for values of resistors R_d $R_a = R_c$ R_b.

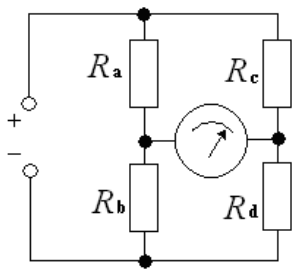

Fig. 4.3: Resistors connected to the Wheatstone bridge

4.1. Measurement setup for Electro-ultrasonic spectroscopy

The block scheme of the electro-ultrasonic measurement setup is shown in Fig. 4.4. It consists of two parts, the electric and the ultrasonic ones.

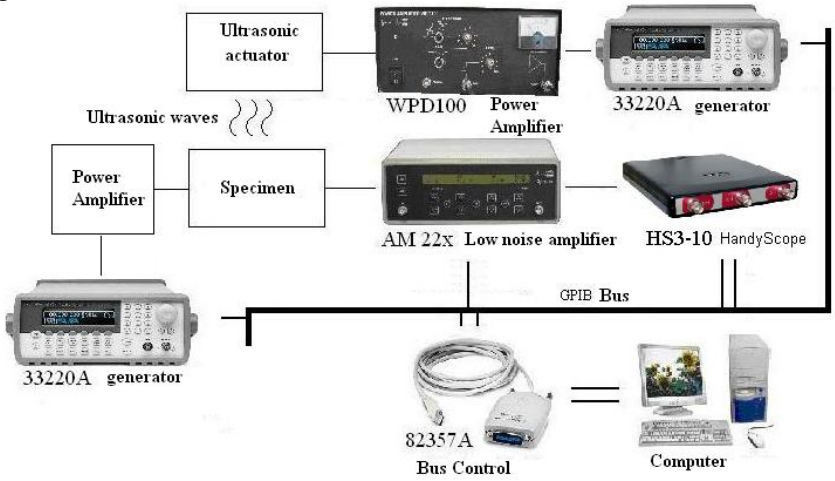

Fig. 4.4: Electro-ultrasonic measurement setup with AC electric signal.

The ultrasonic part contains a signal generator (Agilent), a power amplifier and piezoelectric transmitter. Generator Agilent 33220A can be used in frequency range 1 μHz – 20 MHz for sine and rectangle functions. Maximum length of the programmed signal is 64.000 points and vertical resolution is 64 bits. The power amplifier is consists of WPD 100 in which it is necessary to have power linear actuating harmonic signal on ultrasonic transducer. The measured sample was fixed on the piezoceramic transmitter which is used for ultrasonic signal generation.

Electric part is consists of generator (Agilent), power amplifier, specimen, special filters, A/D converter and computer when the measured signal is stored. Signal from the generator is transformed on higher voltage by power amplifier. This signal is led to the measured sample over the protective resistor. Harmonic signals with frequency higher than the differential frequency component actuating signals are trimmed by the low pass passive filter. The passive filter has cut off frequency 4200 Hz with inhibition 50 dB / decade. The amplifier (AM 22) offers adjustable input gain in the range from -20 to 50 dB by 10 dB step, the frequency band filter with low frequency 30 mHz, 300 mHz, 0.3 Hz, 3 Hz, 30 Hz, 300 Hz, 3 kHz, 30 kHz and 300 kHz, the high frequency filter adjustable in range 3 Hz, 30 Hz, 300 Hz, 3 kHz, 30 kHz and 300 kHz, adjustable output gain in range from 0 to 50 dB by 10 dB. All parameters can be set over GPIB or on the front panel of the amplifier. The amplified signal is led to the A/D converter. As the A/D converter is used digital oscilloscope Agilent 54624A with sampling rate 200 Msa / s or Handyscope HS03. The digitized signal is stored in the computer and noise spectral density frequency dependence evaluated using discrete FFT. The control software was written in Borland C++ Builder and this version is based on Windows operating system. Amplifier AM22 and exciter HTP05 were produced by 3S Sedlak Company. Power amplifier WPD100 was made with help of Prof. K. Hajek. Both generators Agilent are programmable over GPIB interface.

4.2. Proposed Method Sensitivity

To reach high resolution of the proposed method the AC generator with low background noise and signal-to-noise ratio (SNR) higher than 100 dB in the pass-band near the frequency f_i is required. The noise background of this signal increases after the amplification with increasing the amplifier frequency band width and then it is necessary to optimize the frequency band of the amplifier with respect to the signal-to-noise ratio [21].

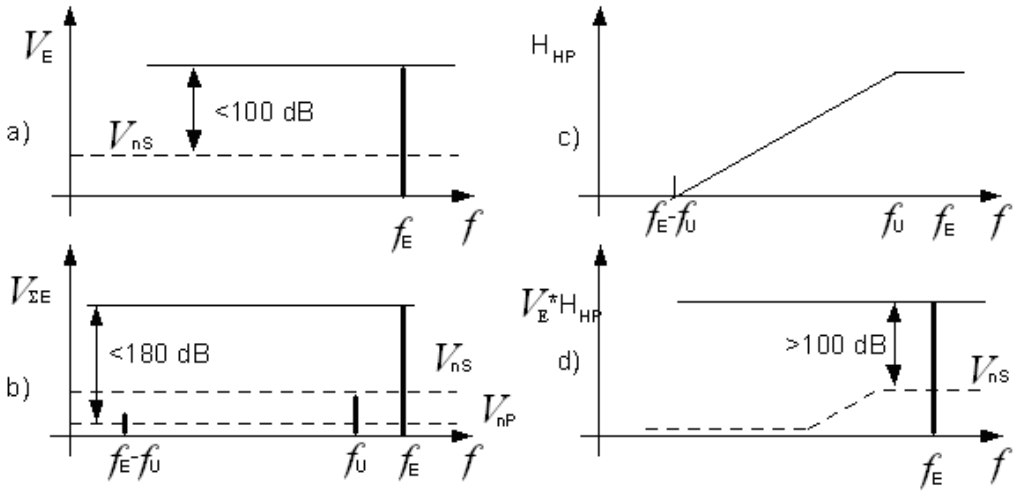

Fig. 4.5: Signals and noise of the AC generator in the frequency domain a) the electrical exciting signal and noise signal (standard generator SNR is about 100 dB), b) SNR in DUT, c) frequency response of AC source HP filter, d) signal and noise after filtration

To increase the AC generator SNR up to 180 dB the measurement set up contains a high-pass filter (HP filter) which transmits exciting signal of frequency f_E, and attenuates the noise in the low frequency band where useful signal of the frequency f_i is measured. Fig. 4.5 c) shows the frequency response of this HP filter. Fig. 4.5 a) represents an exciting signal generated by AC generator before the filtration process while Fig. 4.5 d) represents this signal after the filtration. Since the HP filter is connected to the power amplifier it has to be designed for high voltage and high current load.

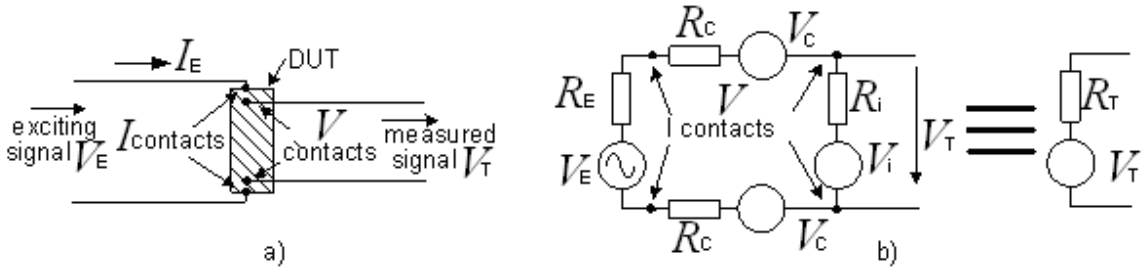

Fig. 4.6: Four-probes method: a) circuitry, b) equivalent DUT electrical diagram: V_E and R_E - exciting generator parameters, V_C and R_C - noise and parasitic modulation of current contacts, V_i and R_i –source of inter-modulated signal on crack , V_T – measured signal.

It is necessary to consider that the current contacts on DUT can create parasitic modulated signal similarly as cracks. I have used four-point connection with current and voltage contacts, where the main current flow through the current contacts as is shown in Fig. 4.6. On the voltage

contacts the signal on intermodulation frequency corresponds to the change of the DUT resistance without contact parasitic modulation effect. This is shown in Fig. 4.6 b). I consider that both R_i and $R_C << R_E$. Therefore the transfer of parasitic voltage V_C to the voltage V_T is much more than 1, because it is divided by resistance divider $R_i/(R_i+2R_C+R_E)$.

This effect can be minimized by soldering or by the other mechanical connections. It is evident that changes of the electrical resistance caused by ultrasonic excitation are very small. Therefore it is necessary to survey the basic sensitivity of proposed method. The limiting factors are the noise of load resistance, preamplifier noise and noise due to the temperature fluctuation caused by the high current density in DUT.

I estimate the maximum sensitivity of my proposed EUS method. Thevenin's model of the measured signal source V_T has an internal resistance R_T (see Fig. 4.6 b)), which can expressed as the parallel combination of resistance R_i and load resistance (R_E+2R_C). Because the $R_i << R_E$, the R_T has very low resistance similar as R_i. I can consider the internal resistance R_T value in the range 0.01 – 1 Ω. For the resistance R = 1 Ω and temperature T = 300 K the thermal noise spectral density S_{ne} is given by:

$$S_{ne} = 4kTR = 1.6x10^{-20}\ \mathrm{V^2/Hz}, \tag{4.1}$$

where k is Boltzmann constant. Then the noise voltage V_n is given by:

$$V_n = \sqrt{S_{ne} \cdot B}\ , \tag{4.2}$$

where B is the effective noise pass-band. Considering the pass-band B = 100 Hz the effective noise voltage of the load resistance is equal to V_n = 1.2 nV. This value is lower than the background noise of the preamplifier. In this case the noise voltage of the preamplifier determines a basic sensitivity of the proposed method. It is evident that resultant noise can be essentially limited by reducing of B value as well as preamplifier noise voltage. For a low noise preamplifier with V_{ne}= 1 nV/√Hz and the pass-band B = 100 Hz, obtain the equivalent noise voltage V_n = 10 nV. Considering the voltage V_T = 0.1 V the detectable relative value of the resistance change can be expressed as

$$\Delta R / R_{DUT} = V_n / V_T = 1x10^{-8} / 0.1 = 1x10^{-7} \tag{4.3}$$

Source resistance R_T is of the order 0.1 Ω and preamplifier noise resistances is 1000 to 10000 times greater. Using transformer can increase the sensitivity 30 to 100 times. On the basis of these conclusions estimate the maximum sensitivity of proposed electro-ultrasonic spectroscopy method on 120 to 160 dB approximately.

The proposed method is based on the mixing principle, where the resultant voltage V_T contains spectral components

$$f_i = \left| \pm nf_E \pm mf_U \right|_{n,m=0,1,2....}\ . \tag{4.4}$$

I will consider the linear parametric mixing system then frequency f_i is given by the superposition or subtraction of exciting frequencies f_E and f_U. It holds

$$f_i = f_E - f_U \ \ or\ \ f_I = f_E + f_U \tag{4.5}$$

There are two methods for the signal detection in:

(i) The low frequency band for $f_i = f_E - f_U$

(ii) The high frequency band for $f_I = f_E + f_U$.

The main advantage of this method is based on the fact that the electrical signal f_i has the frequency different from the frequencies of both exciting signals. This fact allows us to reach high signal to noise ratio and to design NDT method with high resolution and high sensitivity to defects in the DUT.

The electrical excitation signal (on frequency f_E) has high amplitude in comparison with the intermodulation signal which needs the amplifier with high dynamic range. To solve this problem with the high dynamic range for the signal processing, the LP filter with cut-off frequency slightly higher than f_i with sufficient rejection level is used. Then obtain frequency spectrum in low dynamic range, which can be amplified by the low noise preamplifier and measured by selective nano-voltmeter, filtered by BP filter or by FFT analyses.

4.3. Ultrasonic Actuators

I used two ultrasonic actuators. One had cylindrical body with radius 20 mm and the second one with radius 80 mm. Ultrasonic actuators, you can see in Fig. 4.7 (with radius body 20 mm) and Fig. 4.8 (with radius body 80 mm). Each of these actuators has different resonant frequency, how is described in next pages. The ultrasonic actuator with radius body 80 mm (Fig. 4.8) is used for bulkier specimens. The measurement was generally performed on the ultrasonic actuator HTP05.

Fig. 4.7: Ultrasonic actuator with cylindrical body which has radius 20 mm denoted HTP 05

Fig. 4.8: Ultrasonic actuator with cylindrical body which has radius 80 mm denoted HTP02

Actuators consist of two rings of PZT ceramics, copper contacts and metal body. The model of ultrasonic actuator HTP05 is shown in Fig. 4.9. PZT ceramics used for the actuators is described in [22]. Advantages of these actuators are free operation maintenance and easy usage. On the other hand, disadvantage is the fact, that mechanical vibrations of the PZT ceramics are strongly dependent on the temperature and excited frequency from the generator.

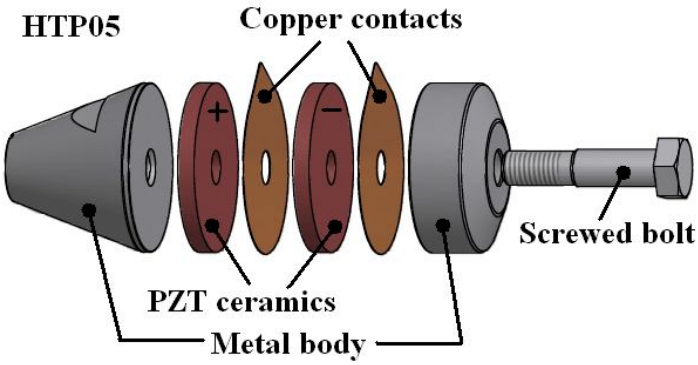

Fig. 4.9: Model of the ultrasonic actuator HTP 05

Serial resistance R_S, capacity C_S, Impedance Z of actuator HTP05 were measured on RLC bridge. Ultrasonic actuator impedance is shown in Fig. 4.10. Impedance is decreasing with frequency. The area of resonances is at frequency range from 30 kHz to 150 kHz. The same area of resonances is shown in Fig. 4.11 and Fig. 4.12, there is serial resistance R_S for HTP05 (Fig. 4.11) and serial capacity C_S for HTP05 (Fig. 4.12). More details of the ultrasonic actuators are written in [23 to 25].

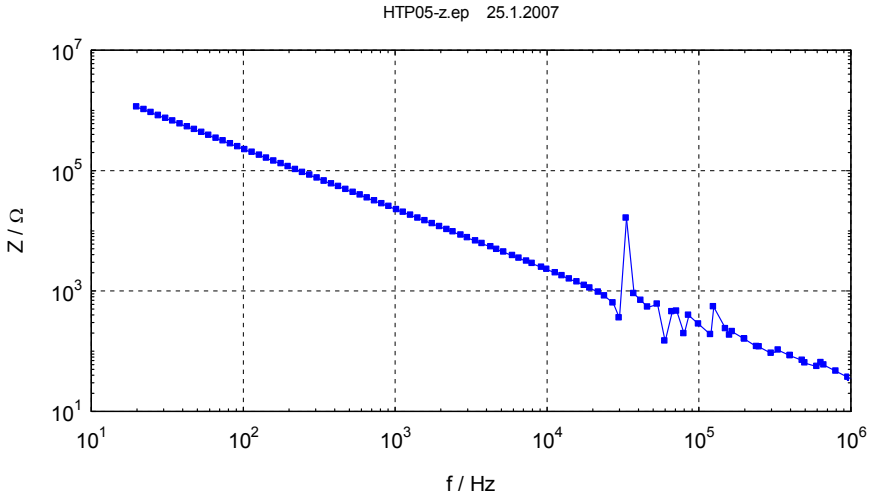

Fig. 4.10: Impedance of the ultrasonic actuator HTP05

Next characteristics were measured on the Faculty of Electrical Engineering and Communication department of Control and Instrumentation. The displacement of mechanical oscillation of these ultrasonic actuators depending on frequency and voltage from electric AC generator connected to the actuators was measured by optical method.

These ultrasonic actuators have different resonant frequencies. Ultrasonic actuators were connected to the AC generator Agilent. Displacement of mechanical oscillation of ultrasonic actuator HTP05 at the frequency of AC generator f_U with constant amplitude $V_U = 5$V is shown in Fig. 4.13.

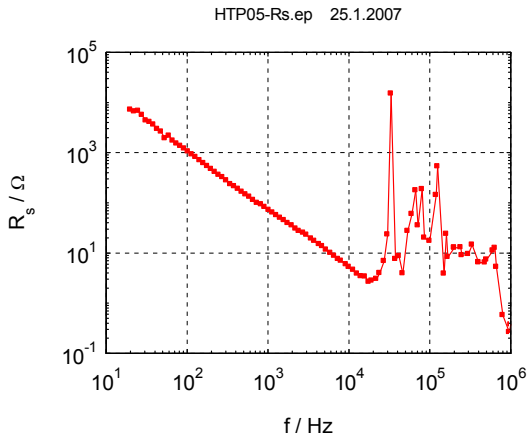

Fig. 4.11: Serial resistance R_S of the ultrasonic actuator HTP05

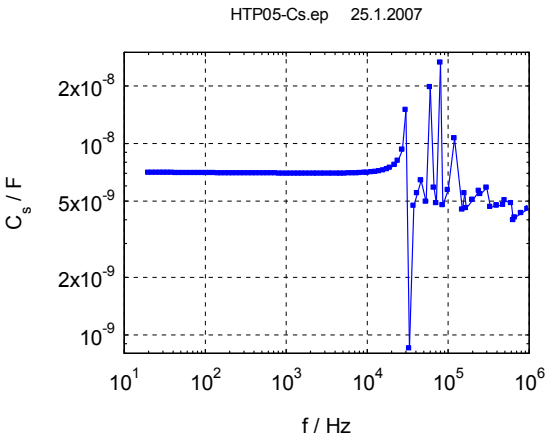

Fig. 4.12: Serial capacity C_S of the ultrasonic actuator HTP05

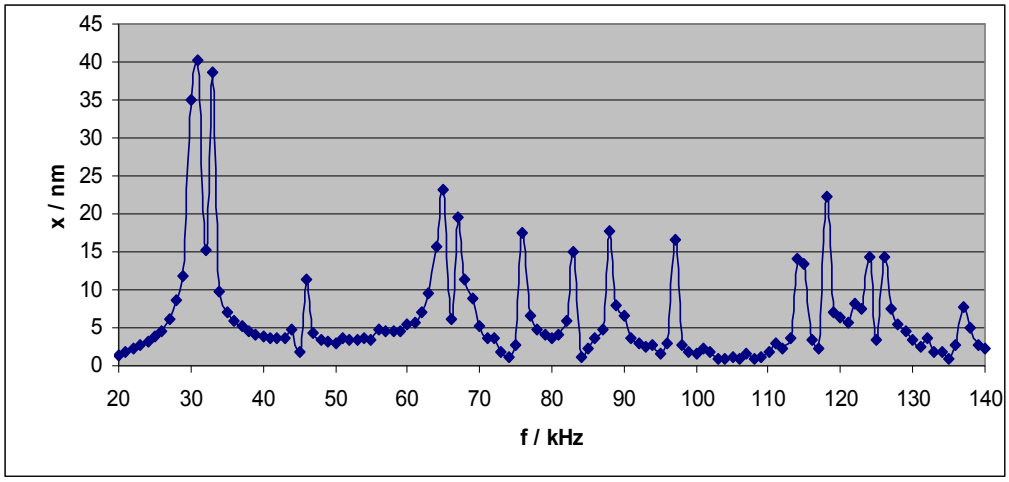

Fig. 4.13: Displacement of mechanical oscillation for ultrasonic actuator HTP05 on the frequency of AC generator f_U with constant amplitude V_U = 5V

There are many resonant frequencies of ultrasonic actuator HTP05 in the Fig. 4.13. The highest resonant frequency is at frequency of electric generator f_U = 30.6 kHz. For this frequency f_U = 30.6 kHz the ultrasonic actuator HTP05 has the highest displacements of mechanical oscillation for constant voltage V_U led to the actuator. On the other hand, the ultrasonic actuator HTP02 has only one resonant frequency, corresponding with frequency of generator f_U = 24 kHz. The displacement of mechanical oscillation dependents on the frequency of generator f_U for constant voltage V_U = 2.5 V led to the ultrasonic actuator HTP02, the displacement is in Fig. 4.14.

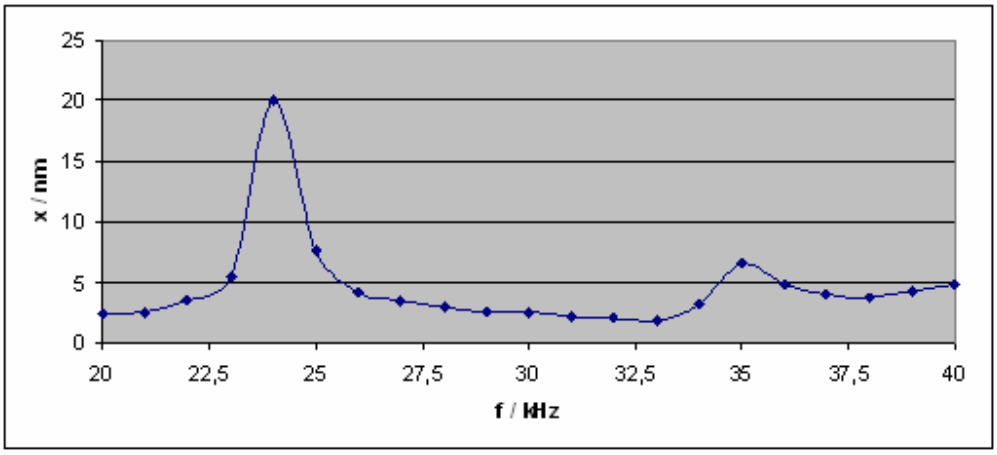

Fig. 4.14: Displacement of mechanical oscillation for ultrasonic actuator HTP02 vs. frequency of AC generator f_U with constant amplitude $V_U = 2.5V$

Displacement of mechanical oscillation has linear dependence on voltage led to the ultrasonic actuator from electric AC generator. Displacement of mechanical oscillation on the ultrasonic actuator HTP05 vs. amplitude of voltage V_U at different frequencies f_U = 25 kHz, 30.6 kHz and 32 kHz you can see in Fig. 4.15. The frequency f_U = 30.6 kHz corresponds with resonant frequency of ultrasonic actuator. For this frequency the displacement of mechanical oscillation is:

$$x = \mathrm{M}\ V_U \tag{4.6}$$

then

$$x = 32 V_U \tag{4.7}$$

where the V_U is AC voltage connected to the ultrasonic actuator
When is applied the same amplitude of voltage variable with different frequency on the ultrasonic actuator then is different mechanical oscillations of the actuator.

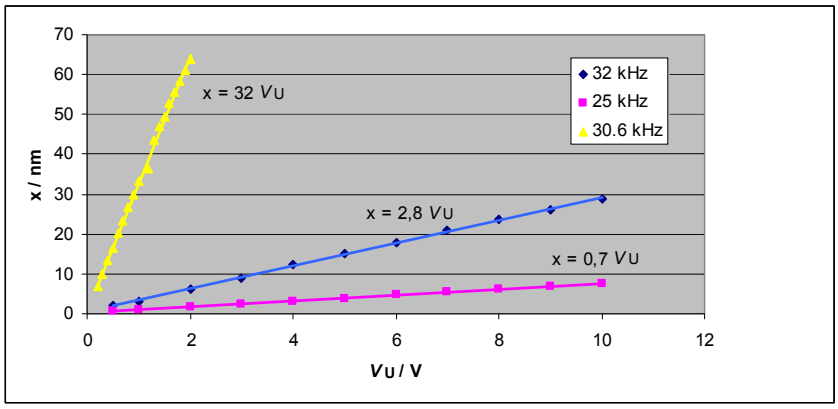

Fig. 4.15: Displacement of mechanical oscillation *x* for ultrasonic actuator HTP05 vs. amplitude of voltage from AC generator with constant amplitude $V_U = 5V$ for different frequencies f_U = 25 kHz, 30.6 kHz and 32 kHz

The linear dependence of the mechanical oscillations of ultrasonic actuator on the amplitude of connected voltage V_U was observed for ultrasonic actuator with radius of body 80 mm also.

Dependence of mechanical oscillations x vs. amplitude of connected AC voltage with frequency f_U = 24.3 kHz, is shown in Fig. 4.16.

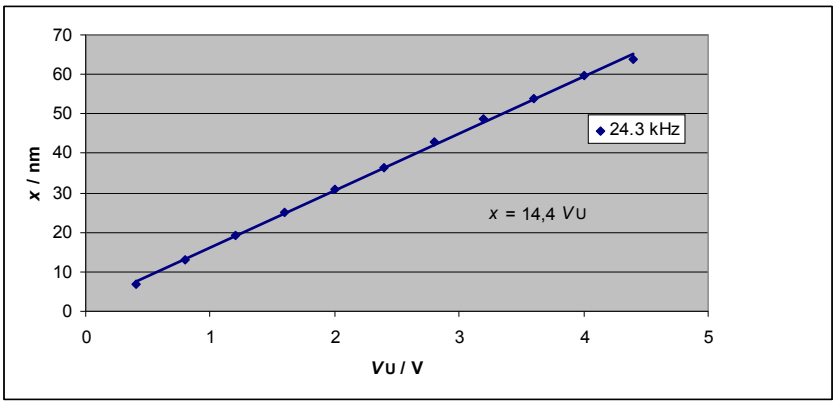

Fig. 4.16: Displacement of mechanical oscillation x for ultrasonic actuator HTP02 vs. amplitude of voltage from AC generator with constant frequency f_U = 24.3 kHz

For example, if is applied AC voltage V_U = 4 V variable with frequency f_U = 24.3 kHz on the ultrasonic actuator HTP02, then the mechanical oscillations has amplitude x = 60 nm. This type of ultrasonic actuator has less resonant frequencies then ultrasonic actuator HTP05.

On the other hand was measured some anomaly dependence of mechanical oscillations on the connected AC voltage on the ultrasonic actuator. I observed when the mechanical oscillations suddenly change the sensitivity on the applied AC voltage. This phenomenon is shown in Fig. 4.17. Mechanical oscillations increases with sensitivity 0.8 / 1V of applied AC voltage and then suddenly change the sensitivity on the more then double of initial value.

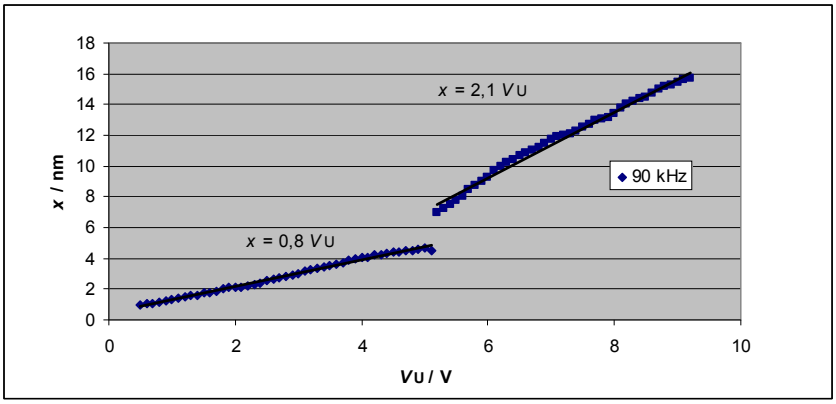

Fig. 4.17: Anomaly which is unfavorable for this measurement

This phenomenon is observed for some specific frequencies of AC voltage connected on the ultrasonic actuator. It is unfavorable for this measurement.

Sensors which were applied on measuring of acoustic emission are based on the same PZT ceramics as ultrasonic transducers. More information about acoustics sensors are detailed described in papers [26 to 28].

5. Experimental results

Electro-ultrasonic spectroscopy was applied on many samples. Thick film resistors, metal samples, granite samples, varistors and so on. In next capture will be shown results from these measurements.

5.1. Measurement on the Cermet Thick Films

5.1.1. Electro-Ultrasonic Spectroscopy with DC electric signal

I evaluated four samples of thick film resistor layers denoted as Sampl-01, Sampl-02, Sampl-03 and Sampl-05. Measured samples were made with different types of resistive pastes (C/Gr conducting particles were suspended in different polymer vehicles). The specimen of the thick film resistor is shown in Fig. 5.1.

Fig. 5.1: Cermet thick film resistor

Resistive pastes were applied on the alumina substrate of dimensions 5 by 40 mm. Resistive layer thicknesses was about 20μm. The contacts were made by dipping silver and one type was used for all the samples. The resistance of my samples was about 1.5 kΩ. The measurements were performed for the exciting ultrasonic signal of frequency 136 kHz where this frequency corresponds to the resonant frequency f_R of the whole system (ultrasonic actuator + sample). The dependence of voltage V_S was measured for different amplitudes of the ultrasonic voltage and for different values of applied DC voltage. The resultant signal in time domain was than evaluated by FFT to obtain the signal spectral density in frequency domain. The voltage V_S can be calculated from following equation:

$$V_S = \sqrt{\Delta f \cdot S_U} \tag{5.1}$$

where Δf is distance between two successive lines in the signal spectra and S_U is signal from noise spectra on frequency f_U.

It is suppose that the sample with higher value of the relative resistance change has more defects in the sample structure comparing to those with lower value of relative resistance change. Measurement on the thick film resistors by electro-ultrasonic spectroscopy with DC electric signal is described in [29]

Results and discussion

The spectral density of the voltage V_S measured on the frequency f_U vs. the amplitude of the ultrasonic signal for different values of DC voltage is shown in Fig. 5.2 for Sampl-01. Probably due to the piezoelectric effect it is measured the nonzero value of voltage V_S even when the DC voltage is zero, $V_E = 0$ V.

The increase of the noise background for DC voltage V_E = 36 V is shown in Fig. 5.3. This is due to that 1/f noise appears in the noise spectrum of measured resistors for higher values of applied DC voltage, which leads to the increase of measuring set-up background noise.

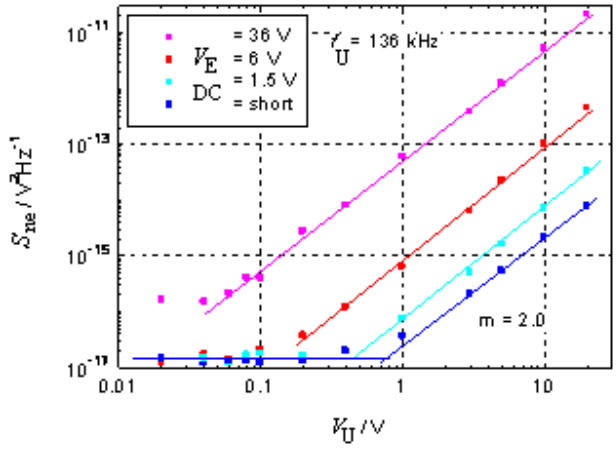

Fig. 5.2: The spectral density of voltage V_S measured on the frequency f_U vs. the amplitude of the ultrasonic signal for different values of DC voltage, measured for Sampl-01.

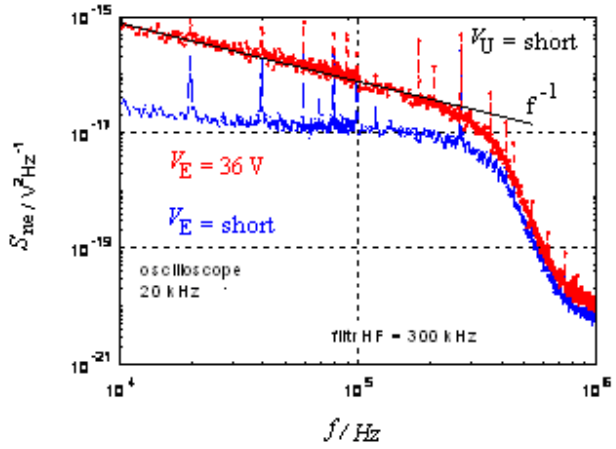

Fig. 5.3: The noise spectrum of measured resistor Sampl-01 for applied DC voltage V_E = 0 V and V_E = 36 V (upper line)

The spectral density of the voltage V_S vs. applied DC voltage for constant value of ultrasonic signal V_U = 10 V is shown in Fig. 5.4.

The spectral density of the voltage V_S vs. DC current for all measured samples is shown in Fig. 5.5. The spectral density of the voltage of V_S increases with approximately the square of DC current which corresponds to the linear increase of voltage V_S with DC current. This is in agreement where the voltage created on the measured structure is proportional to the DC current and ultrasonic excited resistance change. The lost value of V_S is measured for sample Samp-03, which corresponds to the lost ultrasound-excited resistance change of this structure. Voltage V_S can be calculated from the noise spectral density using (5.1).

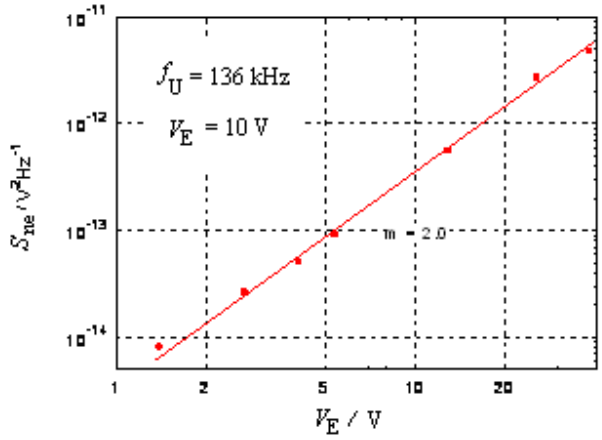

Fig. 5.4: The spectral density of the voltage V_S vs. DC voltage for constant value of ultrasonic signal V_U = 10V

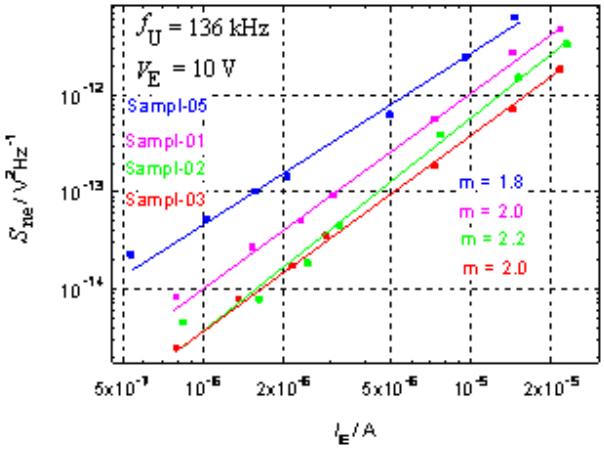

Fig. 5.5: The spectral density of the voltage V_S vs. DC current for Sample 01, 02, 03 and 05

The value of V_S voltage for all measured samples for constant value of DC current I_E = 20 mA and constant value of ultrasonic signal V_U = 10 V is shown in Fig. 5. 6.

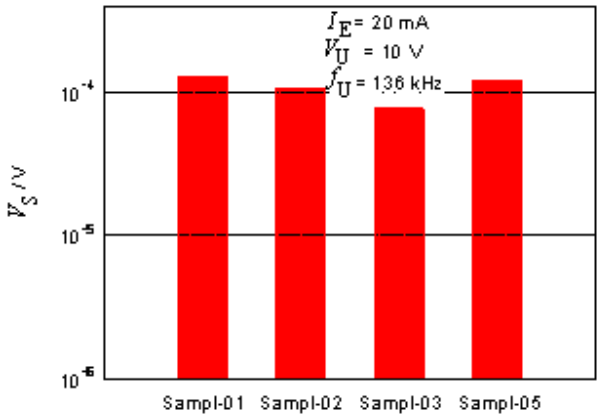

Fig. 5.6: Voltage V_S calculated for Sample 01, 02, 03 and 05, DC current I_E = 20 mA

I found that the relative resistance change $\Delta R/R_X$ is of the order of 10^{-4} percent. The relative resistance change calculated for all the measured samples for constant value of DC current I_E = 20 mA and for constant value of ultrasonic signal V_U = 10 V is shown in Fig. 5.7. The lost value of the relative resistance change is measured for sample Samp-03. The highest value of the relative resistance change is measured for sample Samp-05. It is suppose that the structure quality of sample Samp-03 is better than that of Samp-05.

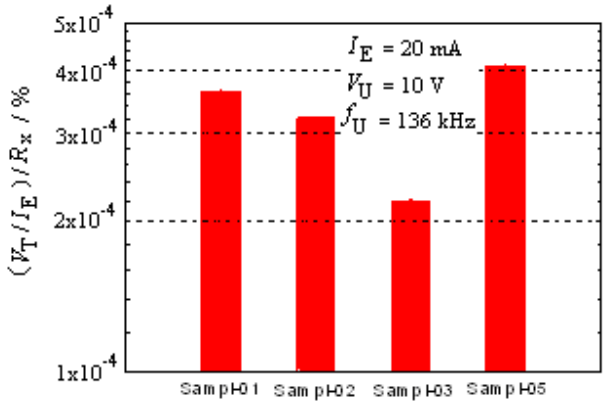

Fig. 5.7: Relative resistance change for all measured samples, DC current I_E = 20 mA

The measurement with DC electric current was performed for more samples on the different frequency of ultrasonic vibration also. The relative resistance change was evaluated before and after second annealing process.

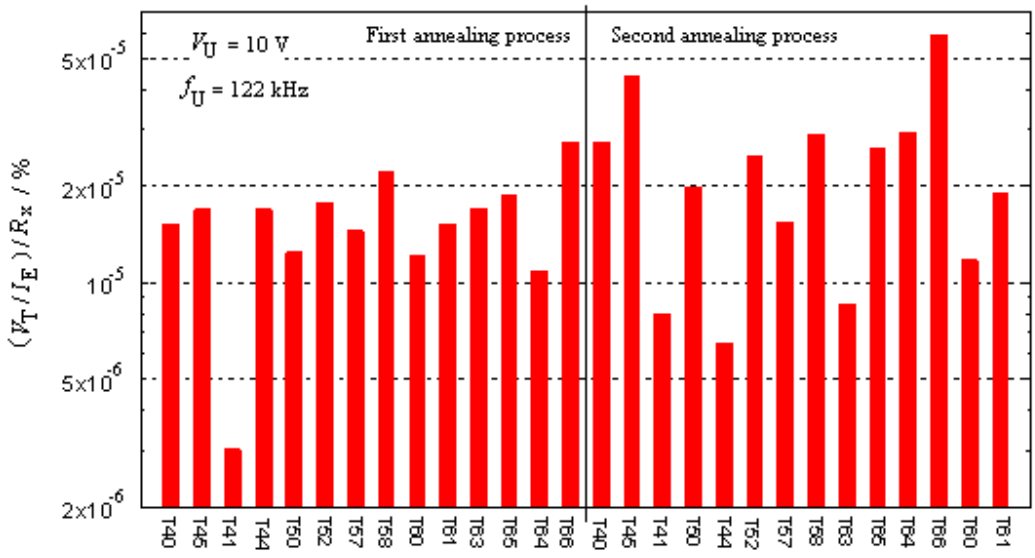

Fig. 5.8: Relative resistance change for all measured samples after the first and second annealing process, for ultrasonic excitation V_U = 10 V and f_U = 122 Hz

The relative resistance change for 14 samples before and after second annealing process for ultrasonic excitation V_U = 10 V and frequency f_U = 122 kHz is shown in Fig. 5.8. For ten samples

was observed increasing of the relative resistance change after second annealing process. For other samples the relative resistance change decreases or fluctuates on the same level which was measured after first annealing process.

Fig. 5.9 shows the relative resistance change for the ultrasonic excitation V_U = 1V variable with frequency f_U = 122 kHz. For this ultrasonic excitation the relative resistance change was increasing for ten samples also after second annealing process.

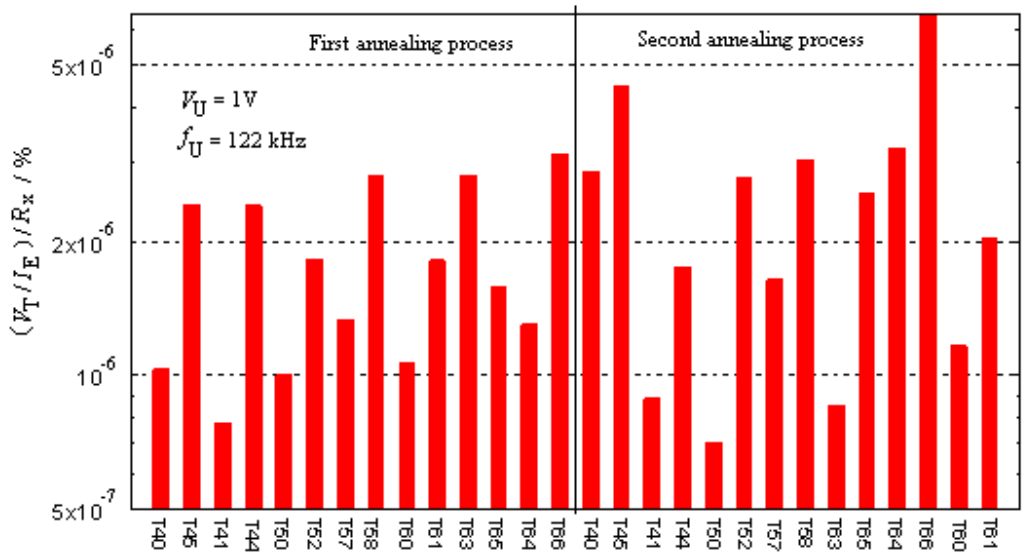

Fig. 5.9: Relative resistance change for all measured samples after the first and second annealing process, for ultrasonic excitation V_U = 1 V and f_U = 122 Hz

Increasing of the relative resistance change due to second annealing process for both ultrasonic excitations V_U = 1 V and 10 V was observed for nine samples (T40, T41, T45, T52, T58, T61, T64, T65 and T66).

Conclusions

I measured four samples of thick film resistor layers denoted as Samp-01, Samp-02, Samp-03 and Samp-05 which were made from different resistive pastes. For all samples the spectral density of V_S increases with the square power of ultrasonic excitation for constant DC voltage and the spectral density of V_S increases with the square power of DC voltage for constant ultrasonic excitation, respectively. This corresponds to the linear increase of voltage V_S with DC current, which is in agreement with the theoretical assumption that voltage v_s created on the measured sample is proportional to I_{DC}. There is observed the piezoelectric effect on my samples. The relative resistance change $\Delta R/R_X$ was calculated and it is of the order of 10^{-4} percent. There we can see that the value of resistive change ΔR is varies for different samples made by one technology. It can be an indicator of the sample quality. It supposes that the samples which have the lost value of ultrasound-excited resistance change it is the better quality structure. In my case was measured the lost value of relative resistance change for sample Samp-03 and the highest value of relative resistance change for sample Samp-05.

When were measured fourteen samples before and after second annealing process, then the relative resistance change was increasing for ten samples for both ultrasonic excitations V_U = 1 V and 10 V variable with frequency f_U = 122 kHz. It supposes that the second annealing process had bad influence on the structure quality of the samples.

5.1.2. Electro-Ultrasonic Spectroscopy with AC electric signal

Measurement with AC electric signal has more sensitivity with respect to noise ratio and useful signal. Here is shown some results on measurements on the thick film resistors layers by electro-ultrasonic spectroscopy with AC electric signal. It was described in many papers, for example [30 to 33].

In order to evaluate the influence of the ultrasonic wave on the measured sample was compared the signal measured on the sample fixed on the piezoceramic transmitter using beeswax with the signal measured on the sample just laying on the top of the transmitter. Measurements were performed for the exciting ultrasonic signal of frequency 31.8 kHz and AC electrical signal of frequency 33.8 kHz. The results of sample T40 measured for $f_E - f_U$ = 2 kHz, V_E = 10 V and V_U = 10 V are shown in Fig. 5.10. For the sample non-fixed on the transmitter no peak is observed on the differential frequency. It shows that signal on the intermodulation frequency is given by the ultrasonic vibrations and other parasitic signal is eliminating.

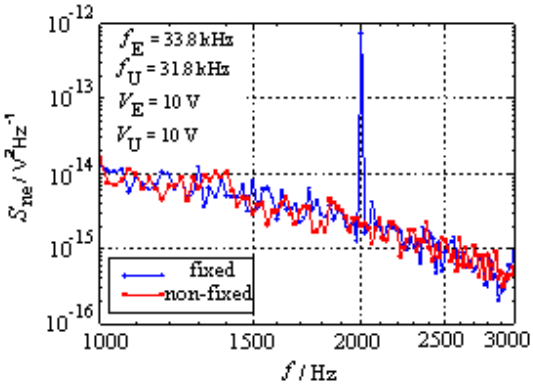

Fig. 5.10: Comparison between the signal measured on the sample fixed on the piezoceramic transmitter using beeswax (blue line) and the signal measured on the sample just laying on the top of the transmitter (red line)

The electro ultrasonic spectroscopy was most applied on the samples of thick film resistor layers. Intermodulation voltage V_i on the resulting frequency $f_E - f_U$ is given by:

$$V_i = \sqrt{\Delta f \cdot S_i} \tag{5.2}$$

where: S_i is signal from the noise spectra on the intermodulation frequency f_E-f_U

By electro-ultrasonic spectroscopy with AC electric signal was evaluate the same samples of thick film resistors layers as in chapter 5.1.1. The samples were fixed on the ultrasonic transmitter (with radius body 20 mm) by beeswax. Ultrasonic transmitter generates the mechanical vibrations on the sample with frequency f_U = 31.8 kHz. The samples were connected simultaneously on the AC electric signal various with frequency f_E = 33.8 kHz. The intermodulation signal on frequency $f_i = f_E - f_U$ was evaluated. The 14 samples were measured before and after second annealing process. The result is shown in Fig. 5.11, where is the relative resistance change computed for each sample for ultrasonic excitation V_U = 10 V and AC electric current I_E = 0.5 mA. In this case the relative resistance change was decreasing with annealing process for most samples (12 samples). It may be indicate that structure of the resistors was improved by annealing process which is contrary of measurement with DC electric current. But there is used different ultrasonic signal frequency and mechanical deformations on the samples are different also.

Then the third annealing process was applied on the samples. The electro-ultrasonic spectroscopy with AC electric signal shows that the relative resistance change decreases again for most samples (9 samples). Relative resistance change for all measured samples after the third annealing process, for ultrasonic excitation V_U = 10 V and f_U = 31.8 kHz is shown in Fig. 5.12.

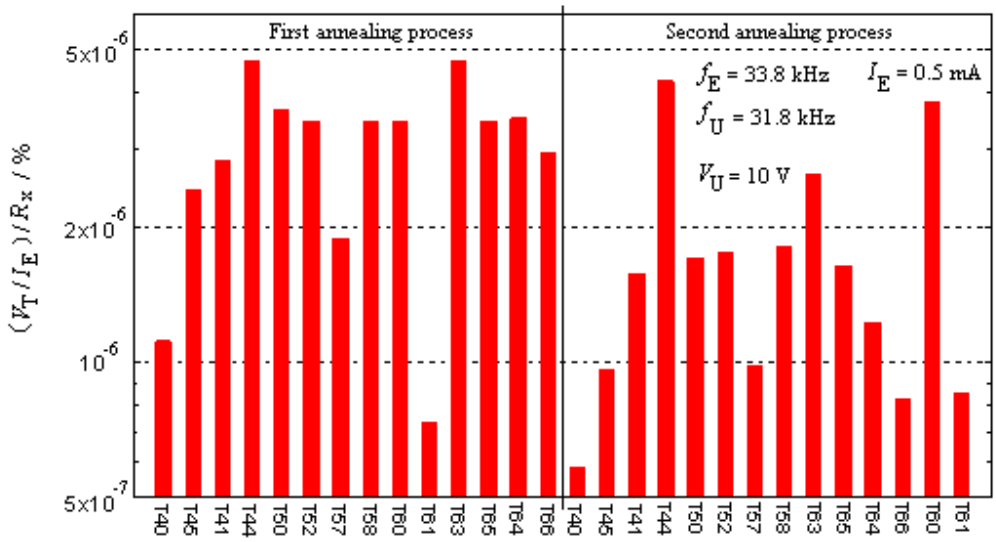

Fig. 5.11: Relative resistance change for all measured samples after the first and second annealing process, for ultrasonic excitation V_U = 10 V and f_U = 31.8 kHz

Why are different results between electro-ultrasonic spectroscopy with AC and DC electric current is not clear. But is it clear that the different frequency of mechanical vibrations has different influence on the resulting resistance change.

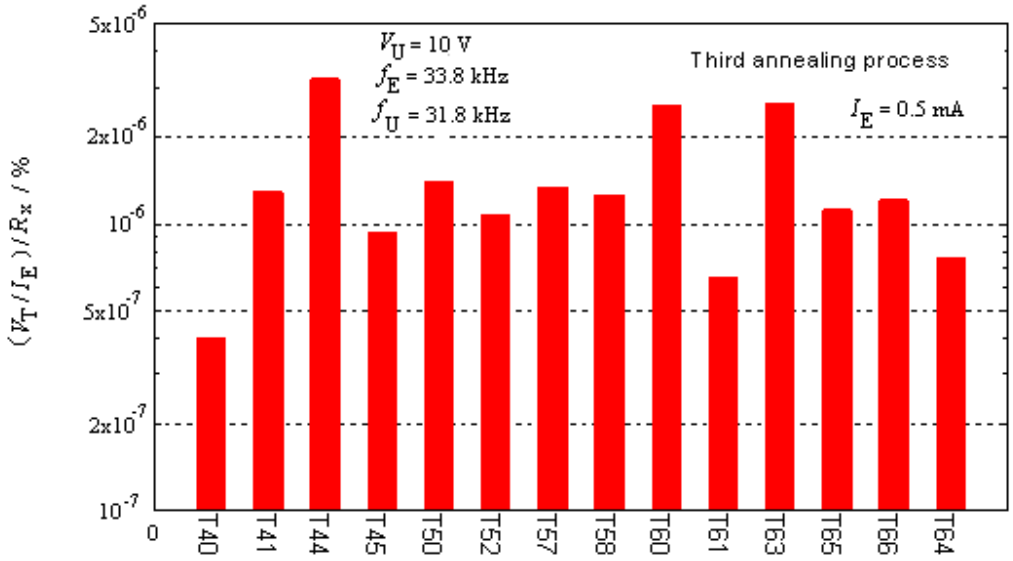

Fig. 5.12: Relative resistance change for all measured samples after the third annealing process, for ultrasonic excitation V_U = 10 V and f_U = 31.8 kHz

Electro-ultrasonic spectroscopy was applied on the sample of cermet thick films. Tested cermet thick film resistors were prepared for the four-point measurements. The sample and its equivalent circuit diagram are shown in Fig. 5.13 and Fig.5.14.

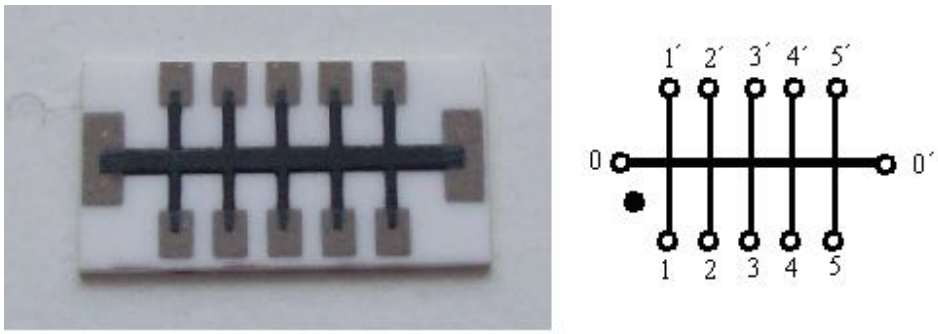

Fig. 5.13: The sample of the cermet thick film resistor

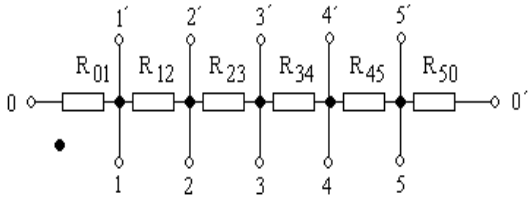

Fig. 5.14: Equivalent circuit diagram for the cermet thick film resistor

Values of resistors in equivalent circuit diagram are shown in Tab. 5.1.

Resistor	R_{01}	R_{12}	R_{23}
R [Ω]	9615	7616	6615
Resistor	R_{34}	R_{45}	R_{50}
R [Ω]	5947	6115	6892

Tab. 5.1 The sample resistance

The resultant signal in time domain was evaluated by FFT to obtain the signal spectral density S_{ne} in frequency domain. Voltage V_i was computed from the measured spectral density.

In this case I studied the dependence of voltage V_i on the resistor length. Total length of the resistor was 18 mm (distance between 0-0'); it was divided by contacts into six parts, each of the length 3 mm. It supposes that intermodulation signal is increasing with the length of resistor.

The ultrasonic frequency was f_U = 31.7 kHz because this frequency corresponds with resonant frequency of ultrasonic actuator. Frequency of electric signal was f_E = 33.9 kHz so the intermodulation signal was measured on the frequency f_i = 2.2 kHz. I evaluated the dependence of intermodulation signal V_i on the electric signal, the ultrasonic signal and the length of resistor. The signal spectral density measured on pin 1´-0´ for electric signal V_E = 7.6 V and ultrasonic signal V_U = 27 V is shown in Fig. 5.15. Sampling frequency is 20 Hz. There is the peak value on the intermodulation signal f_i = 2.2 kHz. Background noise is 10^{-13} V^2Hz^{-1}. The electric filters cut-offs frequencies higher then 3000 Hz.

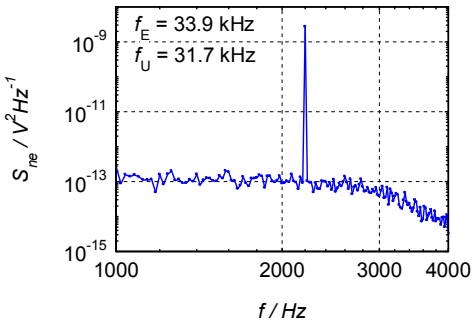

Fig. 5.15: Signal spectral density measured on pin 1´-0´. For electric signal V_E = 7.6 V and ultrasonic excitation V_U = 27 V

The voltage V_i measured on the frequency f_i vs. the electrical current flowing through the structure is shown in Fig. 5.16 for constant ultrasonic signal V_U = 6.78 V. This shown that voltage V_i increases with the increasing length of the sample. Voltage V_i is increasing linearly with electrical current.

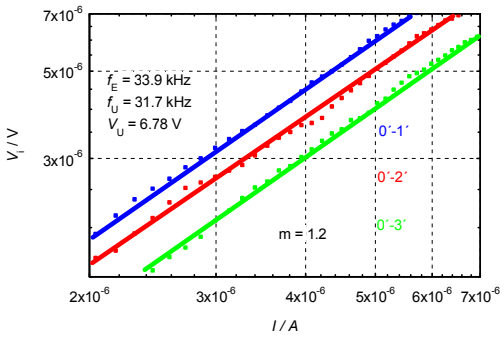

Fig. 5.16: The voltage V_i measured on the frequency f_i vs. the amplitude of the electric signal for pin 1´-0´, 2´-0´ and 3´-0´

The voltage V_i measured on the frequency f_i vs. the ultrasonic signal is shown in Fig. 5.17 for constant electric current I_E = 58 μA. Voltage V_i increases with the increasing length of the sample. Intermodulation voltage V_i is increasing with power of 0.5 for ultrasonic excitation.

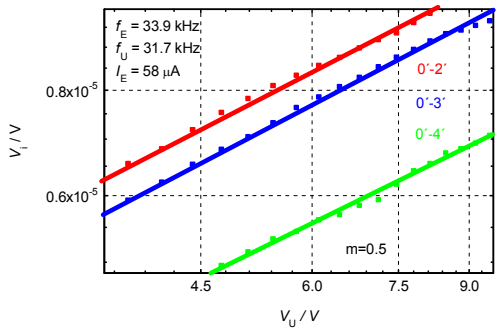

Fig. 5.17: The voltage V_i measured on the frequency f_i vs. the amplitude of the ultrasonic signal for pin 2´-0´, 3´-0´ and 4´-0´

The dependence of voltage V_i on the length of the sample for electric current I_E = 5 μA and ultrasonic excitation V_U = 6.78 V is shown in Fig.5.18. The voltage V_i is increasing linearly with length of the sample except for the last 6 mm. The structure between contacts 4 and 5 contains probably some defects.

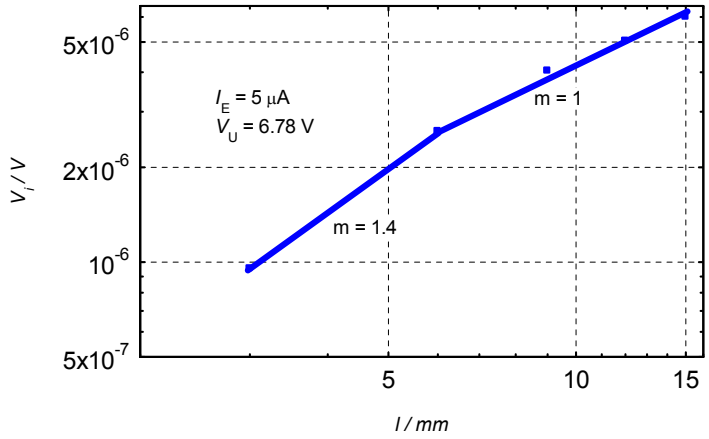

Fig. 5.18: The voltage V_i measured on the frequency f_i vs. the length of the sample

From the measured voltage V_i, I can find the resistance change for each contact. This dependence is shown in Fig. 5.19. The resistance change is increasing with length of the sample.

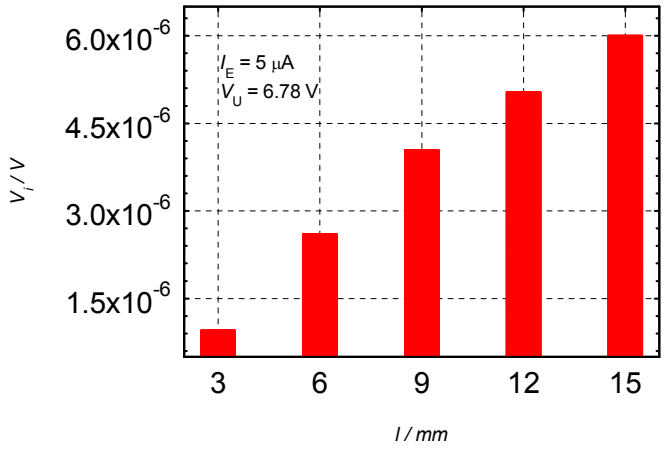

Fig. 5.19: The resistance change ΔR vs. the contacts of the sample for electric current I_E = 5 μA and ultrasonic excitation V_U = 6.78 V

Geometry change due to ultrasonic signal is influences on the thickness of substrate and thick film of resistor. Papers with electro-ultrasonic spectroscopy of polymer-based thick film layers are described in [34 to 36].

Conclusions

Intermodulation voltage V_i increases linearly with ultrasonic excitations when was applied DC and AC constant electric voltage on the sample thick film resistors layers. The same

dependence was observed for constant ultrasonic excitation and different amplitudes of electric current. The resistance change due to ultrasonic excitations was order of 10^{-4} %. On the resistors was applied three times annealing process. From testing electro-ultrasonic spectroscopy by AC current is shown that structure of the resistors was improved by annealing process. Cermet thick film resistor was studied the dependence of voltage V_i on the resistor length. Total length of the resistor was 18 mm (distance between 0-0'); it was divided by contacts into six parts, each of the length 3 mm. The frequency of ultrasonic excitation was f_U = 31.8 kHz and electric signal f_E = 33.9 kHz. The voltage V_i increases linearly with electric current and with power of 0.5 for ultrasonic excitation. The voltage V_i is increasing linearly with length of the sample except for the last 6 mm. The structure between contacts 4 and 5 contains probably some defects. I found the resistance change for each contact. The resistance change is increasing linearly with length of sample. The structure of the sample not contains more defects between contacts 1 up to 4. Some defects are only present between contact 4 and 5.

5.2. Magnesium Composites

5.2.1. The effect of ultrasonic vibrations on sample excited in longitudinal direction

The effect on sample excited in the longitudinal direction will be described first. The sample of Mg alloy with length L = 104 mm, width w = 5 mm, and thickness t = 1.7 mm was fixed on the ultrasonic actuator according to Fig. 5.20.

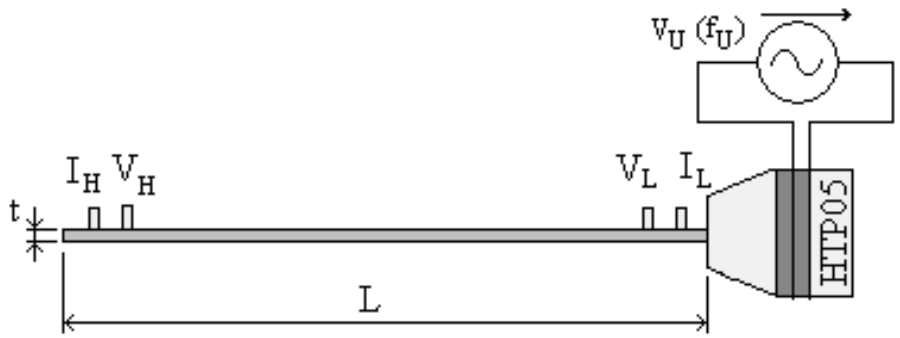

Fig. 5.20: The sample of the Mg alloy flat cross-beam fixed on the ultrasonic actuator, I_L, I_H, and V_L, V_H are current and voltage contacts, respectively.

The dependence of the mechanical amplitude on the AC voltage V_U applied on the ultrasonic actuator was measured and the results are shown in Fig. 5.21. Two different dependences were measured – the first for the ultrasonic actuator itself, and the second for the ultrasonic actuator with fixed sample. The difference between the y-values of these dependences corresponds to the ultrasonic induced sample dilatation for the sample of Mg alloy (see Fig. 5.22).

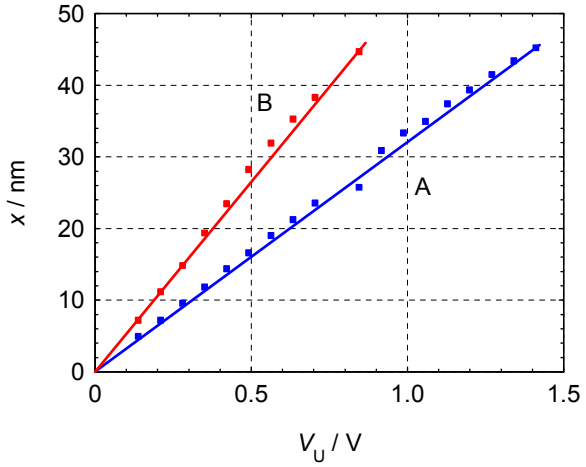

Fig. 5.21: The mechanical amplitude X vs. the AC voltage V_U applied on the ultrasonic actuator at frequency f_U = 30.6 kHz, where lower curve A corresponds to the ultrasonic actuator itself and the upper curve B - for the ultrasonic actuator with fixed sample

The amplitude of ultrasonic vibrations X is proportional to the electrical voltage applied on the ultrasonic actuator (equation 4.6), where the value M = 32 nm/V was measured on the top of the ultrasonic actuator (curve A) and M= 54 nm/V on the top of a fixed sample on ultrasonic actuator (curve B). The measurement was performed on the frequency f_U = 30.6 kHz (see Fig. 5.22). The dependence of the ultrasonic induced sample dilatation ΔL on the voltage V_U applied on the ultrasonic actuator can be estimated from previous experiment.

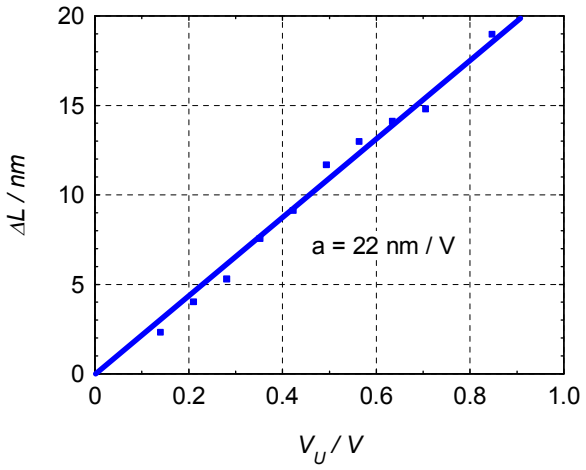

Fig. 5.22: The dependence of the ultrasonic induced sample dilatation ΔL on the voltage V_U applied on the ultrasonic actuator for the sample of Mg alloy measured at the frequency f_U = 30.6 kHz

For the sample dilatation ΔL is proportional to applied voltage V_U with a slope a = 22 nm/V assuming that the both tops of the actuator and the sample oscillate at the same phase. The dependence of the voltage V_i measured on the intermodulation frequency f_i on the AC electric current I_E is shown on Fig. 5.23, for the constant amplitude of the sample dilatation X = 155 nm at frequency f_U = 30.6 kHz.

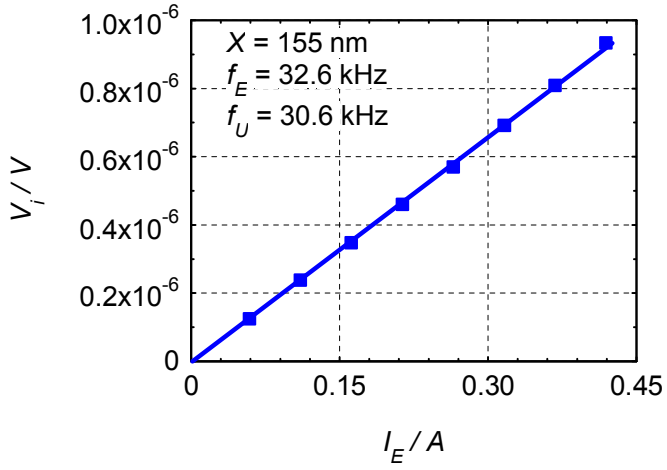

Fig. 5.23: The voltage V_i on intermodulation frequency f_i vs. AC electric current I_E, for the constant amplitude of the sample dilatation X = 155 nm at frequency f_U = 30.6 kHz

The dependence of the intermodulation voltage V_i measured at frequency f_i is shown in Fig. 5.24, for AC electric current I_E = 0.21A, on the amplitude of sample dilatation X. The amplitude of intermodulation signal increases linearly with the amplitude of AC current as well as with the amplitude of sample dilatation X.

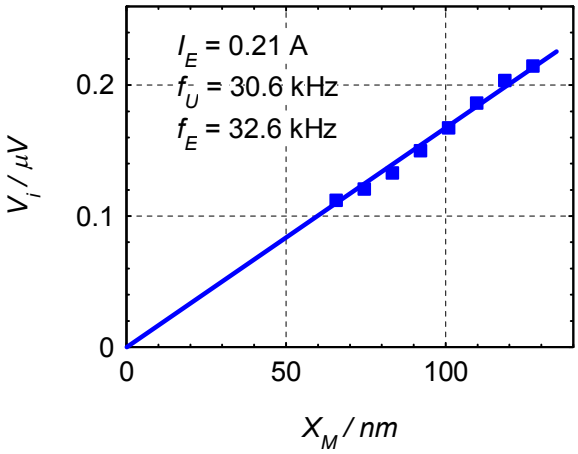

Fig. 5.24: The intermodulation voltage V_i at frequency f_i and electric AC current I_E = 0.21A vs. amplitude of sample dilatation X measured for exciting frequency f_U = 30.6 kHz and f_E = 32.6 kHz

5.2.2. The effect of ultrasonic vibrations on sample excited in transversal direction

Here is described the effect of the ultrasonic excitation on the metallic sample excited in the transversal direction. The sample of a dural flat cross-beam was fixed on the ultrasonic actuator according to Fig. 5.25.

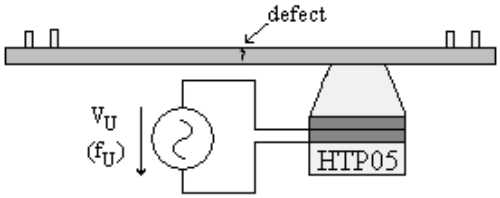

Fig. 5.25: The sample of a dural flat cross-beam with pin hole

NDT testing was performed for the metallic sheets with low electrical resistance and then the AC voltage source was connected through transformer Tr_1. In this case the AC current of frequency f_E applied on the DUT can reach the value up to 1 A. The impedance matching of the signal processing input is realized by transformer Tr_2. This transformer increases the measured voltage without additional noise by 20 to 40 dB.

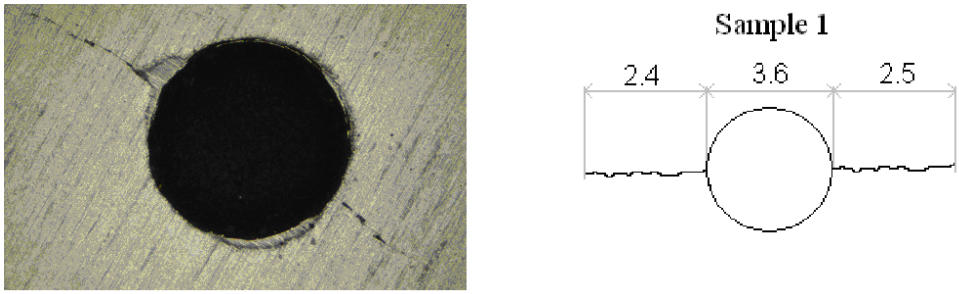

Fig. 5.26: Photo of the pin hole with cracks in the dural flat cross-beam (left) and the size of the hole and cracks (right)

The proposed method was verified by measurements carried out on a set of six dural flat cross-beam samples with a pin hole. Four samples were periodically stressed to obtain cracks around the pin hole (see Fig. 5.26). The other two samples were left for the reference.

During these measurements, the frequency of electrical excitation signal was set to f_E = 35 kHz and the frequency of ultrasonic excitation was set to f_U = 31 kHz. The frequency of intermodulation electrical signal was f_i = 4 kHz. Fig. 5.27 shows a spectral analysis of intermodulation electrical signals for the sample 1 which it consists cracks. The signals were amplified by 40 dB hover Fig. 5.27 shows the measured signal reduced by this amplification. The amplitude of the intermodulation component prior to the amplification is 28 μV. For the comparison the spectral analysis of electrical signals for low stressed sample No 4 is shown in Fig. 5.28. Where the amplitude of the intermodulation component is V_i = 1.5 μV.

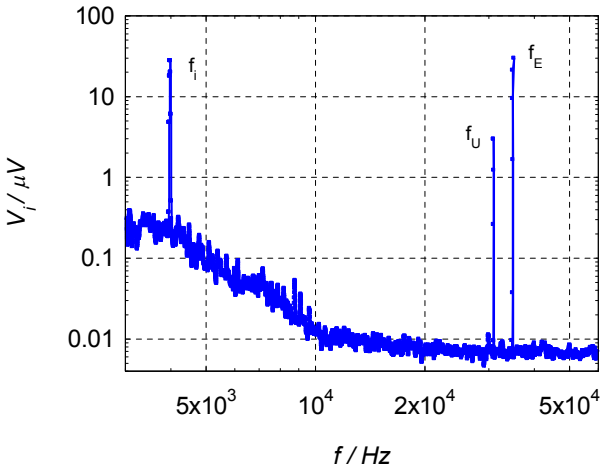

Fig. 5.27: Spectral analysis of electrical signals for sample with cracks for V_E = 9.6 mV, which is attenuated by LP filter to 30 µV

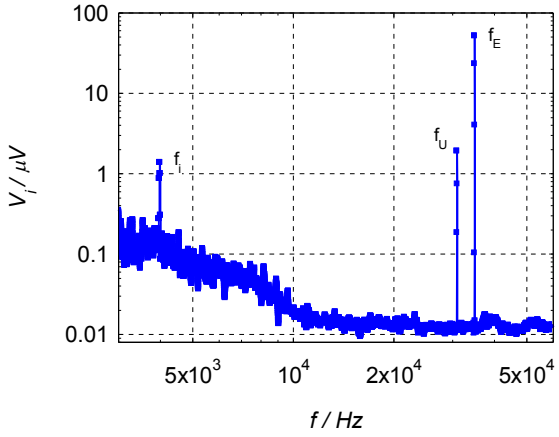

Fig. 5.28: Spectral analysis of electrical signals for the sample No 4 for V_E = 20 mV, which is attenuated by LP filter to 65 µV

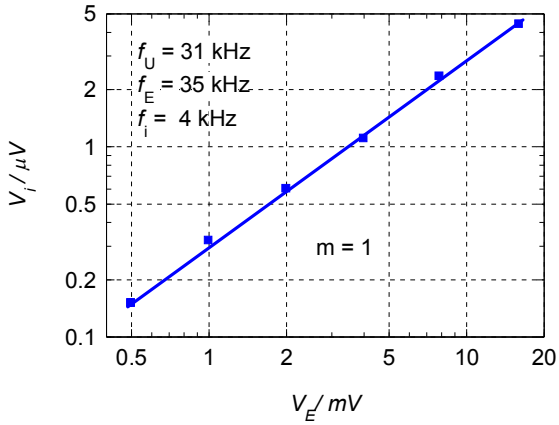

Fig. 5.29: Intermodulation voltages V_i vs. electrical excitation signal V_E for constant value of ultrasonic excitation

The dependence of the intermodulation voltage V_i on the excitation signal V_E for constant value of the ultrasonic excitation is shown in Fig. 5.29, where voltage V_E is measured on the transformer Tr_1 input. The intermodulation voltage V_i is linear function of the signal V_E.

The dependence of the intermodulation voltage V_i on the excitation signal V_U for constant value of the electric excitation is shown in Fig. 5.30. Voltage V_U is measured on the input of the ultrasonic transmitter. Intermodulation voltage V_i for constant value of electrical excitation signal V_E increases with a square of ultrasonic excitation voltage V_U.

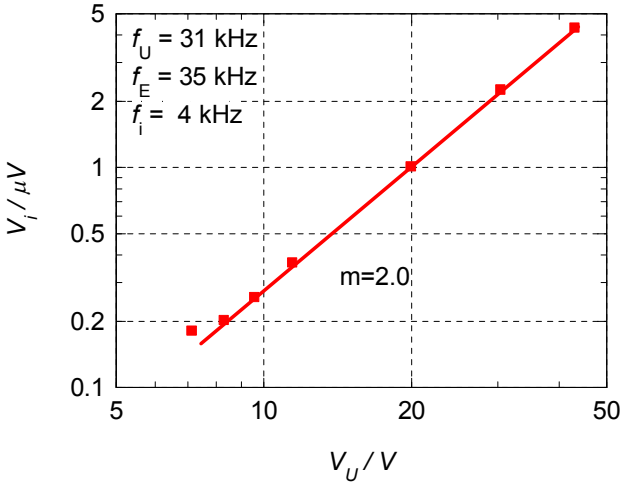

Fig. 5.30: Intermodulation voltages V_i vs. excitation signals V_U for constant value of electrical excitation

Fig. 5.31, shows the resulting intermodulation voltage for all ensembles of samples.

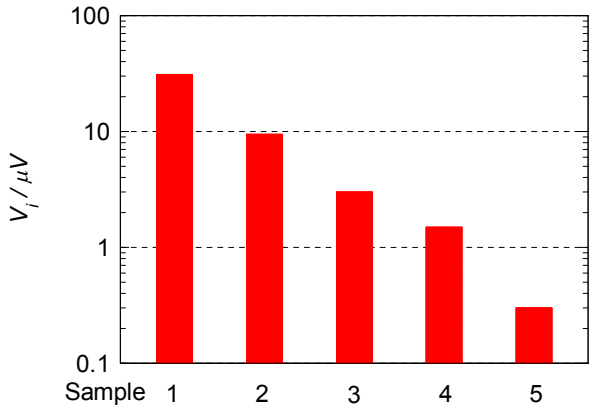

Fig. 5.31: Intermodulation voltages V_i for all measured samples

Table 5.2. The results measured for samples of dural flat cross-beams

Sample No.	1	2	3	4	5
Crack length /mm	4.9	4.4	4.5	3.5	0
V_i / μV	31	9.5	3	1.5	0.3

Table 5.2 shows the comparison of results measured for all the samples No 1 to 4 with cracks and sample No 5 without crack. For the reference sample No 5 the lost value of intermodulation voltage V_i was measured.

It is important that the value of the intermodulation voltage for unstressed reference sample No 5 is not zero. This sample has the amplitude of the intermodulation voltage V_i = 0.3 μV. The sample resistance is influenced not only by the macroscopic cracks, but also by the interaction of ultrasonic signal with inhomogeneities in the sample structure and by the charge carrier mobility change due to the ultrasonic vibrations. There are parasitic effects as an electrical feedback and the piezoresistivity of measured sample as well. The experimental set-up was arranged to minimize these parasitic effects.

Previous results can be explained on the assumption that ultrasonic excitation changes electrical resistance which depends on charge carrier concentration, their mobility and sample structure and geometry. The defects as cracks or dislocations are in analyzed samples due to rolling process or fatigue experiments. The cracks are visible and the length was up to 5 mm. Such samples were chosen to show the outline of new NDT method.

The experiments can be described by intermodulation voltage V_i dependence on electric current I_E or electric voltage V_E and resistance change ΔR due to the ultrasonic excitation with amplitude V_U in the forms which follows from (3.6):

$$v_i(t) = \frac{1}{2} I_E \cos(\omega_E t) \cdot \Delta R \cos(\omega_U t) \tag{5.3}$$

or

$$v_i(t) = \frac{1}{2} V_E \cos(\omega_E t) \cdot \frac{\Delta R}{R} \cos(\omega_U t) \tag{5.4}$$

where R is resistance of all electric circuit

For longitudinal excitation the normalized resistance change is linear function of voltage V_U on ultrasonic actuator because the strain is mainly changed in one direction.

$$\frac{\Delta R}{R} = \mathrm{a} \cdot V_U \tag{5.5}$$

and for transversal excitation the normalized resistance change is quadratic function of voltage V_U on ultrasonic actuator, there is strain changing in two directions.

$$\left(\frac{\Delta R}{R}\right)^2 = \mathrm{b} \cdot V_U \tag{5.6}$$

The a and b constants depend on sample structure, its geometry, cracks characteristics and type of excitation. Similar quadratic dependence of intermodulation voltage on ultrasonic excitation was observed on polymer based carbon and graphite thick film resistors. Electro-ultrasonic spectroscopy on the magnesium composites is described also in papers [37 to 39].

Conclusion

On the defects in metallic samples new harmonic signal is created with frequency given by parametric intermodulation of excitation frequencies f_E and f_U. For the samples with stress

induced cracks higher value of intermodulation voltage is measured. For unstressed referential samples the value of the intermodulation component is influenced by the interaction of ultrasonic signal with inhomogeneities in the sample structure and depends also on the charge carrier mobility change due to the ultrasonic vibrations. I found that the amplitude of intermodulation voltage V_i is the linear function of electrical excitation in both cases of longitudinal and transversal excitations while intermodulation voltage V_i is linear function of ultrasonic excitation for longitudinal excitation and quadratic function for transversal ultrasonic excitation. The signal to noise ratio and high sensitivity for NDT analysis is based on the application of special electrical filters.

5.3. Semiconductors

5.3.1. Monocrystal Si

Specimen of monocrystal Si from Korea was measured by electro-ultrasonic spectroscopy. The specimen was connected by four-point engagement. The sample is illustrated in the Fig. 5.32. Length of the sample was L = 26.6 mm, width and thickness was 3 mm. Resistance between current contacts was 3.7 kΩ and resistance between voltage contacts was 21.9 kΩ.

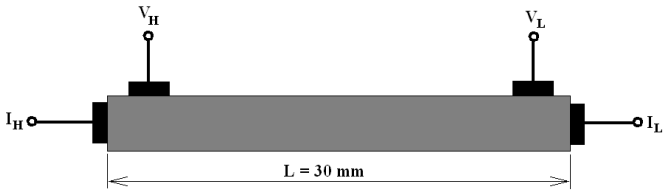

Fig. 5.32: Monocrystal Si. Electric resistance between current contacts is R = 3.7 kΩ and between voltage contacts is R= 21.9 kΩ

Intermodulation voltage V_i measured on the differentia frequency vs. electric voltage connected on the sample is shown in Fig. 5.33. It is for constant ultrasonic excitation V_U = 10 V.

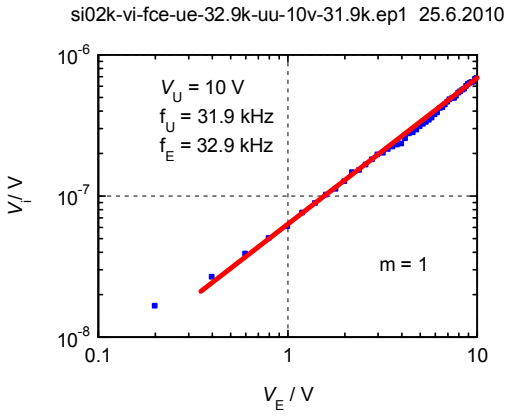

Fig. 5.33: Intermodulation voltage vs. amplitude of electric signal for V_U = 10 V.

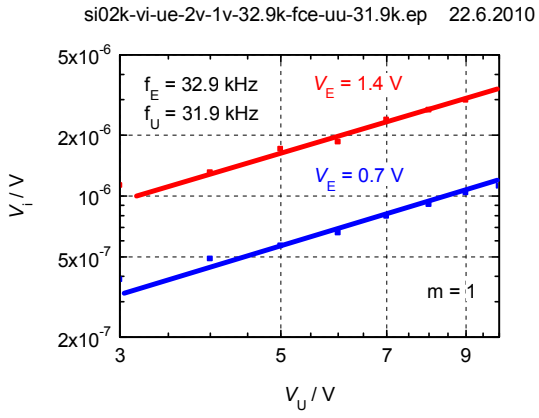

Fig. 5.34: Intermodulation voltage vs. amplitude of ultrasonic excitation for V_E = 0.7 V and 1.4 V

Intermodulation voltage V_i vs. ultrasonic excitation for constant electric voltage V_E = 0.7 V and V_E = 1.4 V connected to the sample is shown in Fig. 5.34. For both dependences the intermodulation voltage increases linearly with electric or ultrasonic excitation. Measurement was performed for ultrasonic signal with frequency f_U = 31.9 kHz and electric signal with frequency f_E = 32.9 kHz.

5.3.2. Monocrystal Si and CdTe

I have measured two samples of monocrystals [40]. Samples were fixed to the ultrasonic actuator by beeswax and connected to the AC voltage. Specimen of monocrystal CdTe is shown in Fig. 5.35 and specimen of monocrystal Si is shown in Fig. 5.36.

Fig. 5.35: Specimen of monocrystal CdTe

Fig. 5.36: Specimen of monocrystal Si

First of all I have measured for constant amplitudes of electric and ultrasonic excitation and for constant frequency of electric signal. Spectral density of intermodulation signal dependence on frequency of ultrasonic actuator for the constant frequency of electric signal f_E = 33.8 kHz is shown in Fig. 5.37.

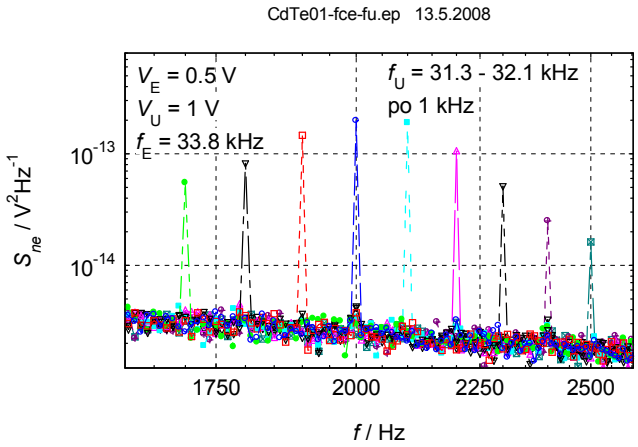

Fig. 5.37: S_{ne} of intermodulation signal vs. frequency of ultrasonic excitation for the frequency of electric signal f_E = 33.8 kHz

The noise background is of the order of 10^{-15} V^2Hz^{-1}. It shown, that the highest intermodulation signal is for frequency f_i = 2 kHz. This frequency corresponds to the ultrasonic excitation on frequency 31.8 kHz. So my measurements were performed for ultrasonic signal on frequency f_U = 31.8 kHz for both samples.

Experimental Results

I evaluated the spectral density of intermodulation signal on frequency f_i for different amplitudes of electric signal and for different amplitudes of ultrasonic excitation. The peak value of intermodulation signal is dependence on AC current flowing throw the structure and on the resistance change except defects and un-homogeneities. Measurements I performed for ultrasonic signal of frequency f_U = 31.8 kHz and for electric signal of frequency f_E = 33.8 kHz. In this case the intermodulation frequency is f_i = 2 kHz.

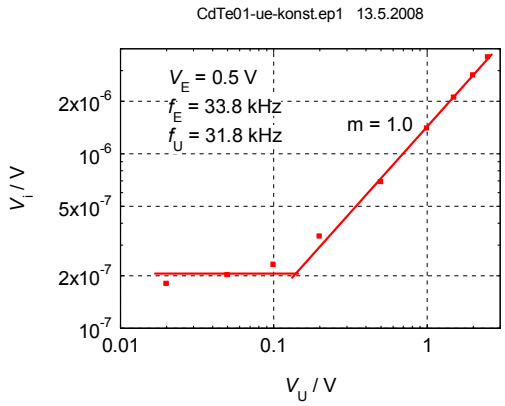

Fig. 5.38: Voltage V_i vs. amplitude of ultrasonic excitation for V_E = 0.5 V. CdTe monocrystal

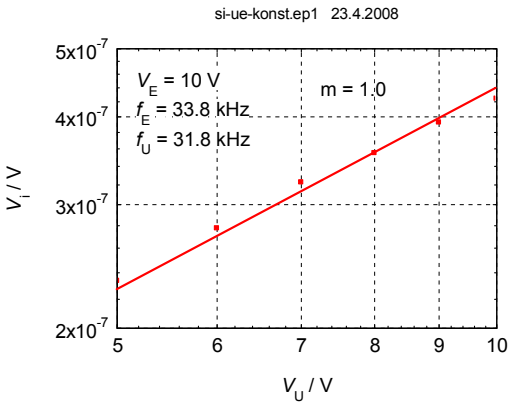

Fig. 5.39: Voltage V_i vs. amplitude of ultrasonic excitation for V_E = 10 V. Si monocrystal

The voltage V_i of the intermodulation signal measured on frequency f_i for different amplitudes of ultrasonic excitation is shown in Fig. 5.38 for CdTe monocrystal and in Fig. 5.39 for Si monocrystal. The sample of silicon was connected to AC voltage of amplitude V_E = 10 V and the sample of Cadmium Telluride was measured for constant AC electric signal V_E = 0.5 V.
It shown, that the voltage V_i of intermodulation signal increases linearly with the ultrasonic excitation for both samples.
The voltage V_i of the intermodulation signal measured on frequency f_i for different amplitudes of electric signal is shown in Fig. 5.40 for Si monocrystal and in Fig. 5.41 for CdTe monocrystal.

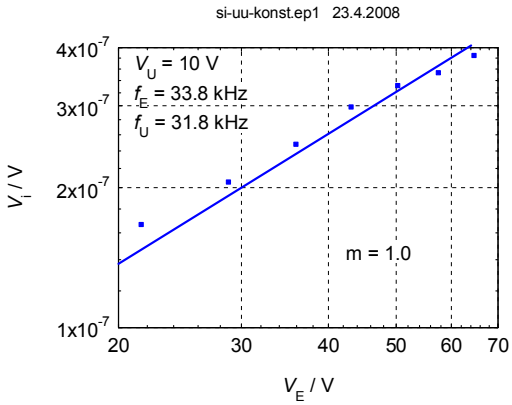

Fig. 5.40: Voltage V_i vs. amplitude of electric signal for V_U = 10 V. Si monocrystal

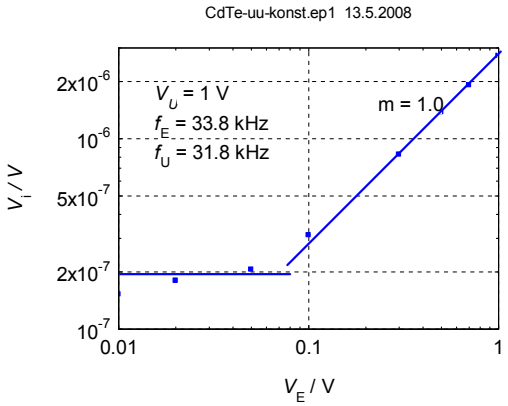

Fig. 5.41: Voltage V_i vs. amplitude of electric signal for V_U = 1 V. CdTe monocrystal

I can compare both samples if I plots the dependence of voltage V_i for different amplitudes of AC current, how is shown in Fig. 5.42.

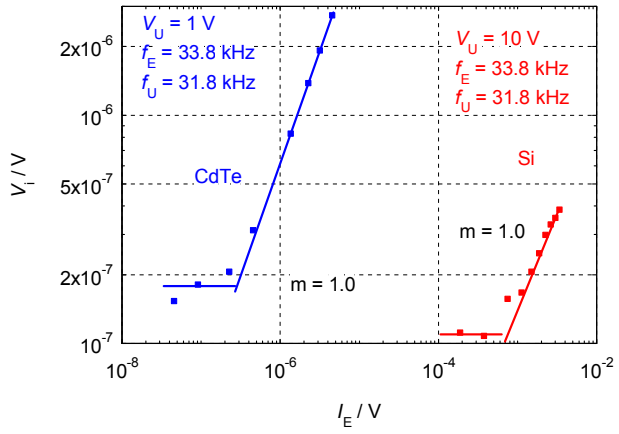

Fig. 5.42: Voltage V_i vs. amplitude of AC current for monocrystal Si and CdTe

If I applied the ultrasonic excitation 10 V and AC current I = 3.55 mA on the sample of monocrystal Si then the relative resistance change is of the order of 10^{-8} percent. For monocrystal CdTe, the relative resistance change is of the order of 10^{-6} percent when I was applied the ultrasonic excitation 1V and AC current 0.69 μA. The value of the relative resistance change defines the sample quality. The relative resistance change for monocrystal Si and CdTe is shown in Fig. 5.43.

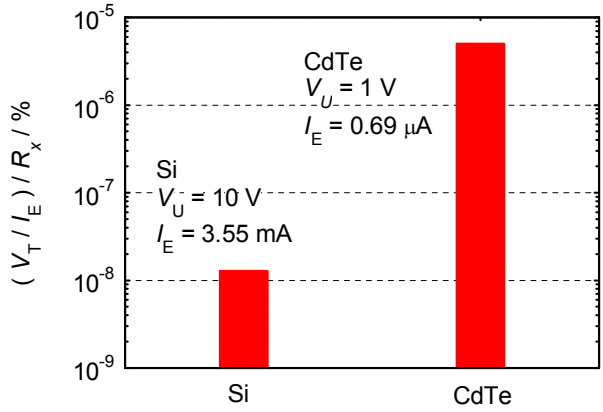

Fig. 5.43: The relative resistance change for monocrystal Si and CdTe

Conclusion

Electro-ultrasonic spectroscopy with AC electric signal was applied on monocrystals. The intermodulation voltage increases linearly with ultrasonic excitation and electric signal for all samples. I calculated that the relative resistance change is of the order of 10^{-8} percent for monocrystal Si and 10^{-6} percent for monocrystal CdTe.

5.4. Measurement on the Varistors

Electro-Ultrasonic spectroscopy was applied on the varistors also from Poland [41, 42]. Four samples of varistors were denoted as PL01, PL02, PL03 and PL04. Two types of varistors are shown in Fig. 5.44.

Fig. 5.44: Specimens of Varistors

Varistors of type on the left side in Fig. 5.44 were denoted PL01 and PL02. Varistors of the second type (Fig. 5.44 on the right side) were denoted PL03 and PL04.

5.4.1. The Dependences on the Electric Excitation

The dependences of the intermodulation voltage V_i on the electric excitation for different values of ultrasonic excitation are shown: in Fig. 5.45 and Fig. 5.46 for samples PL01 and PL02 and for second type in Fig. 5.47 and 5.48 for samples PL03 and PL04.

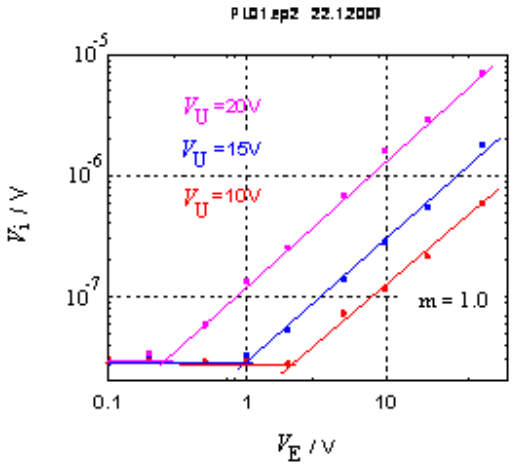

Fig. 5.45: The intermodulation voltage V_i vs. amplitude of electric signal for different ultrasonic excitations. Sample PL01

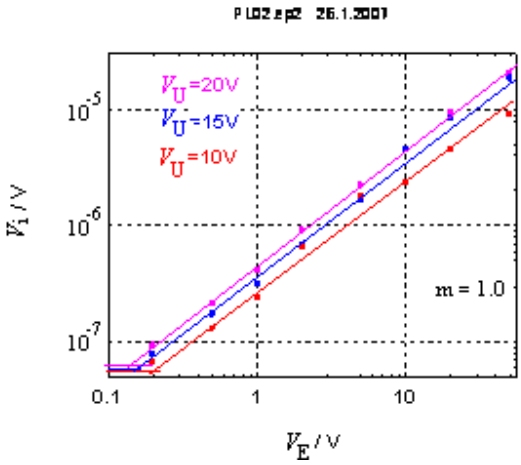

Fig. 5.46: The intermodulation voltage V_i vs. amplitude of electric signal for different ultrasonic excitations. Sample PL02

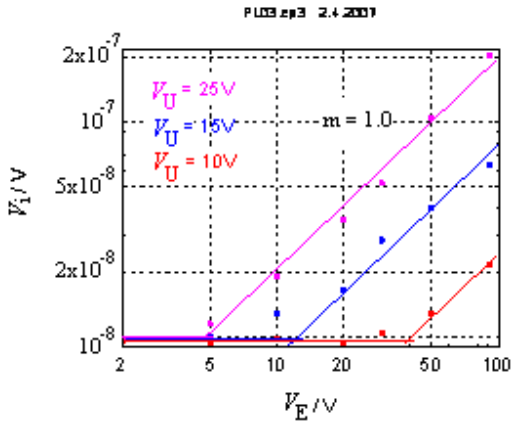

Fig. 5.47: The intermodulation voltage V_i vs. amplitude of electric signal for different ultrasonic excitations. Sample PL03

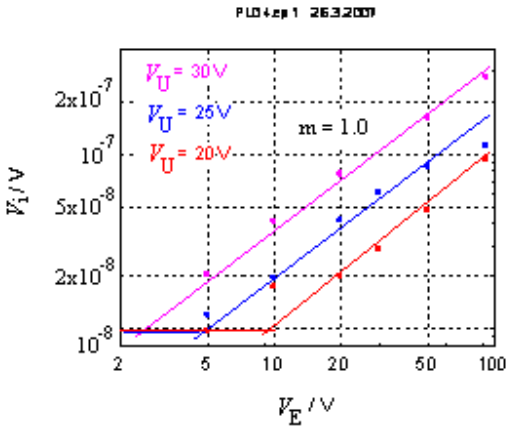

Fig. 5.48: The intermodulation voltage V_i vs. amplitude of electric signal for different ultrasonic excitations. Sample PL04

5.4.2. The Dependences on the Ultrasonic Excitation

The dependences of the intermodulation amplitude V_i on the ultrasonic excitation for the electric excitation V_E = 50 V for samples PL01 and PL02 are shown in Fig. 5.49 and Fig. 5.50. The dependences of the intermodulation amplitude V_i on the ultrasonic excitation for the electric excitation V_E = 92 V for samples PL03 and PL04 are shown in Fig. 5.51 and Fig. 5.52.

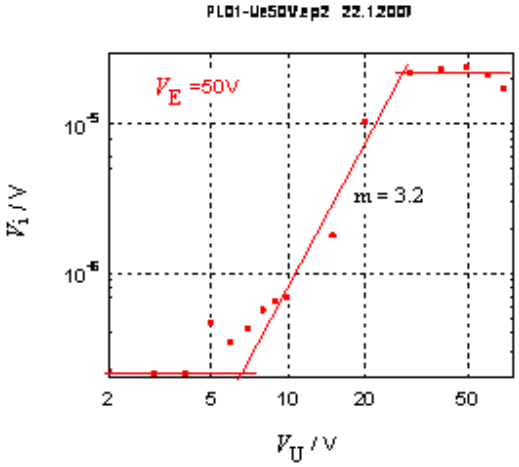

Fig. 5.49: The intermodulation voltage V_i vs. amplitude of ultrasonic excitation for constant electric signal V_E = 50 V. Sample PL01

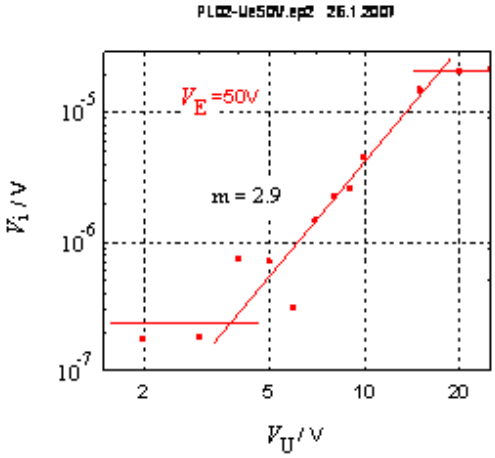

Fig. 5.50: The intermodulation voltage V_i vs. amplitude of ultrasonic excitation for constant electric signal V_E = 50 V. Sample PL02

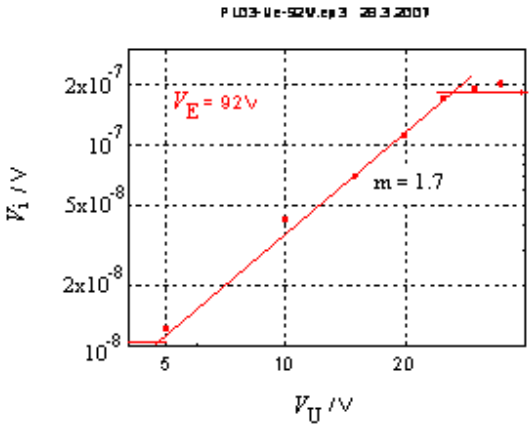

Fig. 5.51: The intermodulation voltage V_i vs. amplitude of ultrasonic excitation for constant electric signal V_E = 92 V. Sample PL03

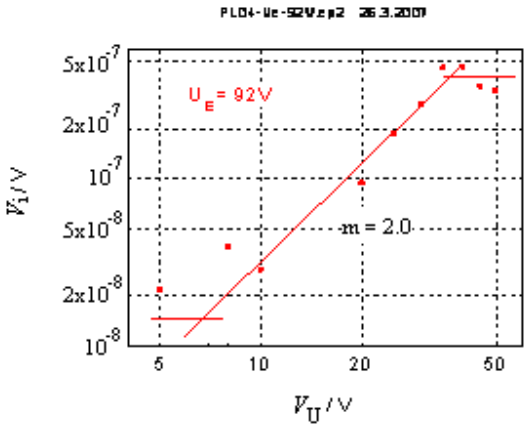

Fig. 5.52: The intermodulation voltage V_i vs. amplitude of ultrasonic excitation for constant electric signal V_E = 92 V. Sample PL04

The amplitude V_i of the intermodulation voltage for samples PL01 and PL02 increases with the ultrasonic excitation with approximately the third power for the V_U above 5 V and reveals the saturation. The saturation occurs for the ultrasonic amplitude value V_U = 18 V for the sample PL02, and for V_U = 30 V for the sample PL01, respectively.

The amplitude V_i of the intermodulation signal for samples PL03 and PL04 increases with the ultrasonic excitation with approximately the square of power for the V_U above 5 V and reveals the saturation also. The saturation occurs for the ultrasonic amplitude value V_U = 27 V for the sample PL03, and for V_U = 35 V for the sample PL04.

CONCLUSION

Four samples of varistors (denoted as PL01, PL02, PL03 and PL04) were measured by electro-ultrasonic spectroscopy. For all samples the intermodulation amplitude V_i increases linearly with electric excitation. For samples PL01 and PL02 intermodulation amplitude V_i increases approximately with the third power of ultrasonic excitation. For samples PL03 and PL04 intermodulation amplitude V_i increases approximately with the square power of ultrasonic excitation. For given electric and ultrasonic excitation the value of V_i can be an indicator of the sample quality. The dependence of the intermodulation amplitude V_i on the ultrasonic excitation reveals the saturation. For given electric excitation the saturation occurs for the lower value V_U for the sample with lower reliability. From my results can conclude, for samples PL01 and PL02, that the structure of sample PL01 is better that that one in sample PL02 and for samples PL03 and PL04, that the structure of sample PL04 is better that that one in sample PL03 and overall that the structure of samples PL03 and PL04 is better that the structure of samples PL01 and PL02

5.5. Measurement on the MOS FET

The electro-ultrasonic spectroscopy was applied on the MOS FET transistor also [43]. The block diagram of the electro-ultrasonic measurement setup is shown in Fig. 5.53. It consists of two parts, the electric and the ultrasonic one.

The ultrasonic part consists of the generator Agilent and the power amplifier WPD 100. The measured sample was fixed on the power piezoceramic transmitter (HTP05) which is used for ultrasonic signal generation.

Electric part consists of a DC voltage source. This signal is led to the measured sample to the V_{GS} (V_G) and V_{DD} (V_D).

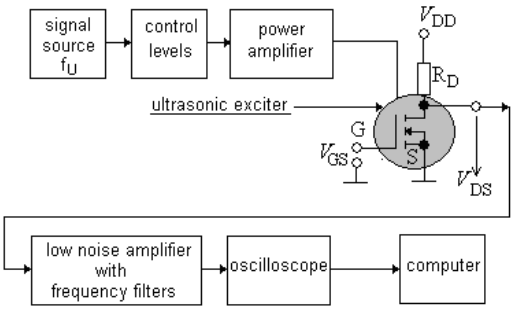

Fig. 5.53: Electro-ultrasonic measurement setup with MOSFET

Experimental

Measurements were performed for the exciting ultrasonic signal of frequency 31.8 kHz where this frequency corresponds to the resonant frequency of the whole system (ultrasonic actuator + sample). The dependence of voltage V_S was measured for different amplitudes of the ultrasonic voltage and for different values of applied DC voltage to the V_{GS} and V_{DD}. The voltage V_S was measured on the frequency of ultrasonic excitation f_U. The resultant signal in time domain was than evaluated by FFT to obtain the signal spectral density in frequency domain. Noise spectral density measured on the sample MOSFET IRF510 is shown in Fig. 5.54 for ultrasonic excitation V_U = short and 1 V. The voltage V_G = 1.28 V and V_D = 3.85 V.

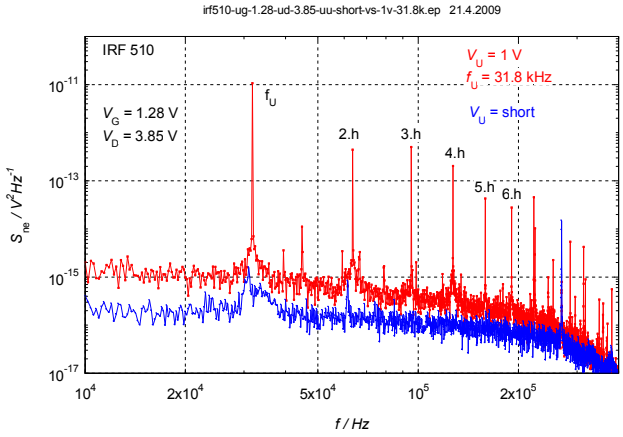

Fig. 5.54: The noise spectrum of the MOSFET IRF510

Results

The dependence of voltage V_S on the ultrasonic excitation and constant applied DC drain voltage V_D = 1.28 V is shown in Fig. 5.55. It is for two values of DC gate voltage V_G (3.82 V and 1.28 V). The voltage V_S measured on the frequency f_U vs. the ultrasonic excitation for constant DC gate voltage V_G is shown in Fig. 5.56. We can see that voltage V_S increases linearly with ultrasonic excitation for constant DC drain V_D and gate V_G voltages.

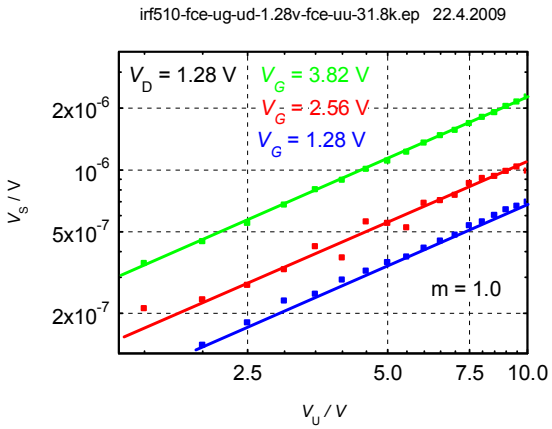

Fig. 5.55: The voltage V_S vs. the amplitude of the ultrasonic excitation for constant drain voltage V_D and different values of gate voltage V_G. Frequency of ultrasonic excitation is f_U = 31.8 kHz.

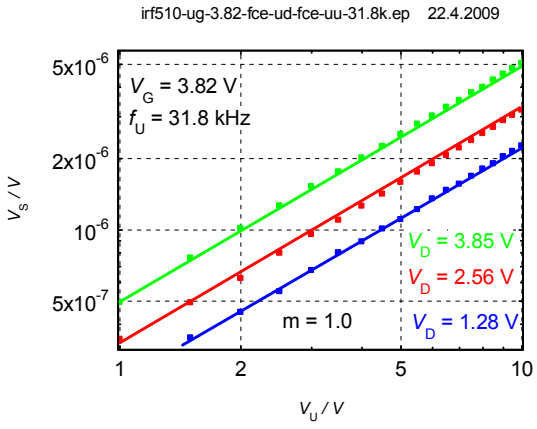

Fig. 5.56: The voltage V_S vs. the amplitude of the ultrasonic excitation for constant drain voltage V_D and different values of gate voltage V_G. Frequency of ultrasonic excitation is f_U = 31.8 kHz.

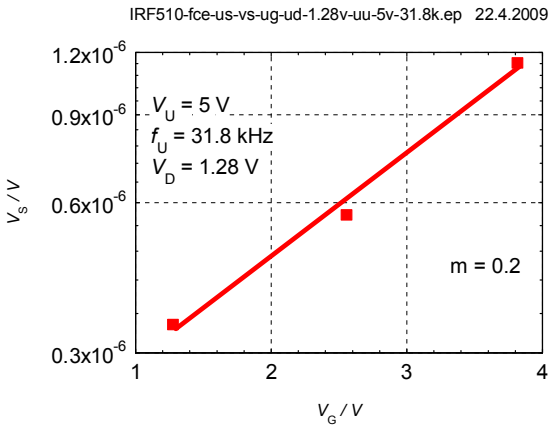

Fig. 5.57: The voltage V_S vs. the amplitude of DC gate voltage V_G. Ultrasonic excitation is V_U = 5 V and V_D is 1.28 V. Frequency of ultrasonic excitation is f_U = 31.8 kHz

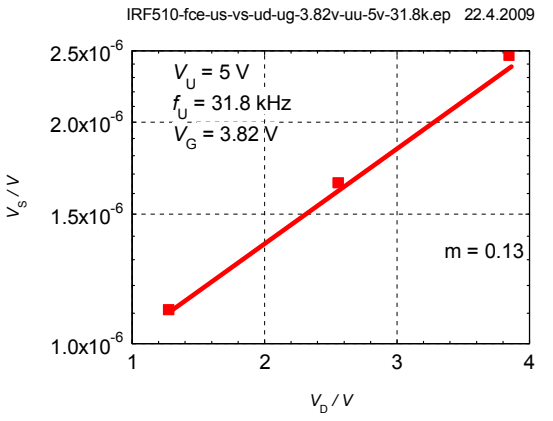

Fig. 5.58: The voltage V_S vs. the amplitude of DC drain voltage V_D. Ultrasonic excitation is V_U = 5 V and V_G is 3.82 V. Frequency of ultrasonic excitation is f_U = 31.8 kHz

The dependence of voltage V_S on the applied DC gate voltage V_G for constant ultrasonic excitation V_U = 5V and DC drain voltage V_D = 1.28 V is shown in Fig. 5.57. The voltage V_S is increasing with power of 0.2 for applied DC gate voltage V_G and for constant ultrasonic excitation and constant DC drain voltage V_D.

The dependence of voltage V_S on the applied DC drain voltage V_D for constant ultrasonic excitation V_U = 5V and DC gate voltage V_G = 3.82 V is shown in Fig. 5.58. The voltage V_S is increasing approximately with power of 0.1 for applied DC gate voltage V_G and for constant ultrasonic excitation and constant DC drain voltage V_D.

Conclusion

Sample of MOSFET IRF510 was measured by electro-ultrasonic spectroscopy. I analyzed signal on the frequency of ultrasonic excitation f_U for different amplitudes on DC drain and gate voltages.

The voltage V_S increases:

- linearly with ultrasonic excitation for constant DC drain and gate voltages,
- with power of 0.2 for applied DC gate voltage V_G and for constant ultrasonic excitation and constant DC drain voltage V_D,

Approximately with power of 0.1 for applied DC gate voltage V_G and for constant ultrasonic excitation and constant DC drain voltage V_D.

5.6. Rock Samples

Non-destructive testing by the ultrasonic wave is applied on rock samples also [44, 45]. Electro-ultrasonic spectroscopy was applied on the granite sample [46 to 48]. An electric resistance of the granite sample is of the order of R = 10 MΩ. Since material has many inhomogeneities in the structure, I suppose high level of measured intermodulation signal on frequency f_i.

5.6.1. Electro-Ultrasonic spectroscopy on the rock sample

Measurements

I measured on frequency of ultrasonic actuator f_U = 31.7 kHz. This frequency corresponds with resonant frequency of ultrasonic actuator and fixed granite sample. Frequency of the electric signal was f_E = 33.7 kHz so the intermodulation signal was on frequency f_i = 2 kHz. Gradually, I increased the electric signal and the ultrasonic signal and then I searched the level of this intermodulation component on frequency f_i. Fig. 5.59 represents measured the noise spectral density of the granite sample Z01. There is the intermodulation signal on frequency 2 kHz and noise background decrease on frequency approximately 3 kHz which is given by the electric filters. Background noise is of the order of 10^{-13} V^2Hz^{-1}.

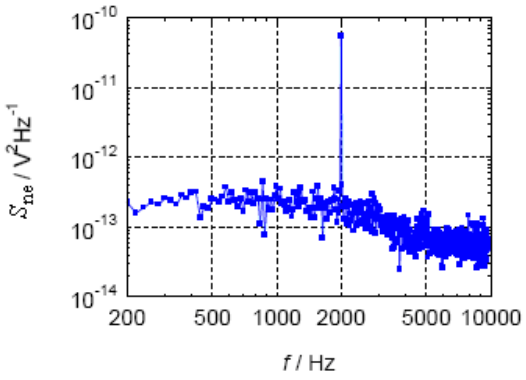

Fig. 5.59: Noise spectral density of granite sample Z01 in frequency range from 200 Hz to 10 kHz. Frequency f_E = 33.7 kHz and f_U = 31.7 kHz

The first measurement on the granite sample by electro-ultrasonic spectroscopy is presented. Research is at the beginning. I tested the rock sample of granite denoted Z01. This sample had shape of prism 50 x 50 x 11 mm^3 (Fig. 5.60).

Fig. 5.60: The rock sample of granite. There is electric contact on the sample fixed by DiAg paste

Electric contacts were fixed on the sample by dipping silver, how is shown in Fig 5.60. Sample was fixed on the ultrasonic transducer HTP05 by beeswax. First was connected the ultrasonic transducer on the constant level of AC voltage of frequency f_U = 31.7 kHz. Electric AC signal of frequency f_E = 33.7 kHz and different level of amplitude V_E was led on the sample. I evaluated intermodulation voltage on frequency f_i how is shown in Fig. 5.61. The intermodulation voltage V_i on the frequency f_i increases linearly with electric signal V_E.

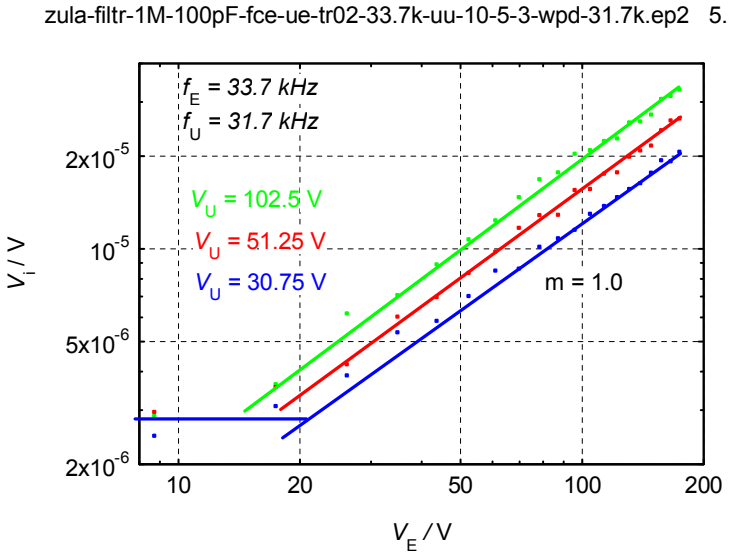

Fig. 5.61: The intermodulation voltage V_i vs. electric voltage for constant ultrasonic excitation V_U = 102.5, 51.25 and 30.75 V

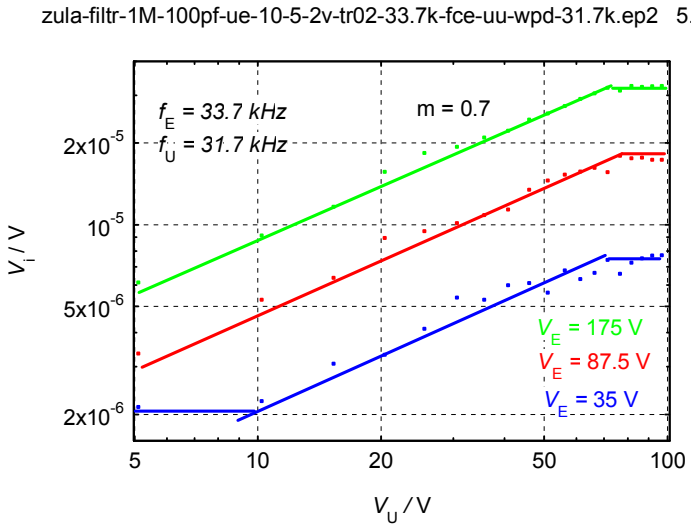

Fig. 5.62: The intermodulation voltage V_i vs. ultrasonic excitation for constant electric voltage V_E = 175, 87.5 and 35 V

On the second step I connected the sample on the AC voltage with the same frequency f_E = 33.7 kHz with constant level for amplitudes of electric signal. Intermodulation voltage was measured for different level of amplitudes of AC voltage led to the ultrasonic transducer with

frequency f_U = 31.7 kHz also. The intermodulation voltage V_i depends on ultrasonic excitation for constant electric AC voltage is shown Fig. 5.62. There is shown that intermodulation voltage V_i is increasing with 0.7 power for ultrasonic excitation. The saturation of ultrasonic excitation appears for amplitudes V_U = 70 V and higher voltages led on the ultrasonic actuator.

This part is based on the combined usage of two modern nondestructive testing methods, the electro-ultrasonic spectroscopy and the diagnostics of mechanically stressed solid dielectric materials by the electromagnetic (EME) and acoustic (AE) emission signals.

The granite sample was measured by the electro-ultrasonic spectroscopy. Then mechanical load (provided by hydraulic press) was applied on this sample. Generally, an application of mechanical stress leads to micro-cracks formation in stressed solid dielectric materials. Cracks generation is accompanied by generation of the electromagnetic (EME) and acoustic (AE) emission signals, which can be measured by appropriate sensors. Continual measurement and real-time processing and evaluation of these signals can be used for quantitative sample damage estimation. After mechanical load application the sample measuring was conducted one more time by means of the electro-ultrasonic spectroscopy.

The force of mechanical load applied on the granite sample and events intensity after time is shown in Fig. 5.63 and Fig. 5.64. Fig. 5.63 is for first mechanical load and Fig. 6.64 is for second mechanical load. Events intensity represents generating micro cracks in the structure of the granite sample during mechanical load.

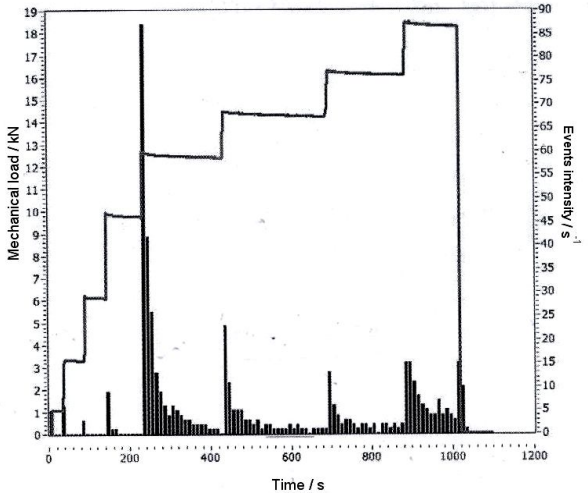

Fig. 5.63: The force of the first mechanical load applied on the granite sample and events intensity after time

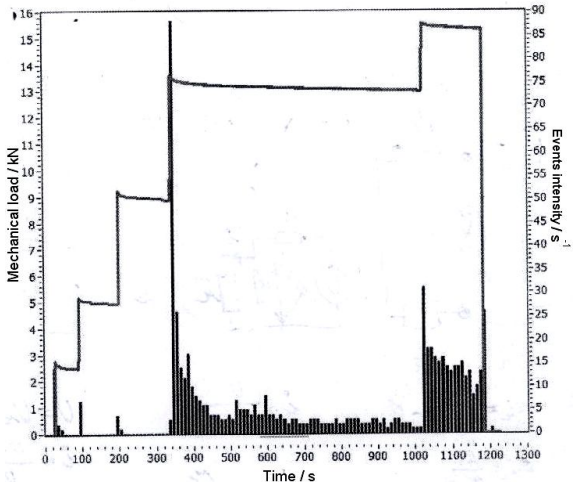

Fig. 5.64: The force of the second mechanical load applied on the granite sample and events intensity after time

The voltage V_i (measured on intermodulation frequency f_i) depending on the granite sample damage is shown in Fig. 5.65. You can see increase of the intermodulation voltage V_i due to cracks contains in the sample structure.

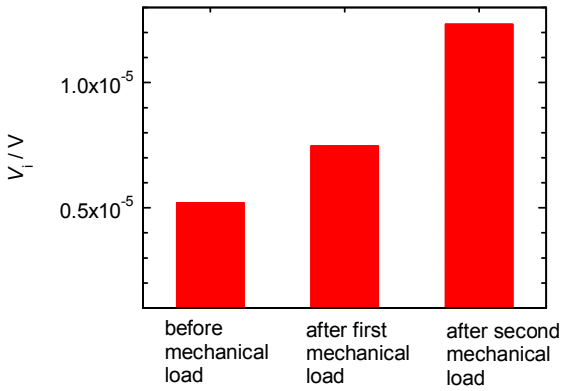

Fig. 5.65: Intermodulation voltage V_i increasing with number of cracks in the granite sample

Conclusion

I tested the rock sample of granite denoted Z01. This sample had shape of prism 50 x 50 x 11 mm3.

The voltage V_i in dependence on ultrasonic excitation appears the saturation. The saturation of ultrasonic excitation occurs for ultrasonic voltage V_U = 70 V for different constant electric voltage V_E = 175, 87.5 and 35 V. The voltage V_i increases approximately with the 0.7 power of ultrasonic excitation for the granite sample Z01.

I found, that intermodulation voltage V_i increases with the damage of the granite sample.

6. Conclusion and Discussion

Electro ultrasonic spectroscopy is based on interaction of two signals: electric AC signal and ultrasonic signal. A new harmonic signal of the frequency f_i is created as a result of resistance change due to variation of the crack effective area by ultrasonic excitation. The intermodulation frequency f_i is given by the subtraction of excitation frequencies f_E and f_U. Amplitude of the intermodulation signal on frequency f_i is influenced by the electric current flowing through the sample structure and ultrasonically induced resistance change due to the defects and inhomogeneities in the sample structure. High sensitivity of this method follows from the fact that the signal giving information on tested sample has frequency different from the exciting signals.

Ultrasonic signal is applied on the sample, in a frequency range from 15 kHz up to 150 kHz. The wavelength of the ultrasonic waves is smaller then mean free path of carriers, thus, the ultrasonic wave does not influence the carriers directly. Ultrasonic excitation changes the geometry of the sample only, in the range of elastic deformations (the non-destructive geometry change). Thus standing wave is created on the sample by ultrasonic vibration. Resistance of the sample is changing similarly to piezoresistive effect. The sample structure is

changing in its all volume due to this excitation. The geometry change inside the sample depends on the type of wave (longitudinal, transversal or torsion wave), frequency of oscillations and position where is defect situated inside the sample. Orientation of cracks considering is also important the wave propagation.

All materials contain cracks and micro-cracks in their structure. My attempt is to detect these cracks. Electro-Ultrasonic spectroscopy is non–destructive testing method which can describe quality and reliability of the tested sample.

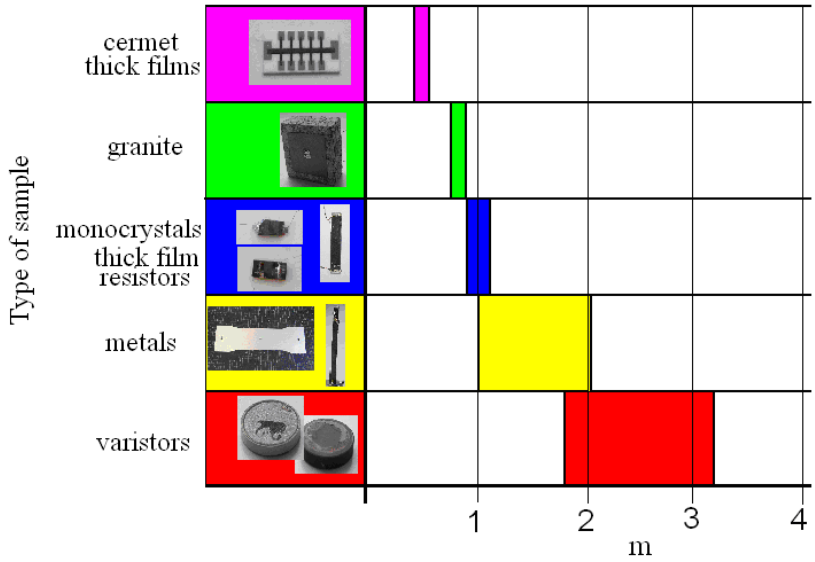

Fig. 6.1: The slope of dependence of intermodulation voltage on ultrasonic excitation

I found that the amplitude of the intermodulation voltage V_i is linear function of electrical excitation for constant ultrasonic excitation. It was observed for all measured samples.

The amplitude of intermodulation component depends on the ultrasonic excitation by several factors such as sample geometry, material, wave propagation etc. Fig. 6.1 shows, how the dependence of intermodulation voltage on ultrasonic excitation changes its slope in order to various samples.

The intermodulation voltage increases linearly with ultrasonic excitations for most samples. It is obviously for longitudinal ultrasonic standing wave generations on the sample. It occurs then the direction of electrical current is parallel to direction of ultrasonic excitation. When ultrasonic excitation works in pendicular direction to electrical current, the different behavior of intermodulation voltage may be observed. It was observed for measurement on the metal samples where a metal plate was excited longitudinal and transversal wave directions. The gauge factor is influenced by the cracks, defects and inhomogeneities of the material. In other words sample with defects is more sensitive on the ultrasonic excitation then sample without defects. If the samples are excited by the same ultrasonic wave then the dependent of the intermodulation voltage on the ultrasonic excitation is the same.

I measured various types of samples, such as thick film resistors, metal samples of magnesium alloy, aluminium and dural plates, monocrystals Si and CdTe, varistors and granite samples.

7. Contribution of the work

Ultrasonic signal is widely used in non-destructive testing methods. Typical ultrasonic testing inspection system is based on several functional units, pulser and receiver, transducer. Ultrasonic transducer generates high frequency ultrasonic energy. This energy is in the form of waves and it is introduced and propagates through the material. If material contains a crack in the path of sound wave then part of the energy will be reflected back from the flaw surface. Advantages of ultrasonic inspection are [49]:

- It is sensitive to both surface and subsurface discontinuities.
- The depth of penetration for flaw detection or measurement is superior to other NDT methods.
- Only single-sided access is needed when the pulse-echo technique is used.
- It is highly accurate in determining reflector position and estimating size and shape.
- Minimal part preparation is required.
- Electronic equipment provides instantaneous results.
- Detailed images can be produced with automated systems.
- It has other uses, such as thickness measurement, in addition to flaw detection.

On the other hand, disadvantages are follows:

- Surface must be accessible to transmit ultrasound.
- It normally requires a coupling medium to promote the transfer of sound energy into the test specimen.
- Materials that are rough, irregular in shape, very small, exceptionally thin or not homogeneous are difficult to inspect.
- Cast iron and other coarse grained materials are difficult to inspect due to low sound transmission and high signal noise.
- Linear defects oriented parallel to the sound beam may go undetected.

The method of the nondestructive measurement has never been described before and our department is the first one to do it. To provide nondestructive tests the ultrasonic signal is used. But quite different method is applied here. In case of elektro-ultrasonic spectroscopy, the ultrasonic signal of low frequency is used only to generate standing mechanical oscillations in specimen. It causes the deformation of the specimen in the elastic range and contained structural defects could be revealed. The more structural defects the specimen has the more sensitive its reaction to the ultrasound signal is. Moreover, it could be used to examine the influence of mechanical oscillations on different electronic components. Each mechanical system is loaded with oscillations of different intensity. Damaged component or material could have different properties under the influence of these oscillations. It could cause fatal consequences. The method of electro ultrasonic spectroscopy could prevent these situations. By means of this method materials, components or the whole circuits which don't comply with required properties under generated oscillations could be found out. This dissertation demonstrates practical measurements by means of electro ultrasonic spectroscopy for both conductive materials and semi-conductive ones or materials with high resistance.

Advantages of electro-ultrasonic inspection are:

- Examine all defects and inhomogeneities in the volume sample.
- It is very simple method and not need high power voltage.

Disadvantages of the electro-ultrasonic inspection:

- Tested material must have measured electrical resistance.
- Measured signal can by covered by the background noise of the measurement setup.
- Different quality contacts between sample and ultrasonic actuator

I founded that electro-ultrasonic spectroscopy can be applied on the sample with high and low material resistance. The samples with high material resistance are for example granite and varistors.

8. References

[1] VAN DEN ABEELE, K., CARMELIET, J., Single Mode Nonlinear Resonant Acoustic Spectroscopy (SIMONRAS) for damage detection in quasi-brittle materials. 1999 http://www.bwk.kuleuven.ac.be/bwk/sr99/bwf.htm#bf1.1

[2] OBRAZ, J., Zkoušení materiálu ultrazvukem, SNTL, Praha, 1989

[3] HEFNER, Š., Ultrazvuková spektroskopie v pevných látkách, Disertační práce, VUT FEKT, Brno 2006.

[4] HÁJEK, K., SEDLÁKOVÁ, V., MAJZNER, J., HEFNER, Š., ŠIKULA, J., Non-linearity and noise characterisation of thick-film resistors after high voltage stress, In *3rd European Microelectronics and Packaging Symposium with Table Top Exhition. Lanskroun: IMAPS CZ&SK*. 2004, s. 421 - 426, ISBN 80-239-2835-X.

[5] ARNOLD, W., HIRSEKORN, S., KOPYCINSKA, M., RABE U., REINSTADTLER, M., Nonlinear Effects in Ultrasonic Transmission in Atomic Force Microscope Contacts, In *16th International Symposium on Nonlinear Acoustics*. 2002, Russia, Moscow, August 2002.

[6] JOHNSON, P., TEN CATE J. A., Non-destructive Testing of Materials By Nonlinear Elastic Wave Spectroscopy. http://www.ees11.lanl.gov/nonlinear/diagnostics.html

[7] ZAITSEV, V.Yu., SAS, P., Nonlinear response of a akly damaged metal sample: a dissipative mechanism of vibroacoustic interaction, *Journal of Vibration and Control*, 2000.

[8] DEBYE, P., A method for the determination of the mass of electrolyte ions, J. Chem. Phys., 1,13-16,1933

[9] WILLIAMS. M., An Electrokinetic Transducer, The review of scientific instruments, 19, 10, 640-646, 1948

[10] KUKOZ F.I., KUKOZ, L.A., The nature of audioelectro-chemical phenomena, Russ. J. Phys. Chem. 36 (1962) pp. 367-369

[11] O'BRIEN, R.W., Electro-acoustic effects in a dilute suspension of spherical particles, J. Fluid Mech., 190, 71-86, 1988

[12] GLAUSER, A.R., ROBERTSON P.A., LO, C.R., An electrokinetic sensor for studying immersed surfaces, using focused ultrasound, Sensors Actuators B, 80, 1, 68-82, 2001

[13] LÜTHI, B., Physical acoustics in the solid state, ISBN 9783540229100, (2005)

[14] AKSHISER A. 1939 *J. Phys*. (U.S.S.R.) 1, 289

[15] PARMENTER R. H. 1953, The Acousto-Electric Effect, *Phys. Rev*. 89, 990, (1953)

[16] INREICH G., Acoustodynamic Effects in Semiconductors, *Phys. Rev*. 104, 321, (1956)

[17] GRIMALDI, C., RYSER, P. and STRÄSSLER, S., Gauge factor enhancement driven by heterogeneity in thick-film resistors, J. Appl. Phys. 90, 322 (2001), 6 pages.

[18] PAPAKOSTAS, T. V., and WHITE, N. M., Influence of substrate on the gauge factor of polymer thick-film resistors, J. Phys. D: Appl. Phys. 33 (2000) L73–L75

[19] PALLÀS-ARENY, R., BSTER, J. G., Sensors and signal conditioning, second edition, 2001, ISBN: 0-471-33232-1

[20] KANDA, Y., Piezoresistance effect in silicon, Sensors and Actuators, 28A, 1991, 83-91.

[21] ŠIKULA, J.; HÁJEK, K.; SEDLÁKOVÁ, V.; TOFEL, P.; MAJZNER, J. Improved Signal to Noise Ratio of Electro- ultrasonic Spectroscopy. *ElectroScope - http://www.electroscope.zcu. cz,* 2008, roč. 2008, č. 6, s. 1-4. ISSN: 1802- 4564.

[22] HEFNER, Š., MAJZNER, J., HAVRÁNEK, J., ŠIKULA, J. NOISE CHRACTERISTICS OF PIEZOCERAMICS SAMPLES. In *New Trends in Physics 2004*. 2004, Brno, s. 36 - 39, ISBN 80-7355-024-5.

[23] MAJZNER, J. Optimalizace poměru signál/šum piezokeramického senzoru, *Disertační práce*, VUT FEKT, Brno, 2006

[24] SEDLÁK, P. Matematický model piezokeramického senzoru, *Disertační práce*, VUT FEKT, Brno, 2006

[25] SEDLAK, P., MAJZNER, J., TOFEL, P., SIKULA, J. Piezoelectric Transducers: Electrical and Noise Characteristics Modeling. *In Defektoskopie 2006 Proceedin,*. Brno*: Czech Society for Nondestructive Testing,* 2006.s. 217-224. ISBN: 80-214-3290-X

[26] ŠIKULA, J., ŠTRUNC, M., MAJZNER, J., HÁJEK, K. Electrical noise and sensitivity of piezoceramic sensors. In *Proc. of NDT 2003*. 2003.

[27] SEDLÁK, P., MAJZNER, J., HEFNER, Š. Frekvenční charakteristiky snímačů akustické emise. In *Defektoskopie 2003*. 2003, Praha, s. 211 - 215, ISBN 80-214-2475-3.

[28] SEDLÁK, P., MAJZNER, J., HEFNER, Š., BLÁHA, M. Piezoceramics Sensors: Signal to Noise Ratio. In *3rd European Microelectronics and Packaging Symposium with Table Top Exhition. Lanskroun: IMAPS CZ&SK*. 2004, s. 666 - 671, ISBN 80-239-2835-X.

[29] TOFEL, P.; SEDLÁKOVÁ, V.; ŠIKULA, J. Thick Film Resistor Testing by Electro - Ultrasonic Spectroscopy with DC Electric Signal. In *Reliability and Life-time Prediction ISSE2008*. 1. Hungary: 2008. s. 56-57. ISBN: 978-963-06-4915-5.

[30] SEDLÁKOVÁ, V.; ŠIKULA, J.; TOFEL, P.; KOPECKÝ, M.; HÁJEK, K. THICK FILM RESISTORS NDT BY ELECTRO- ULTRASONIC SPECTROSCOPY. In *Vth workshop NDT in progress*. 2009. s. 247-252. ISBN: 978-80-214-3968- 9.

[31] HAJEK, K., SEDLAKOVA, V., MAJZNER, J., HEFNER, S., SIKULA, J. Non-linearity and noise characterisation of thick-film resistors after high voltage stress. In *Proceedings of 3rd European Microelectronics and Packaging Symposium*. Prague (Czech Republic), 2004, June 16 – 18, s. 421 – 426, ISBN 80-239-2835-X.

[32] SEDLÁKOVÁ, V.; TOFEL, P.; ŠIKULA, J.; TACANO, M. Noise, Non-Linearity and Electro-Ultrasonic Spectroscopy for Testing of Resistors. *Passive Component Industry Magazine,* 2008, roč. 2008 (10), č. 6, s. 23-27.

[33] SEDLAKOVA, V., MELKES F., DOBIS, P., SIKULA, J. TACANO, M., HASHIGUCHI, S. Non-linearity changes induced by current stress in thick film resistors. *In Proceedings of CARTS,* 2004, San Antonio, Texas, (U.S.A.), 2004, s. 154 – 157, ISSN 0887-7491.

[34] SEDLÁKOVÁ, V.; TOFEL, P.; ŠIKULA, J. Long Term Stability of Polymer Based Resistors Tested by Noise, Non-Linearity and Electro- Ultrasonic Spectroscopy. In *17th European Microelectronics and Packaging Conference & Exhibition*. Italie: 2009. s. 1-5. ISBN: 978-1-4244-4722- 0.

[35] TOFEL, P.; ŠIKULA, J.; SEDLÁKOVÁ, V.; CHVÁTAL, M. Electro Ultrasonic Spectroscopy of Cermet Thick Films. In *32nd International Spring Seminar on Electronics Technology*. Brno: 2009. s. 188-189. ISBN: 978-1-4244-4260- 7.

[36] SEDLÁKOVÁ, V.; ŠIKULA, J.; TOFEL, P.; MAJZNER, J. Electro-ultrasonic spectroscopy of polymer-based thick film layers. *Microelectronics Reliability,* 2008, roč. 48, č. 6, s. 886-889. ISSN: 0026-2714.

[37] TOFEL, P.; ŠIKULA, J.; TROJANOVÁ, Z. NONLINEAR ULTRASONIC SPECTROSCOPY OF MAGNESIUM COMPOSITES. In *NEW TRENDS IN PHYSICS 2007*. Brno, Czech Republic: Ing. Zdeněk Novotný CSc., 2007. s. 146-149. ISBN: 978-80-7355-078-3.

[38] TOFEL, P.; ŠIKULA, J.; HÁJEK, K.; TROJANOVÁ, Z.; BUMBÁLEK, L. Cracks detection in Mg alloy by electro- ultrasonic spectroscopy. *Key Engineering Materials,* 2011, roč. 465, č. 1, s. 350-353. ISSN: 1662- 9795.

[39] TOFEL, P.; ŠIKULA, J.; SEDLÁKOVÁ, V.; TRČKA, T. Electro Ultrasonic Spectroscopy of Magnesium Composites. *Jemná mechanika a optika,* 2010, roč. 55, č. 5/ 2010, s. 142-144. ISSN: 0447- 6441.

[40] TOFEL, P.; ŠIKULA, J.; SEDLÁKOVÁ, V. NDT OF SINGLE CRYSTAL CDTE AND SI BY ELECTRO- ULTRASONIC SPECTROSCOPY. In *Vth Workshop NDT in Progress.* Praha: 2009. s. 305-310. ISBN: 978-80-214-3968- 9.

[41] TOFEL, P.; ŠIKULA, J. ELECTRO- ULTRASONIC SPECTROSCOPY FOR TESTING QUALITY OF RESISTIVES MATERIALS. In *Student EEICT 2009.* 2009. s. 171-175. ISBN: 978-80-214-3870- 5.

[42] TOFEL, P.; ŠIKULA, J.; HASSE, L. The Non-Linear Electro-Ultrasonic Spectroscopy. In *30th International Spring Seminar on Electronics Technology*. Cluj-Napoca, Romania: Dan Pitica, 2007. s. 196-197. ISBN: 978-973-713-174-4.

[43] TOFEL, P.; ŠIKULA, J.; PARAČKA, P. ELECTRO- ULTRASONIC SPECTROSCOPY OF MOSFETS. In *IEEE Workshop Králíky 2009.* 2009. s. 285-288. ISBN: 978-80-214-3938- 2.

[44] GUYER, R.A., McCALL, K.R., BOITNOTT, G.N., HILBERT, L.B., PLONA, TJ. Quantitative use of Preisach-Mayergoyz space to find static and dynamic moduli in rock, *J. Geophys. Res.* 102, s. 5281-5293, 1997.

[45] BEARD M. D., LO M. J. S. Non-destructive testing of rock bolts using guided ultrasonic waves. International Journal of Rock Mechanics and Mining Science, Volume 40, Issue 4, Pages 527-536, ISSN: 13651609, 2003

[46] TOFEL, P.; TRČKA, T. Diagnostika žulového vzorku pomocí elektro- ultrazvukové spektroskopie. In *DISEE 2010, DIELEKTRICKÉ A IZOLAČNÉ SYSTÉMY V ELEKTROTECHNIKE A ENERGETIKE*. 2010. s. 74-77. ISBN: 978-80-227-3366- 3.

[47] TOFEL, P.; CHVÁTAL, M. GRANITE SAMPLE AND ELECTRO- ULTRASONIC SPECTROSCOPY. In *STUDENT EEICT 2010.* Brno: 2010. s. 134-138. ISBN: 978-80-214-4079-1.

[48] TOFEL, P.; ŠIKULA, J. NON-DESTRUCTIVE TESTING OF A ROCK SAMPLE BY NON-LINEAR ULTRASONIC SPECTROSCOPY. In *NEW TRENDS IN PHYSICS 2007.* Brno, Czech Republic: Ing. Zdeněk Novotný CSc, 2007. s. 142-145. ISBN: 978-80-7355-078-3.

[49] http://www.ndt-ed.org/EducationResources/CommunitzCollege/Ultrasonics/Introduction/description.htm

List of symbols

[]	matrix
α_{sw}	attenuation of the sound wave
α_T	temperature coefficient
γ_{ij}	shear strain
$\Delta\theta$	temperature change
ε	strain
$[\varepsilon_{rs}]$	relative permittivity matrix
$\emptyset$	volume fraction of dispersed phase
λ	wave length
μ	mobility
μ_d	dynamic electrophoretic mobility
ζ	potential of dispersion and emulsion
π_L	piezoresistive coefficient
ρ	electrical resistivity
σ	electrical conductivity, mechanical stress
ω_E, ω_U	angular frequency of electric / ultrasonic excitation
A	cross-section area
B	effective noise pass-band
C	capacity
$[C_E]$	elastic matrix
C_P, C_S	parallel / serial equivalent circuit capacity
CVI	colloid vibration potential
c	stiffness tensor
E	Young's modulus
$\vec{E}$	vector of electric field intensity
E_{ae}	acousto electric field
E_{DC}	direct electric field
e	electric charge
$[e]$	coupling matrix
F	force

$\vec{F}$	force vector
f	frequency
f_E, f_U	frequency of electric / ultrasonic excitation
f_i, f_I	intermodulation frequency on low / high frequency band
f_R	resonant frequency
Δf	distance between two successive lines in the signal spectra
GF	Gauge factor
GF_L	longitudinal gauge factor
GF_T	transverse gauge factor
I_{AW}	intensity of acoustic wave
i_{AC}	alternating current amplitude
i_{DC}	direct current
$\vec{J}$	current density vector
k	wave number, Boltzmann constant
k_u	ultrasonic transfer constant
L	length of the sample
ΔL	change of the length
M	ultrasonic constant dependent on frequency
n	density of carriers
n_e, n_h	density of electrons / holes
n_p, n_m	density of particles / fluid
PZT	lead zirconate titanate
R	electric resistance
R_C	resistance of current contact
R_{DUT}	sample resistance under test
R_E	electric signal generator resistance
R_P, R_S	parallel / serial equivalent circuit resistance
ΔR	resistance change
S_{ne}	noise spectral density
T	temperature
t	time, thickness
V_C	parasitic voltage on current contacts

V_n	noise voltage
V_{ne}	noise voltage for a low noise preamplifier
V_S	voltage measured on the sample on the ultrasonic frequency
V_s	sound velocity
V_T	total voltage measured on the sample
v	Poisson's ratio
v_d	drift velocity
v_i	intermodulation voltage
W	width of the sample
x	amplitude of displacement
x_m	amplitude of mechanical vibrations
Z	impedance

Curriculum Vitae

Name:	Pavel Tofel
Born:	September 19th 1981 in Valašské Meziříčí
Contact:	xtofel01@stud.feec.vutbr.cz
Nationality:	Czech
Sex:	Male

Education

2001 – 2006	**Brno University of Technology / Faculty of Electrical Engineering and Communication / Electrical Engineering and Computer Science - Cybernetics, Control and Measurements**
	State exam passed in June 2006
	Diploma thesis - Object sorting based on shape
2006 – 2011	**Brno University of Technology / Faculty of Electrical Engineering and Communication / Department of Physics**
	Ph.D. study
	Ph.D. Thesis - Non-linear Electro - Ultrasonic Spectroscopy of Resistors, State exam passed in June 2011

Experience

2002 –	Brno University of Technology / Faculty of Electrical Engineering and Communication: Technical worker
2008	Main investigator of Grant project FRVS 2016/2008/G1 Modernizace laboratoře pro elektro-ultrazvukovou spektroskopii
2010	Main investigator of Grant project FRVS 3034/2010/G1 Modernizace laboratoře pro diagnostiku elektronických součástek pomocí Elektro-Ultrazvukové spektroskopie

Languages

English